The Tibet ASγ Experiment

Masato TAKITA, ICRR, U. of Tokyo
(For the Tibet ASγ collaboration)

Externalreview, @ICRR, 16/Jan/2013

CONTENTS

1. Tibet ASγ Experiment

The Tibet ASγ Collaboration

M.Amenomori(1), X.J.Bi(2), D.Chen(3), W.Y.Chen(2), S.W.Cui(4), Danzengluobu(5), L.K.Ding(2), X.H.Ding(5), C.F.Feng(6), Zhaoyang Feng(2), Z.Y.Feng(7), Q.B.Gou(2), H.W.Guo(5), Y.Q.Guo(2), H.H.He(2), Z.T.He(4,2), K.Hibino(8), N.Hotta(9), Haibing Hu(5), H.B.Hu(2), J.Huang(2), W.J.Li(2,7), H.Y.Jia(7), L.Jiang(2), F.Kajino(10), K.Kasahara(11), Y.Katayose(12), C.Kato(13), K.Kawata(3), Labaciren(5), G.M.Le(2), A.F.Li(14,6,2), C.Liu(2), J.S.Liu(2), H.Lu(2), X.R.Meng(5), K.Mizutani(11,15), K.Munakata(13), H.Nanjo(1), M.Nishizawa(16), M.Ohnishi(3), I.Ohta(17), S.Ozawa(11), X.L.Qian(6,2), X.B.Qu(2), T.Saito(18), T.Y.Saito(19), M.Sakata(10), .K.Sako(12), J.Shao(2,6), M.Shibata(12), A.Shiomi(20), T.Shirai(8), H.Sugimoto(21), M.Takita(3), Y.H.Tan(2), N.Tateyama(8), S.Torii(11), H.Tsuchiya(22), S.Udo(8), H.Wang(2), H.R.Wu(2), L.Xue(6), Y.Yamamoto(10), Z.Yang(2), S.Yasue(23), A.F.Yuan(5), T.Yuda(3), L.M.Zhai(2), H.M.Zhang(2), J.L.Zhang(2), X.Y.Zhang(6), Y.Zhang(2), Yi Zhang(2), Ying Zhang(2), Zhaxisangzhu(5), X.X.Zhou(7)

(1)Department of Physics, Hirosaki University, Japan
(2)Key Laboratory of Particle Astrophysics, Institute of High Energy Physics, Chinese Academy of Sciences, China
(3)Institute for Cosmic Ray Research, University of Tokyo, Japan
(4)Department of Physics, Hebei Normal University, China
(5)Department of Mathematics and Physics, Tibet University, China
(6)Department of Physics, Shandong University, China
(7)Institute of Modern Physics, SouthWest Jiaotong University, China
(8)Faculty of Engineering, Kanagawa University, Japan
(9)Faculty of Education, Utsunomiya University, Japan
(10)Department of Physics, Konan University, Japan
(11)Research Institute for Science and Engineering, Waseda University, Japan
(12)Faculty of Engineering, Yokohama National University, Japan
(13)Department of Physics, Shinshu University, Japan
(14)School of Information Science and Engineering, Shandong Agriculture University, China
(15)Saitama University, Japan
(16)National Institute of Informatics, Japan
(17)Sakushin Gakuin University, Japan
(18)Tokyo Metropolitan College of Industrial Technology, Japan
(19)Max-Planck-Institut f¥"ur Physik, Deutschland
(20)College of Industrial Technology, Nihon University, Japan
(21)Shonan Institute of Technology, Japan
(22)RIKEN, Japan
(23)School of General Education, Shinshu University, Japan

Yangbajing Cosmic Ray Observatory

90˚522**E**, 30˚102**N**, 4,300 m a.s.l. (606g/cm^2)

Yangbajing,
Tibet, China
4300 m a.s.l. = 606 g/cm^2

Tibet Air Shower Array

Tibet III (37000 m^2)

Total 789 detectors
Mode Energy
~3 TeV
Angular Resolution
~0.9 deg @ 3 TeV
Trigger Rate
~1700 Hz

Research Purpose

Complementary to Air Cherenkov Telescopes
Wide-field-of-view（~2sr）high-duty cycle CR telescope

1. **3TeV~100TeV cosmic γ rays**
2. **3TeV ～100 PeV primary cosmic rays**

-> Origin, acceleration of cosmic rays

3. **The Sun's shadow in cosmic rays**
（Shielding effect on cosmic rays by the Sun)
-> Global structure of solar and interplanetary magnetic fields

Longitudinal development of AS

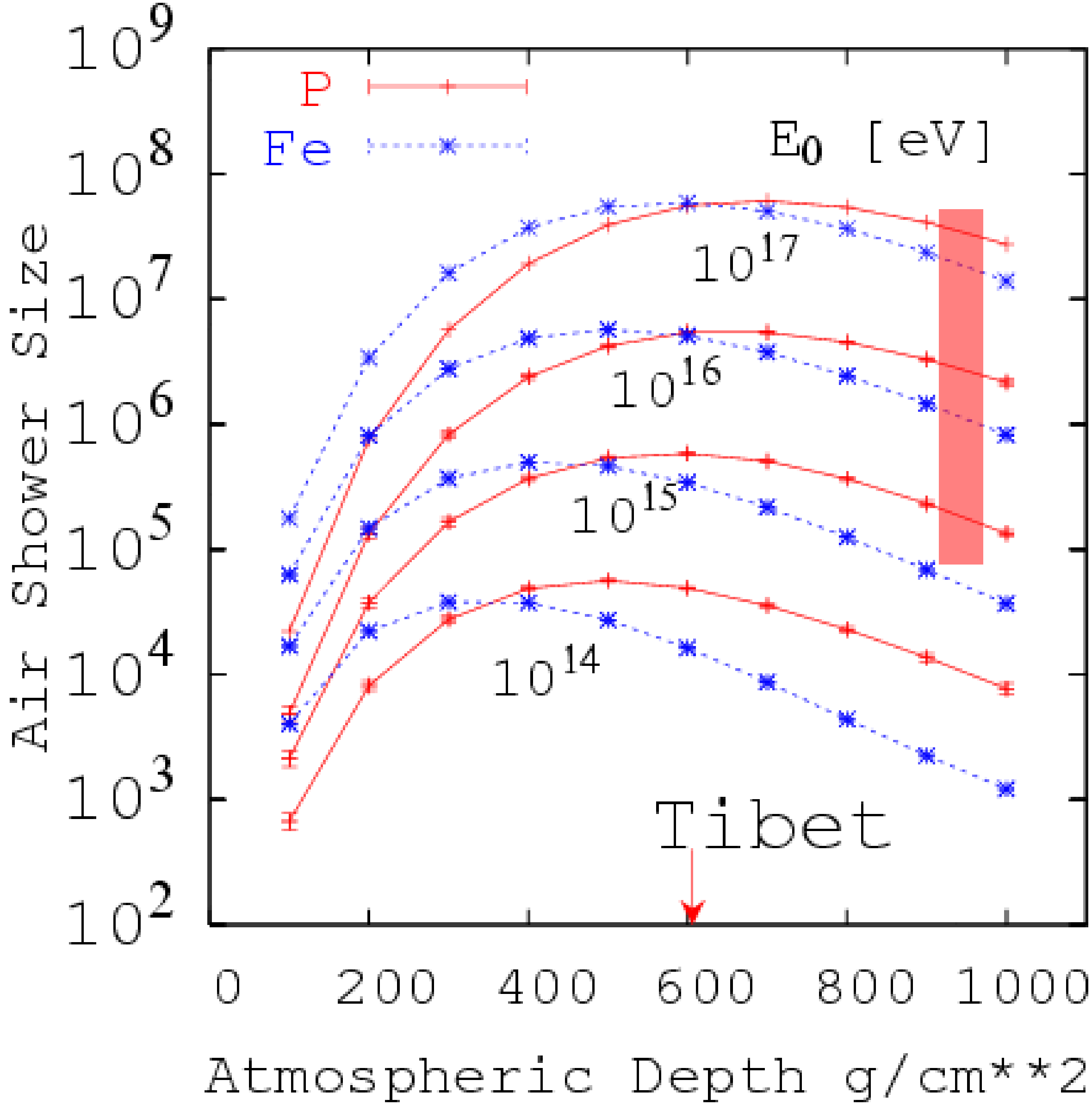

Why Tibet?

1. TeV CR/γ

   Attenuation

   @sea level

2. Good Energy determination in Knee

   (10^{15}-10^{16}eV)

   (p or Fe)

Tibet-III Air Shower (AS) Array

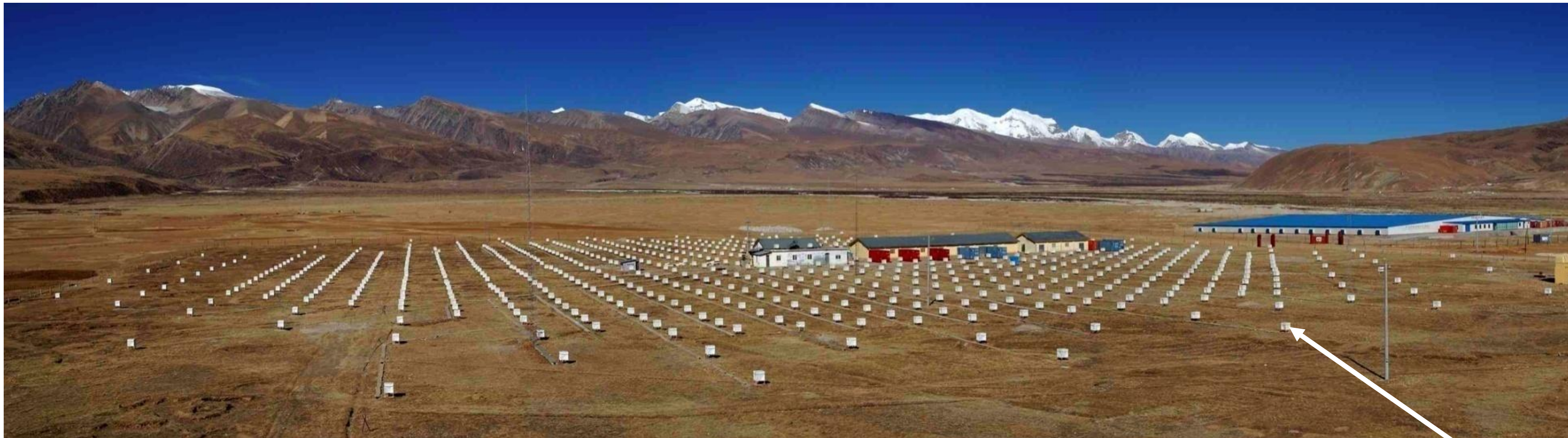

☐ Number of Scinti. Det.	0.5 m^2 x 789
☐ Effective Area for AS	~37,000 m^2
☐ Energy region	~TeV - 100 PeV
☐ Angular Resolution (Gamma rays)	~0.4 @10 TeV ~0.2 @100 TeV
☐ Energy Resolution (Gamma rays)	~70% @10 TeV ~40% @100TeV
☐ F.O.V.	~2 sr

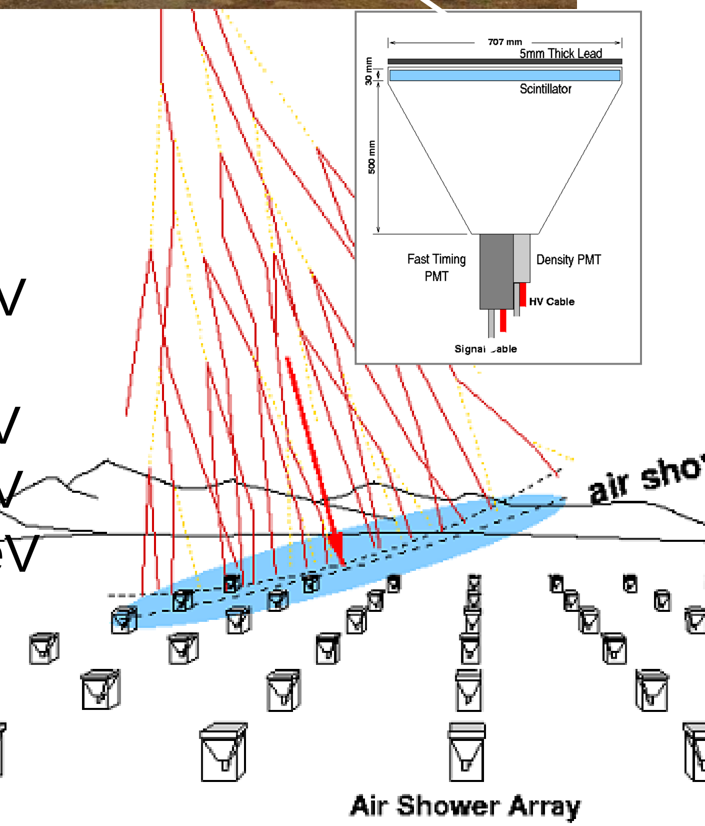

2nd particles Timing & Energy deposit

Detection Principle

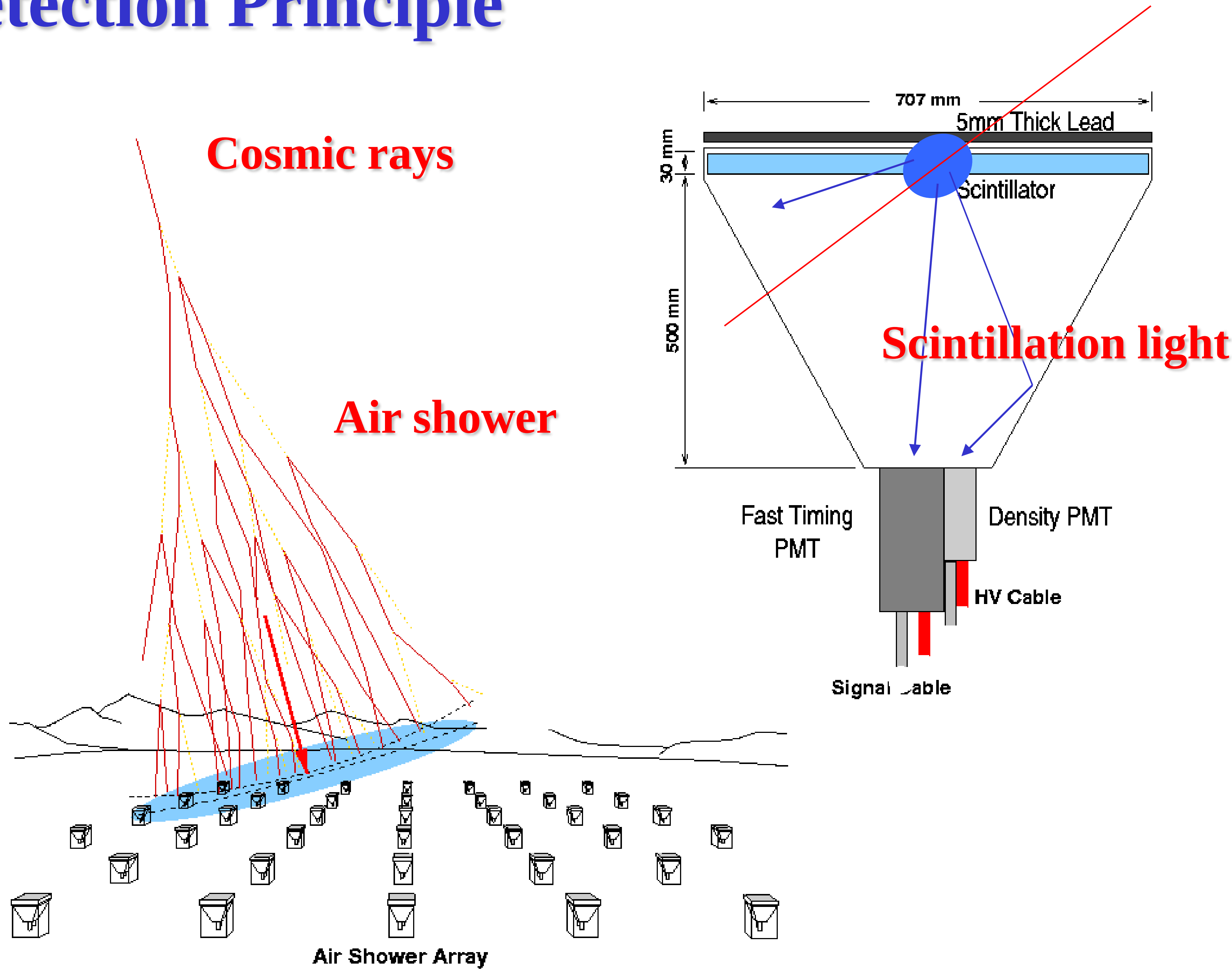

Air Shower Detection

2nd particle density → Cosmic ray energy

2nd particle timing → Cosmic ray direction

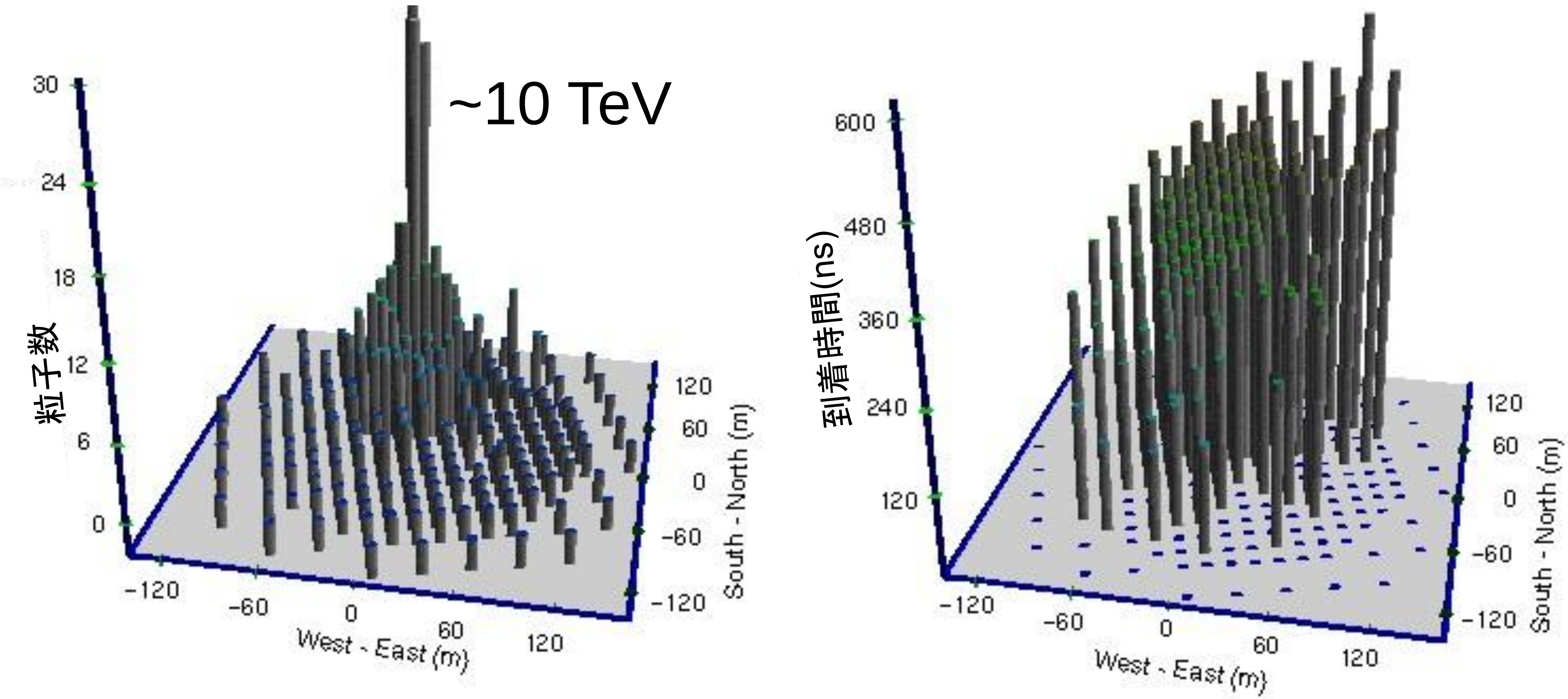

Air shower rate triggered by Tibet III ~1700Hz

Performance by Moon's Shadow

The Astrophysical Journal, 692, 61–72(2009)

- □Absolute Energy Scale
- □Angular Resolution
- □Pointing Accuracy

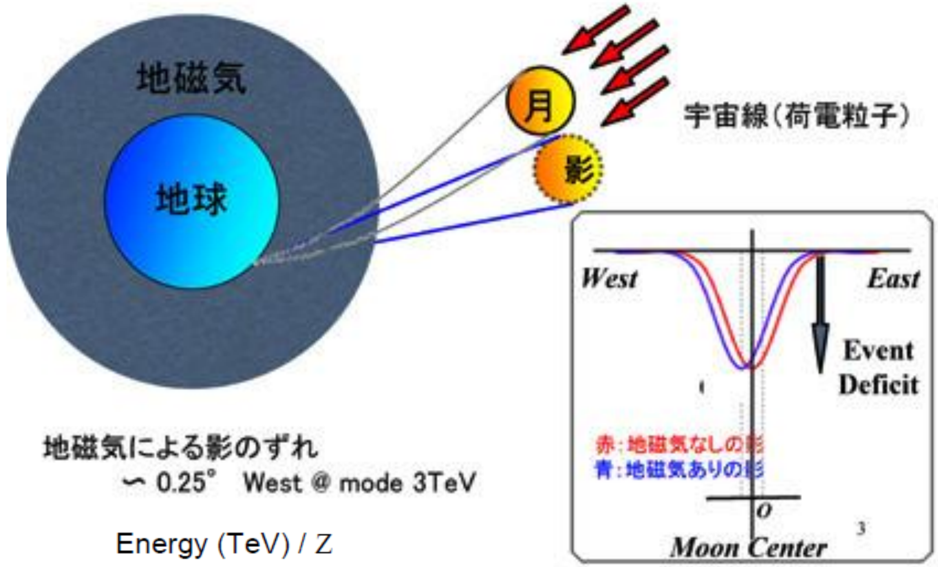

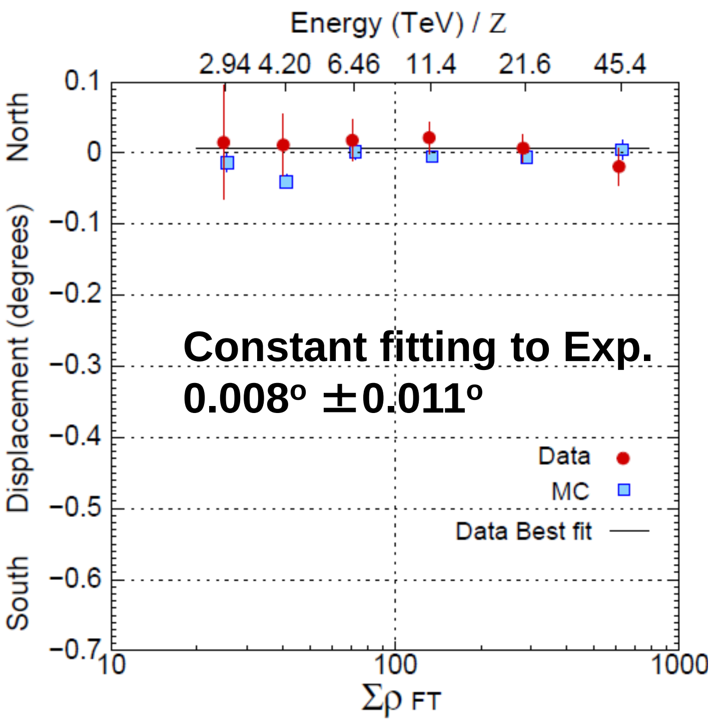

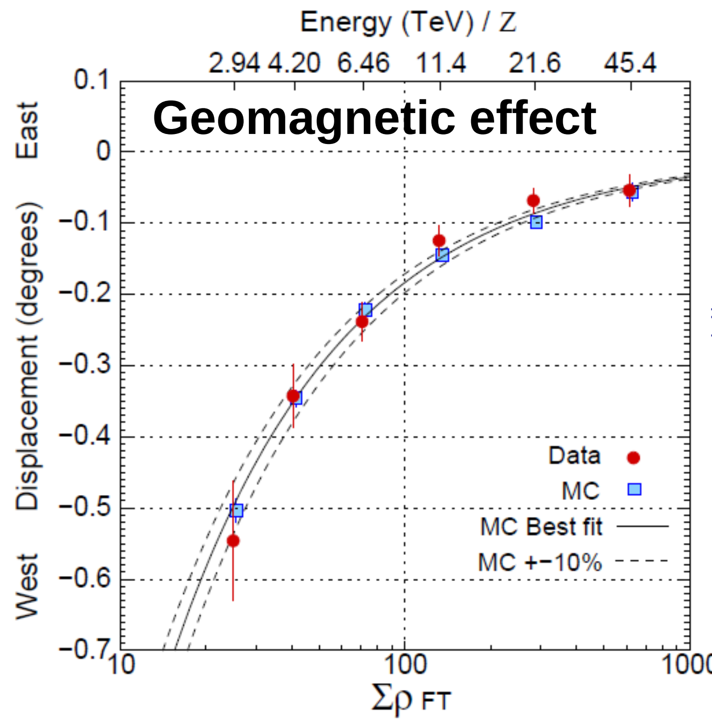

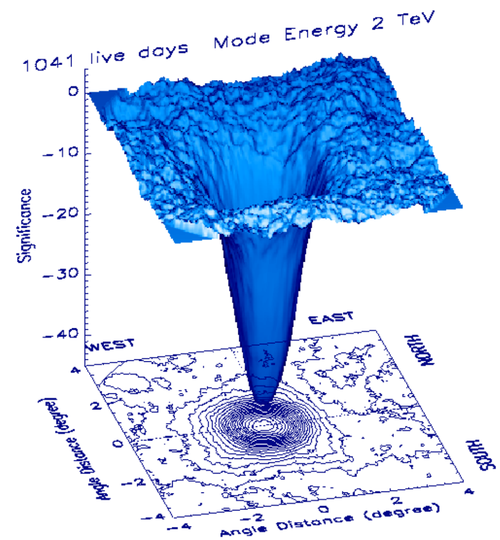

Pointing Error < 0.011°

Absotute Energy Scale Error < 12%
+4.5%(±8.6stat.±6.7syst.)%

Search for TeV anti-protons by the Moon's shadow

3TeV 40σ

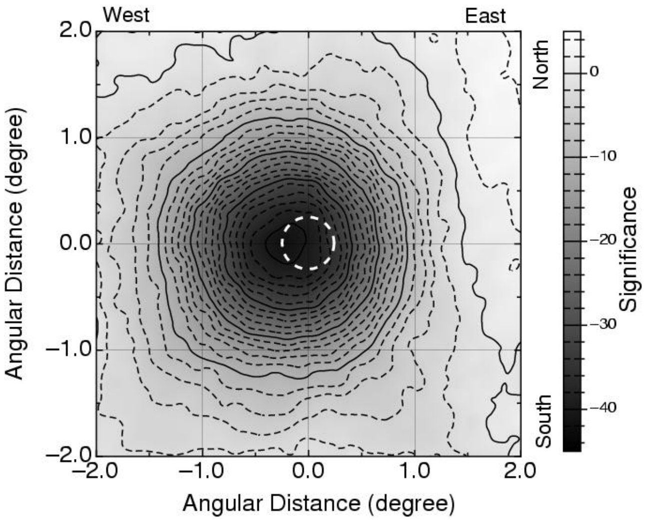

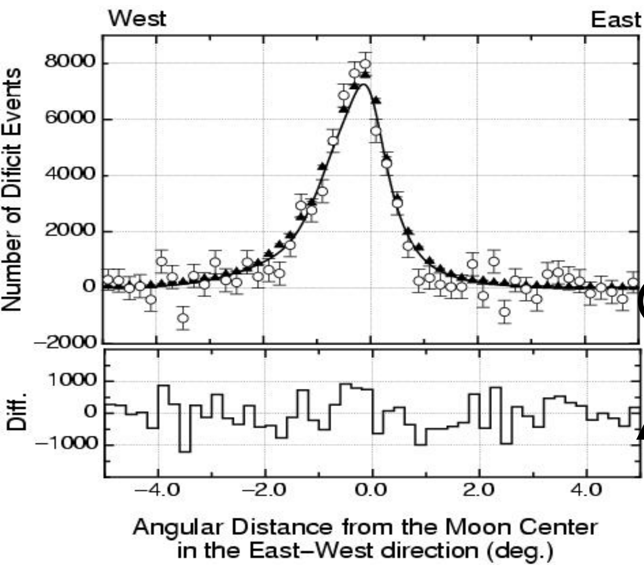

0.23°

Westward

○ :DATA

△ :MC

Amenomori et al.
Astroparticle Physics, 28, (2007) 137-142

Tibet III

7% of CR @90%C.L.

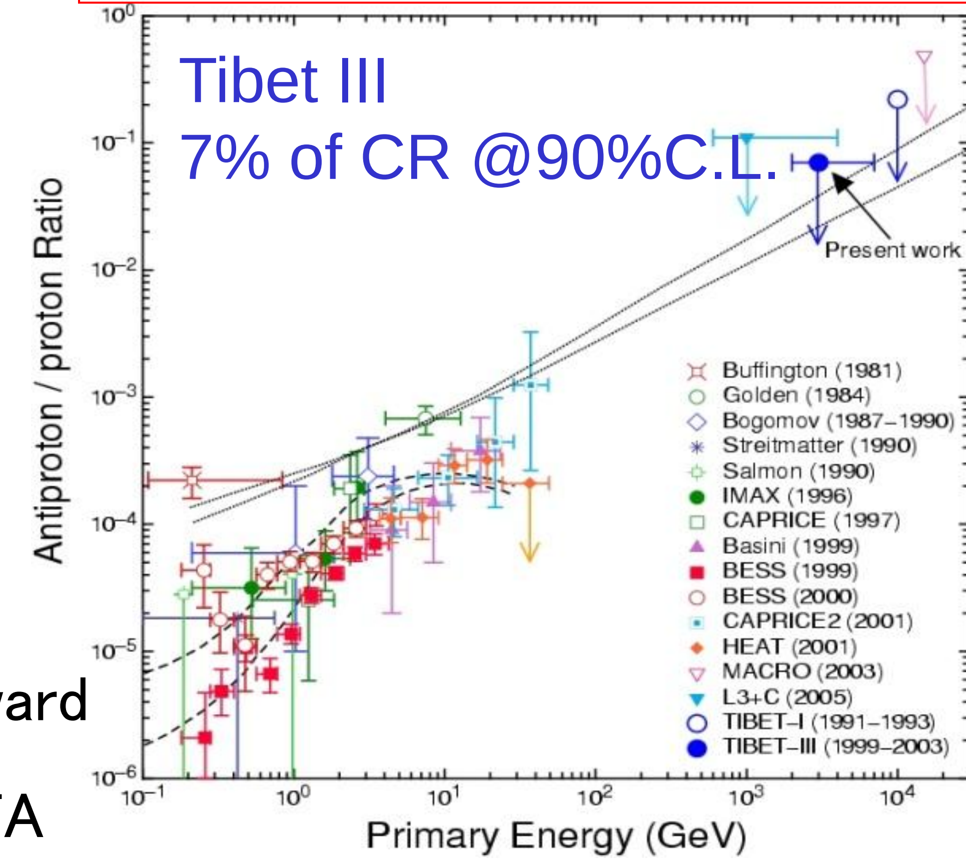

Dashed line: leaky box

M.Simon et al. ApJ 499 (1998)250.

Dotted line: extragalactic anti-matter model

S.A. Stephan et al. Space Sci. Rev. 46 (1987) 31.

2. γ-ray physics

Cosmic Ray Anisotropy at sidereal time frame (Tibet ASγ)

Anisotropy Map

Amenomori et al, Science, 314, 439 (2006)

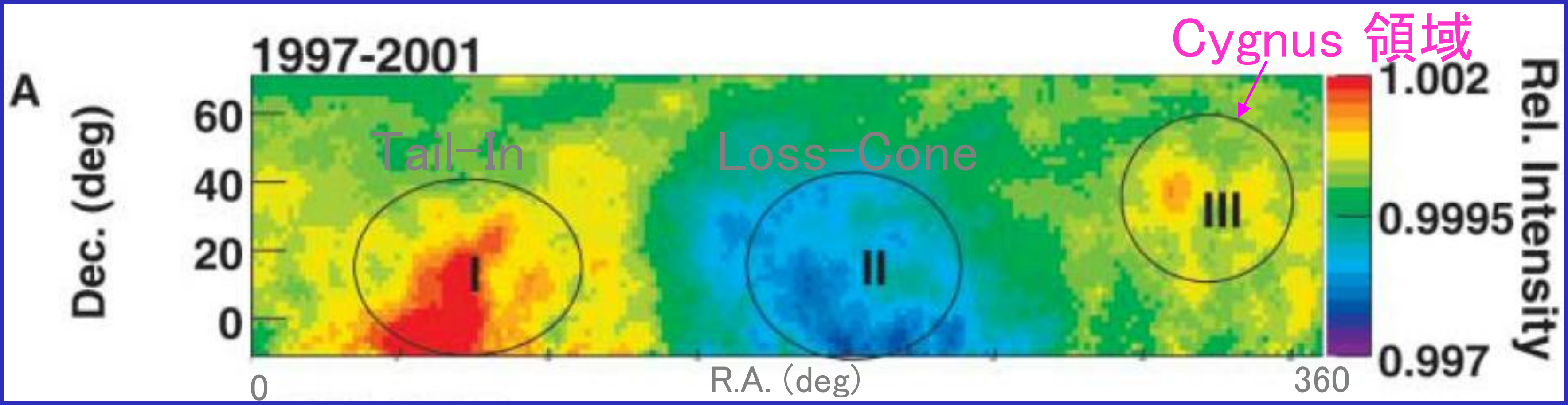

Cygnus Region

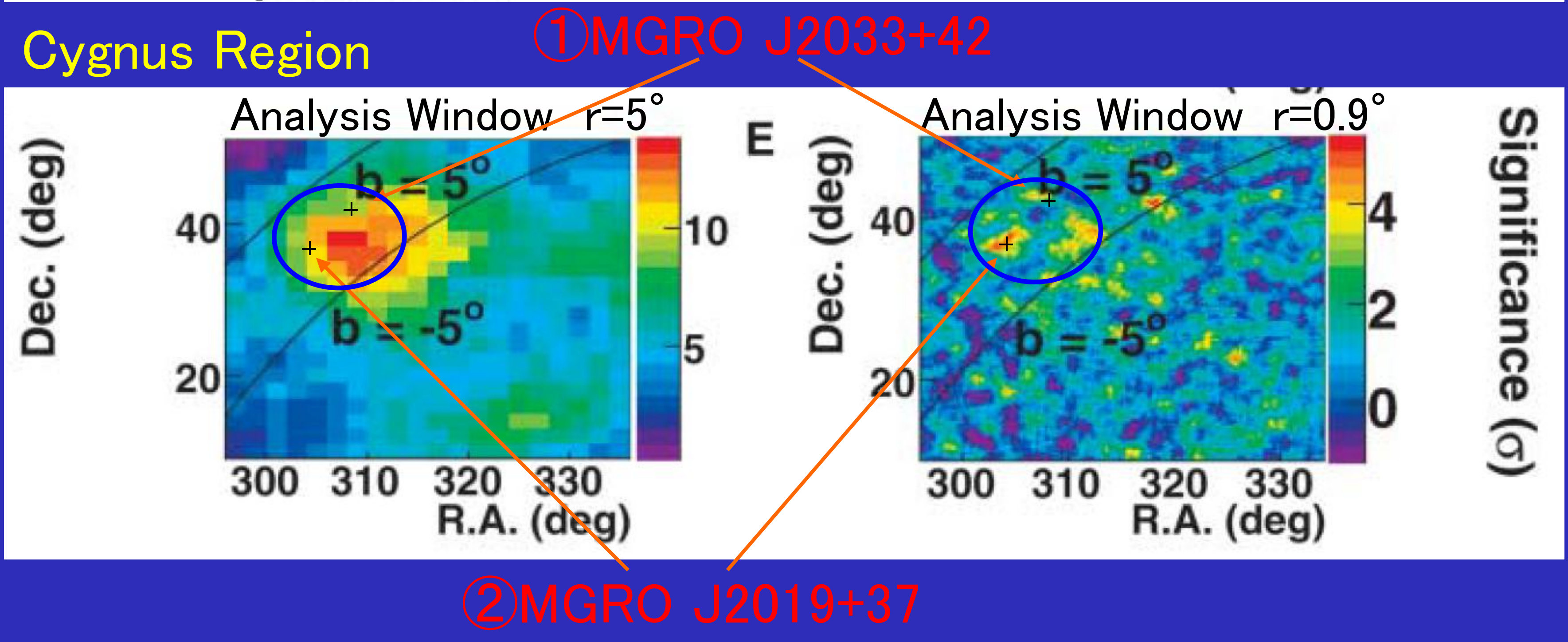

Cygnus領域 Milagro 全天サーベイ(2007年)

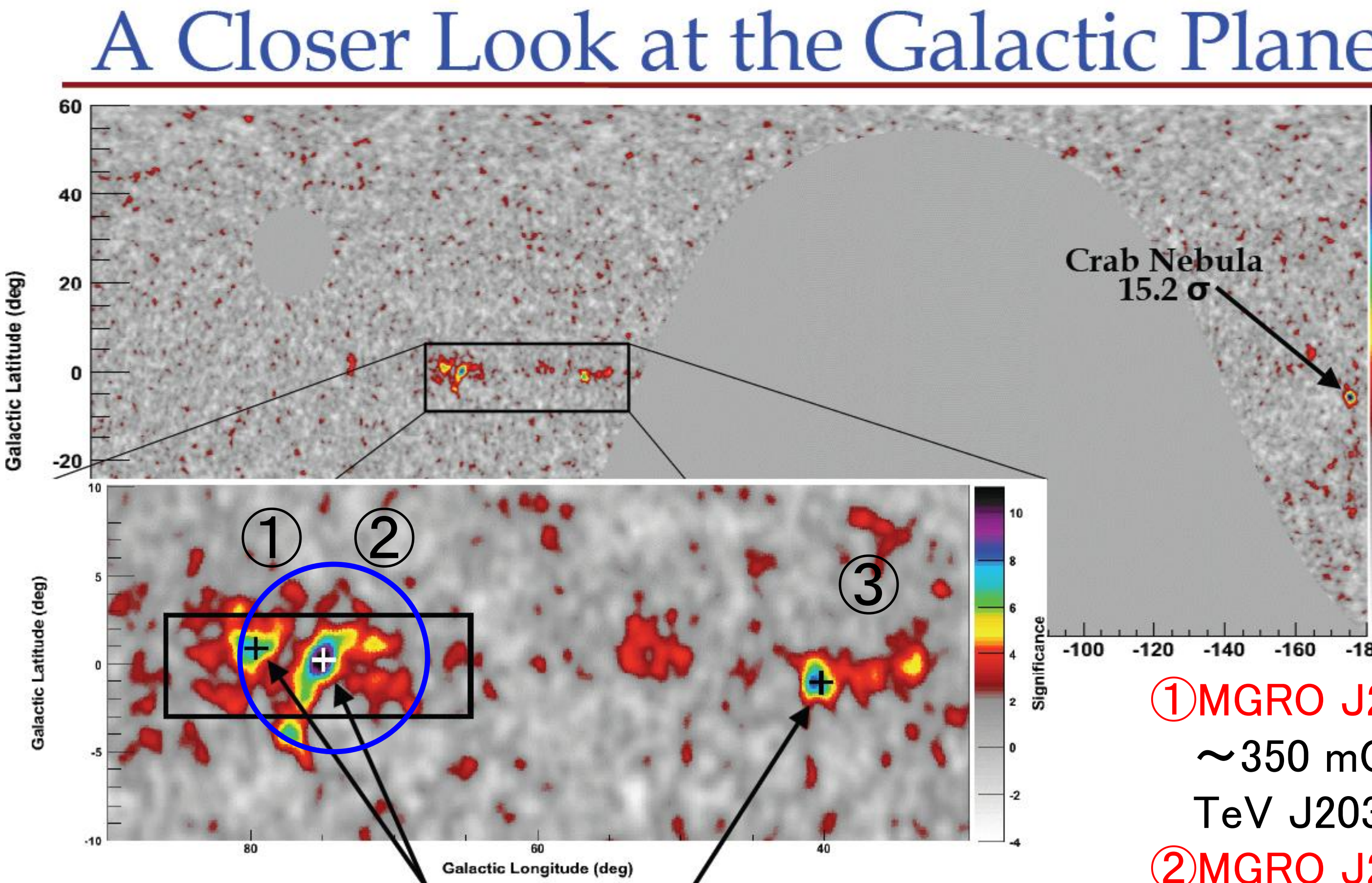

- Cygnus region shows two new TeV gamma-ray sources
- Diffuse emission from Cygnus region
- A new TeV source at low declinations

12TeV

①MGRO J2033+42
～350 mCrabs Diffuse
TeV J2032+4130?

②MGRO J2019+37
～500 mCrabs Diffuse

③MGRO J1909+06
～850 mCrabs Point-like?

First GLAST Symposium,
A. Abdo, "Discovery of TeV Gamma Ray Emission from the Cygnus Region with Milagro Using a New Background Rejection Technique"
http://glast.gsfc.nasa.gov/science/symposium/2007/thursday/7.3_Abdo.pdf

Observation of TeV Gamma Rays from the Fermi Bright Galactic Sources with the Tibet Air Shower Array (Amenomori et. al.)

ApJ 709(2010)L6-L10

(**arXiv:0912.0386**)

Introduction

Large Area Telescope(LAT)
on the Fermi Gamma-Ray
Space Telescope

Lanched in June 2008

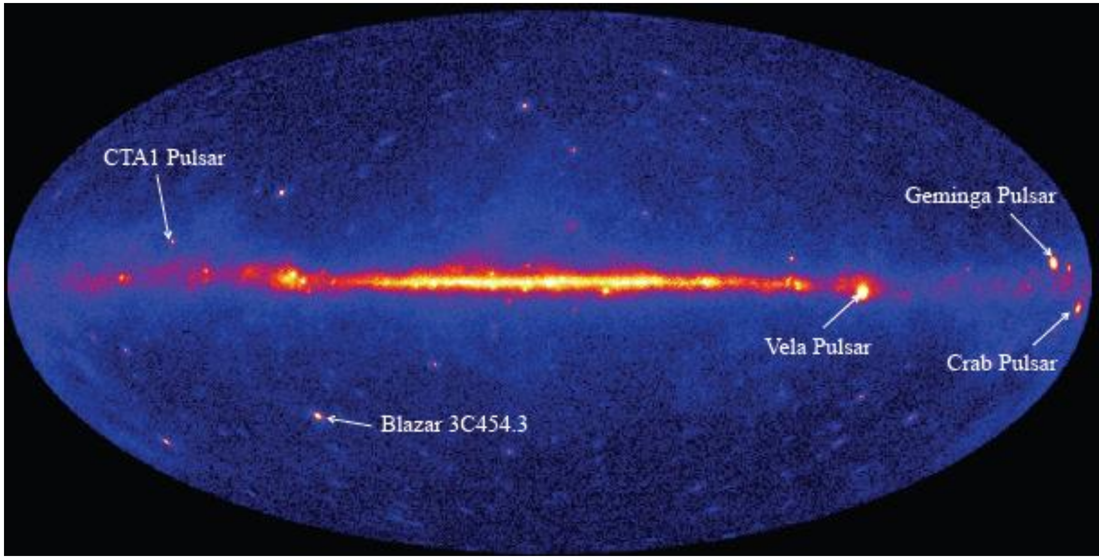

FERMI/LARGE AREA TELESCOPE BRIGHT GAMMA-RAY SOURCE LIST
Abdo, A. A. et al. 2009, ApJS, 183, 46 (July 2009, astrp-ph submitted in Feb. 2009)

Fermi LAT 3 month observation
>100MeV,
>10σ

205 most significant sources (120 extragalactic sourcs)
A typical 95% uncertainty radius of source position: 10′ ～ 20′

Milagro Observation of TeV Emission from Galactic Sources
In the Fermi Bright Source List *(Abdo, A. A. et al 2009, ApJ, 700, L127)*

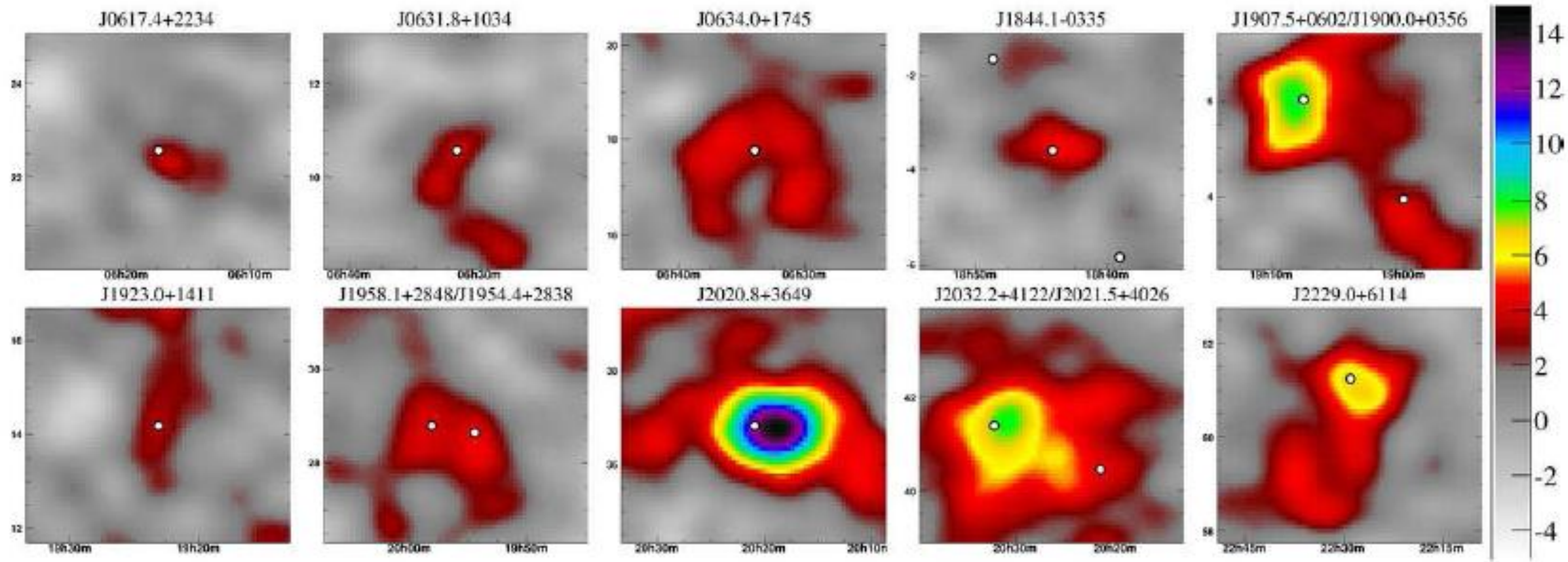

Fig. 1.— The 3σ sources from Table 1, omitting the Crab. Each frame shows a 5°x5° region with the LAT sources indicated by white dots. The data has been smoothed by a Gaussian of width varying between 0.4° and 1.0°, depending on the expected angular resolution of events. Horizontal axes show Right-Ascension and vertical axes show Declination. The colors indicate the statistical significance in standard deviations.

34 sources selected from 205 Fermi sources
(Not extragalactic & Dec.>-5.0°)

Eγ ∼ 35 TeV

PSR	16
HXB	1
SRN	5
UNID	12

Milagro Results

Name (0FGL)	type	RA (deg)	DEC (deg)	l (deg)	b (deg)	Flux ($\times 10^{-17}$ TeV^{-1} sec^{-1} cm^{-2})	Signif. (σ's)	TeV assoc.
J0007.4+7303	PSR	1.85	73.06	119.69	10.47	< 90.4	2.6	
J0030.3+0450	PSR	7.60	4.85	113.11	-57.62	< 20.9	-1.7	
J0240.3+6113	HXB	40.09	61.23	135.66	1.07	< 26.2	0.7	LSI +61 303
J0357.5+3205	PSR	59.39	32.08	162.71	-16.06	< 16.5	-0.1	
J0534.6+2201	PSR	83.65	22.02	184.56	-5.76	162.6 ± 9.4	17.2	Crab
J0613.9-0202	PSR	93.48	-2.05	210.47	-9.27	< 60.0	-0.0	
J0617.4+2234	SNR[a]	94.36	22.57	189.08	3.07	28.8 ± 9.5	3.0	IC443
J0631.8+1034	PSR	97.95	10.57	201.30	0.51	47.2 ± 12.9	3.7	
J0633.5+0634	PSR	98.39	6.58	205.04	-0.96	< 50.2	1.4	
J0634.0+1745	PSR	98.50	17.76	195.16	4.29	37.7 ± 10.7	3.5	MGRO C3 Geminga
J0643.2+0858		100.82	8.98	204.01	2.29	< 30.5	0.3	
J1653.4-0200		253.35	-2.01	16.55	24.96	< 51.0	-0.5	
J1830.3+0617		277.58	6.29	36.16	7.54	< 32.8	0.2	
J1836.2+5924	PSR	279.06	59.41	88.86	25.00	< 14.6	-0.9	
J1844.1-0335		281.04	-3.59	28.91	-0.02	148.4 ± 34.2	4.3	
J1848.6-0138		282.16	-1.64	31.15	-0.12	< 91.7	1.7	
J1855.9+0126	SNR[a]	283.99	1.44	34.72	-0.35	< 89.5	2.2	
J1900.0+0356		285.01	3.95	37.42	-0.11	70.7 ± 19.5	3.6	
J1907.5+0602	PSR	286.89	6.03	40.14	-0.82	116.7 ± 15.8	7.4	MGRO J1908+06 HESS J1908+063

14 sources were detected with >3σ

J1911.0+0905	SNR[a]	287.76	9.09	43.25	-0.18	< 41.7	1.5	
J1923.0+1411	SNR[a]	290.77	14.19	49.13	-0.40	39.4 ± 11.5	3.4	HESS J1923+141
J1953.2+3249	PSR	298.32	32.82	68.75	2.73	< 17.0	0.0	
J1954.4+2838	SNR[a]	298.61	28.65	65.30	0.38	37.1 ± 8.6	4.3	
J1958.1+2848	PSR	299.53	28.80	65.85	-0.23	34.7 ± 8.6	4.0	
J2001.0+4352		300.27	43.87	79.05	7.12	< 12.1	-0.9	
J2020.8+3649	PSR	305.22	36.83	75.18	0.13	108.3 ± 8.7	12.4	MGRO J2019+37
J2021.5+4026	PSR	305.40	40.44	78.23	2.07	35.8 ± 8.5	4.2	
J2027.5+3334		306.88	33.57	73.30	-2.85	< 16.0	-0.2	
J2032.2+4122	PSR	308.06	41.38	80.16	0.98	63.3 ± 8.3	7.6	TEV 2032+41 MGRO J2031+41
J2055.5+2540		313.89	25.67	70.66	-12.47	< 17.6	-0.0	
J2110.8+4608		317.70	46.14	88.26	-1.35	< 24.1	1.1	
J2214.8+3002		333.70	30.05	86.91	-21.66	< 20.7	0.6	
J2229.0+6114	PSR	337.26	61.24	106.64	2.96	70.9 ± 10.8	6.6	MGRO C4
J2302.9+4443		345.75	44.72	103.44	-14.00	< 13.2	-0.6	

Tibet-III Data Analysis

All-sky Data by the Tibet-III Array (Phase 1-9 Ver.B4)

$\Sigma\rho_{FT} > 10^{1.25}$ && zenith $<40^o$
Inout && 1.25p Any4 && Residual Error <1.0m
Search Window Size: $R_s(\Sigma\rho_{FT}) = 6.9 / \sqrt{\Sigma\rho_{FT}}$ (Variable)

1999 Nov – 2008 Dec
1915.5 live days

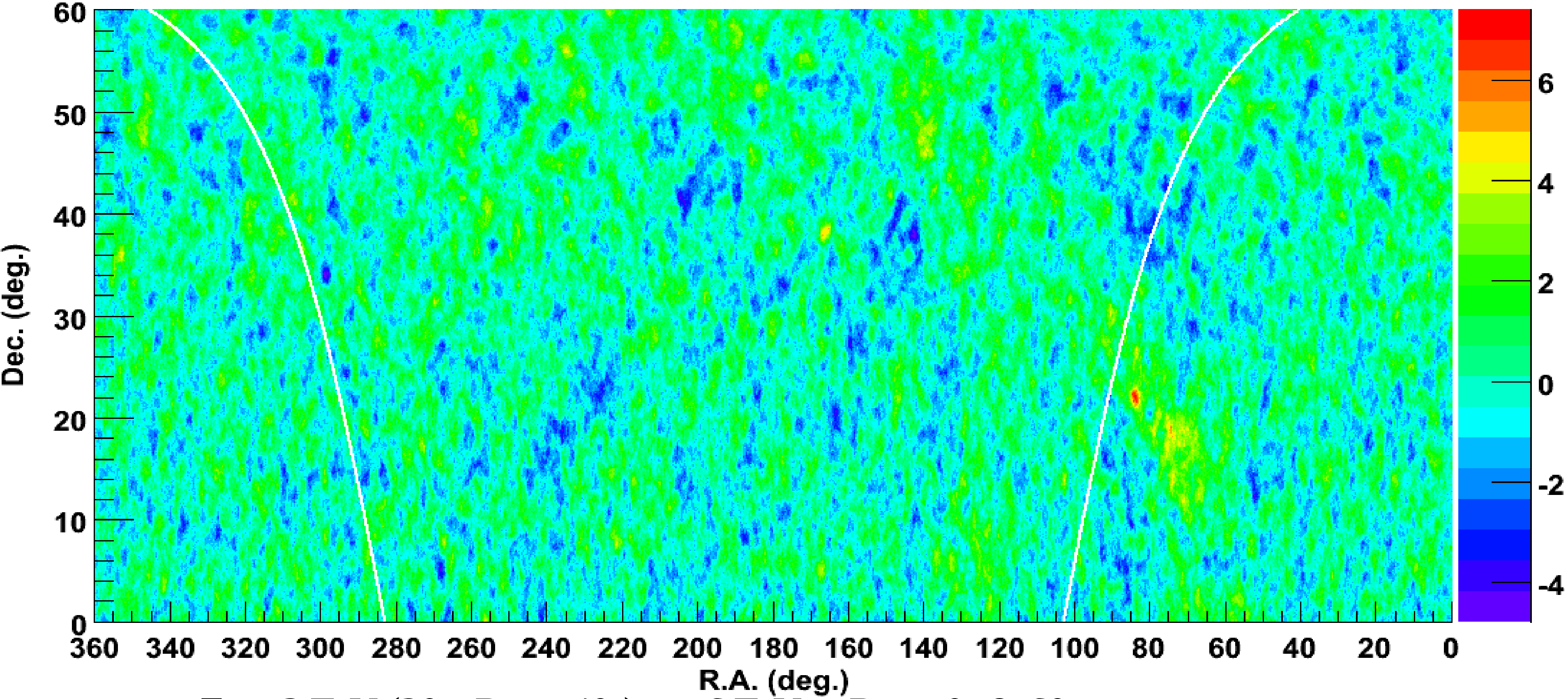

$E\gamma \sim 3$ TeV (20^o<Dec.<40^o), ~ 6 TeV at Dec.=0^o & 60^o

Target sources in the Fermi Bright Source List

The Fermi Bright Source List: 205 sources

Not identified as extragalactic: 85 sources

0^o < Declination < 60^o 27 sources

Pulsar (PSR)	13
Supernova remnant (SNR)	5
Unidentified	9

Table 1
Summary of the Tibet-III Array Observations of the *Fermi* Sources

Fermi LAT Source (0FGL)	Class	R.A. (deg)	Decl. (deg)	Tibet-III Signi. (σ)	Milagro[a] Signi. (σ)	Source Associations
J0030.3+0450	PSR	7.600	4.848	1.7	−1.7	
J0357.5+3205	PSR[b]	59.388	32.084	−1.7	−0.1	
J0534.6+2201	PSR	83.653	22.022	6.9	17.2	Crab
J0617.4+2234	SNR	94.356	22.568	0.2	3.0	IC 443
J0631.8+1034	PSR	97.955	10.570	0.3	3.7	
J0633.5+0634	PSR[b]	98.387	6.578	2.4	1.4	
J0634.0+1745	PSR	98.503	17.760	2.2	3.5	Geminga
J0643.2+0858		100.823	8.983	−1.2	0.3	
J1830.3+0617		277.583	6.287	−0.2	0.2	
J1836.2+5924	PSR[b]	279.056	59.406	−0.3	−0.9	
J1855.9+0126	SNR	283.985	1.435	0.7	2.2	W44
J1900.0+0356		285.009	3.946	1.0	3.6	
J1907.5+0602	PSR[b]	286.894	6.034	2.4	7.4	MGRO J1908+06 HESS J1908+063
J1911.0+0905	SNR	287.761	9.087	1.7	1.5	G43.3 − 0.2
J1923.0+1411	SNR	290.768	14.191	−0.3	3.4	W51 HESS J1923+141

Geminga

Tibet-III 2σ
∼0.3 Crabs

Table 1
Summary of the Tibet-III Array Observations of the *Fermi* Sources

Tibet-III 2σ〜0.3 Crabs

Fermi LAT Source (0FGL)	Class	R.A. (deg)	Decl. (deg)	Tibet-III Signi. (σ)	Milagro[a] Signi. (σ)	Source Associations
J1953.2+3249	PSR	298.325	32.818	−0.0	0.0	
J1954.4+2838	SNR	298.614	28.649	0.6	4.3	G65.1+0.6
J1958.1+2848	PSR[b]	299.531	28.803	0.1	4.0	
J2001.0+4352		300.272	43.871	−0.5	−0.9	
J2020.8+3649	PSR	305.223	36.830	2.2	12.4	MGRO J2019+37
J2021.5+4026	PSR[b]	305.398	40.439	2.2	4.2	
J2027.5+3334		306.882	33.574	−0.3	−0.2	
J2032.2+4122	PSR[b]	308.058	41.376	2.4	7.6	TeV J2032+4130 MGRO J2031+41
J2055.5+2540		313.895	25.673	−0.0	−0.0	
J2110.8+4608		317.702	46.137	0.3	1.1	
J2214.8+3002		333.705	30.049	−1.0	0.6	
J2302.9+4443		345.746	44.723	−0.0	−0.6	
LAT PSR J2238+59[c]	PSR[b]	339.561	59.080	2.5	4.7	

Cygnus region

New Fermi-LAT Pulsar, Not included in analysis

All 7 sources >2σ are associated with pulsars. →PWNs?

Six of them are coincident with Milagro sources.

Remaing one have still positive significance 1.4σ by Milagro.

Statistics

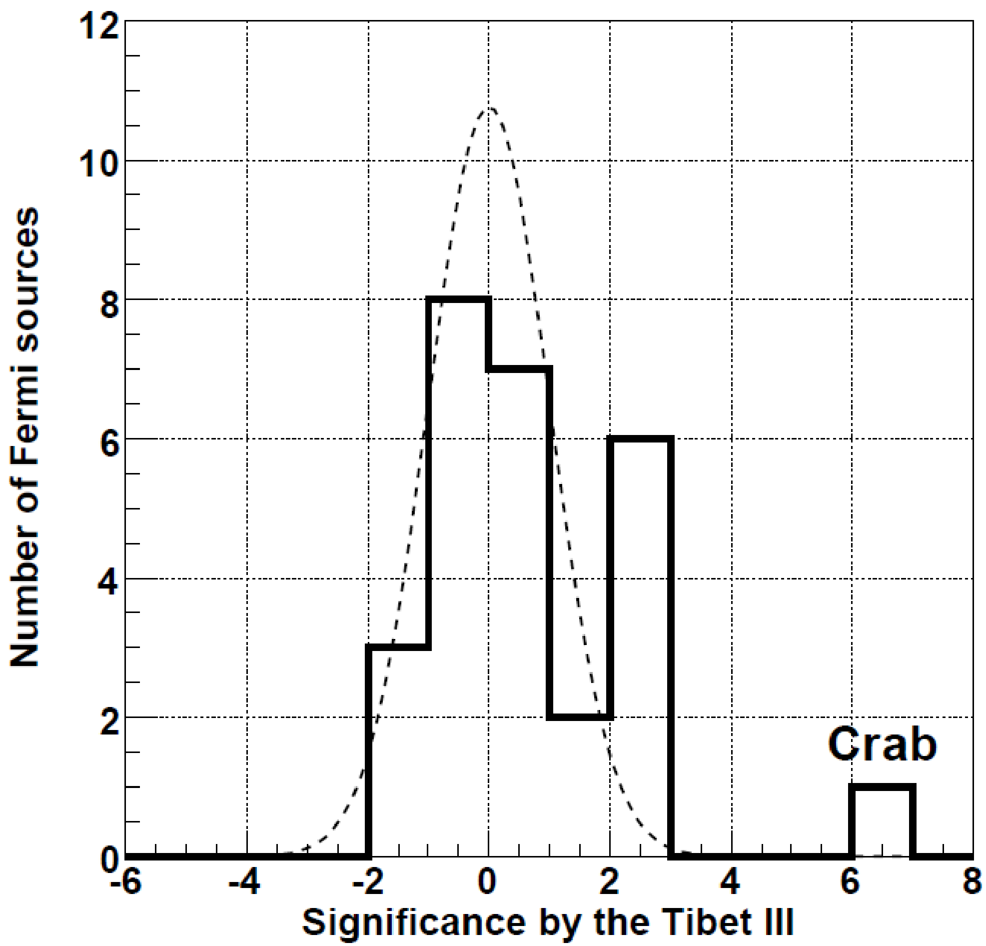

Total: 27 sources

>2σ: 7 sources

Fig. 1.— Histograms show significance distribution of the *Fermi* bright sources observed by the Tibet-III array. The dashed curve indicates the expected normal Gaussian distribution.

Chance Probability

Expected number of sources >2σ
27 × 0.02275 (2σ Upper prob.) = 0.61

Upper probabiriy for 7 events against λ=0.61
assuming Poisson statistics

$$p(A=7)=1-\sum_{k=0}^{A-1}\frac{e^{-\lambda}\lambda^{k}}{k!}$$

$$= 3.8 \times 10^{-6} \sim 4.5\sigma$$

Without Crab
λ = 26 × 0.02275 (2σ Upper prob.) = 0.59
P(A=6) = 3.6 × 10^{-5} ∼ 4σ

Flux consistency between the Tibet-III and the Milagro

	Tibet σ	Milagro σ	Expected σ from Milagro
J0534.6+2201	6.9	17.2	-
J0633.5+0634	2.4	1.4	0.56
J0634.0+1745	2.2	3.5	1.40
J1907.5+0602	2.4	7.4	2.97
J2020.8+3649	2.2	12.4	4.97
J2021.5+4026	2.2	4.2	1.68
J2032.2+4122	2.4	7.6	3.05

Underestimated?

J2020.8+3649 flux:

Tibet-III (30±14)% of the Crab flux above 3 TeV

Milagro (67±7)% of the Crab flux above 35 TeV

$\Delta = 2.3\sigma$

difference between them is calculated to be 2.3σ. It can be interpreted by either statistical fluctuation, harder energy spectrum than the Crab, or an extended source instead of the assumed point-like source in this analysis.

Tibet-III

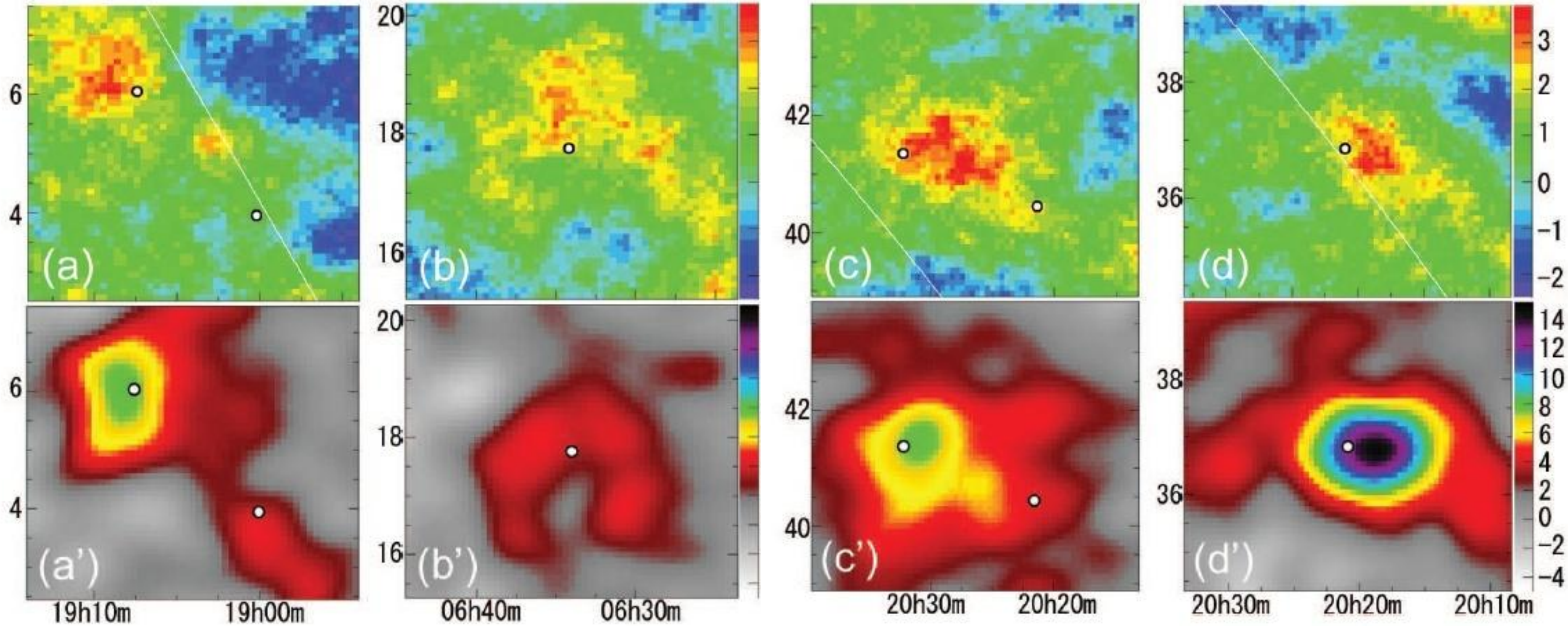

Milagro

Fig. 2.— Comparisons of significance maps around the *Fermi* sources between the Tibet-III array (a)–(d) and the Milagro experiment (a’)–(d’) taken from Abdo et al. (2009c). Selected are *Fermi* sources with $\geq 2\sigma$ significance by the Tibet-III array and $\geq 3\sigma$ by the Milagro experiment except for the Crab. White points in each image show the *Fermi* source positions: (a)(a’) J1907.5+0602/J1900.0+0356; (b)(b’) J0634.0+1745 (Geminga); (c)(c’) J2021.5+4026/J2032.2+4122; (d)(d’) J2020.8+3649. The horizontal axis, vertical axis, and color contours indicate the right ascension, declination, and significance, respectively.

3. Knee Physics

TIBET Hybrid Experiment

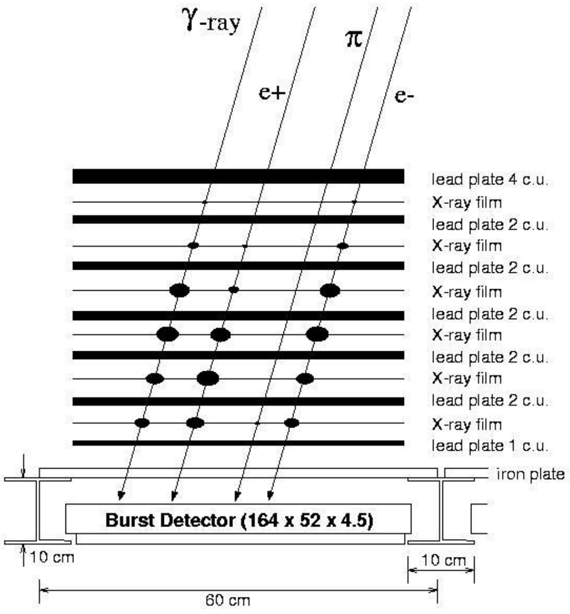

How to obtain proton spectrum?

Hybrid system

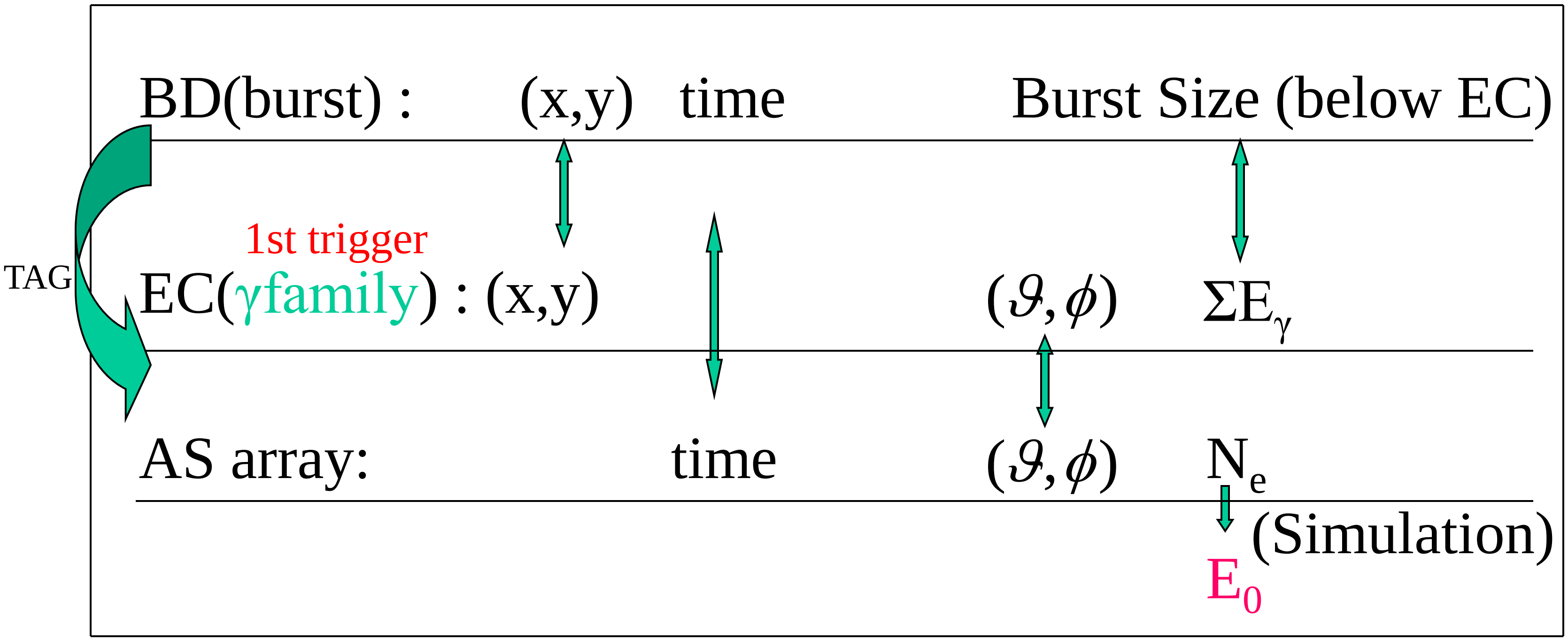

EC-Xray film image → Scanner (GUI Software) → family detection

AS+family matching event → ANN (Correlations) → Proton Identification ~100 eV/699 days

Artificial Neural Network

JETNET 3.5

Parameters for training: N_γ, ΣE_γ, $\langle R_\gamma \rangle$, $\langle ER_\gamma \rangle$, N_e, θ

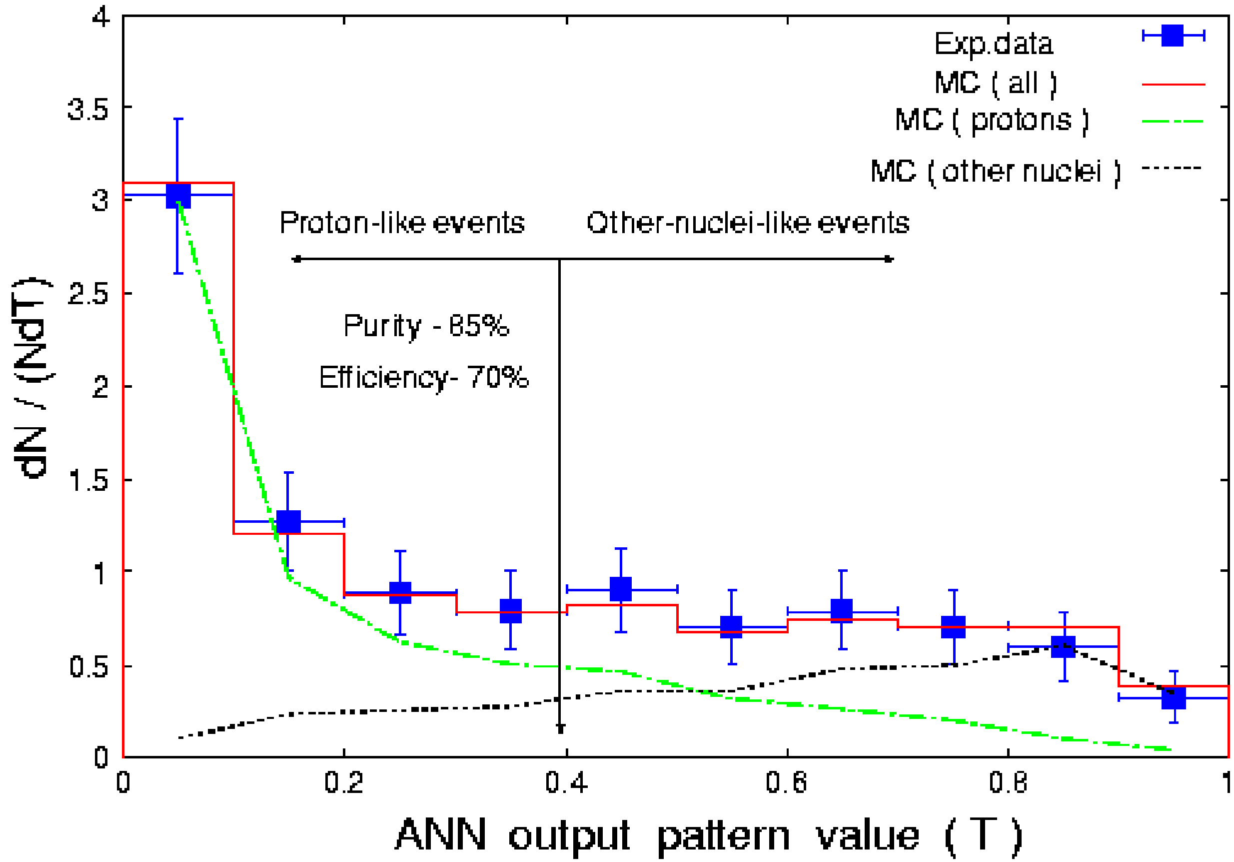

Primary proton spectrum

(a) (by QGSJET model)

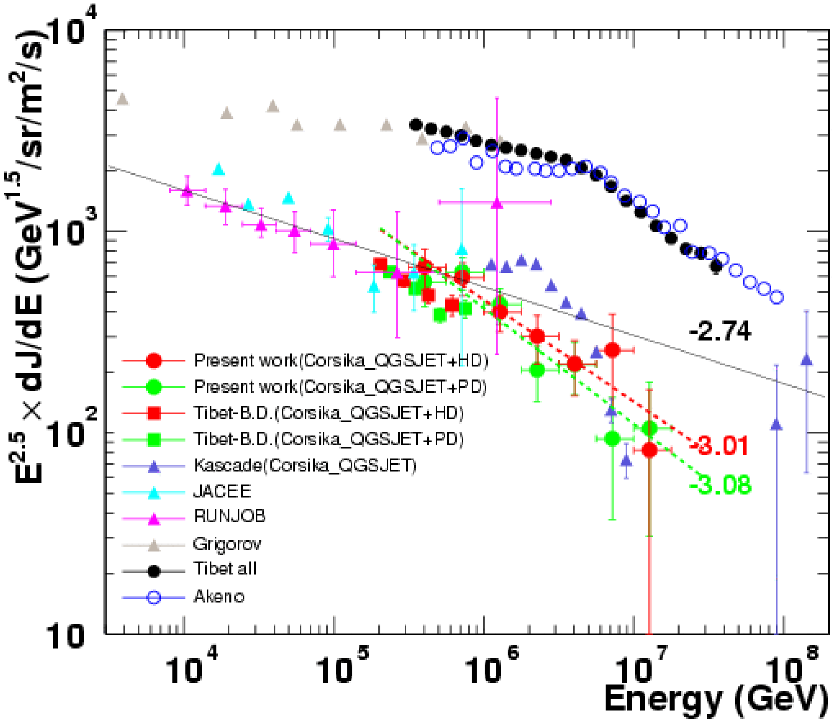

(b) (by SIBYLL model)

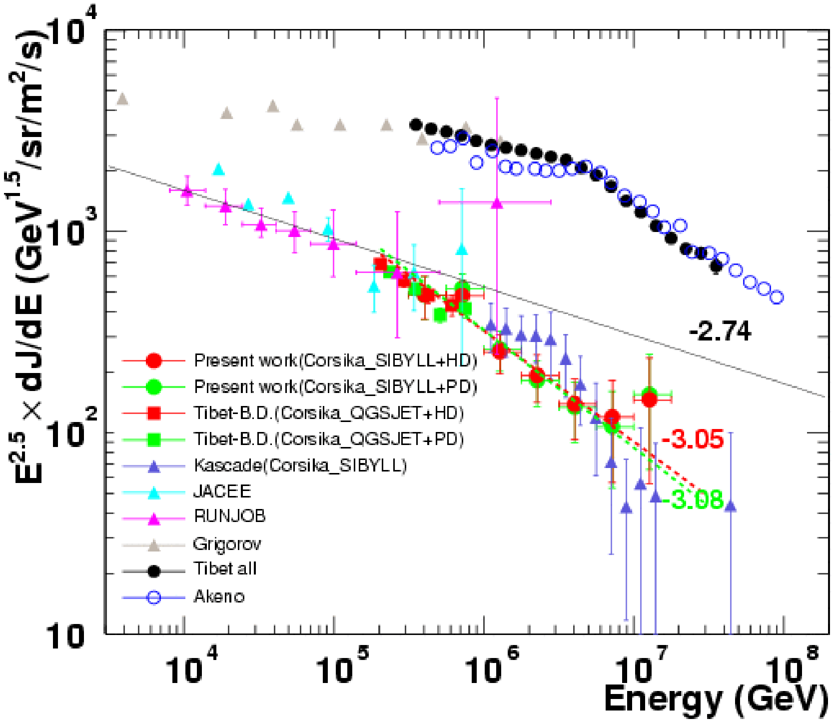

(KASCADE data: astro-ph/0312295)

Primary helium spectrum

(a) (by QGSJET model)

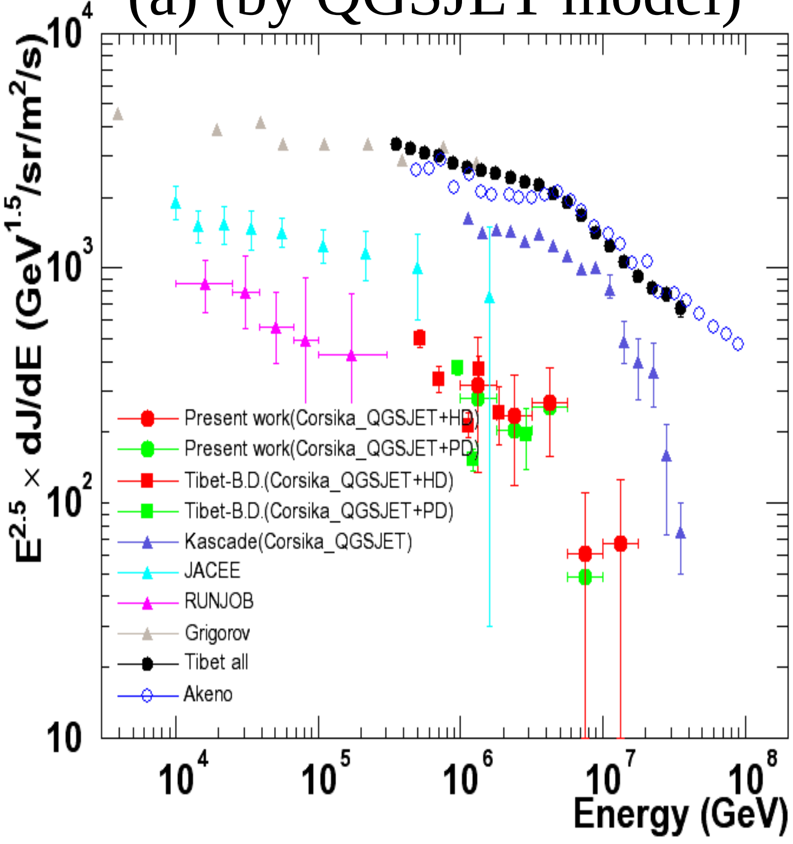

(b) (by SIBYLL model)

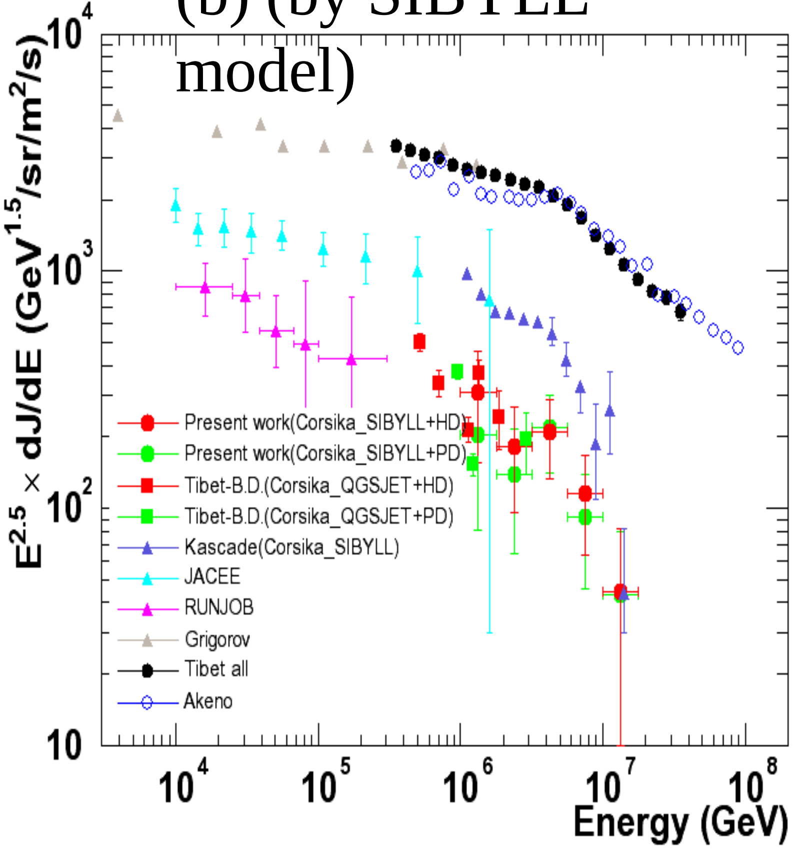

p+helium selection: purity=93%, efficiency=70%

Primary Cosmic Ray Energy Spectrum

CORSIKA_QGSJET

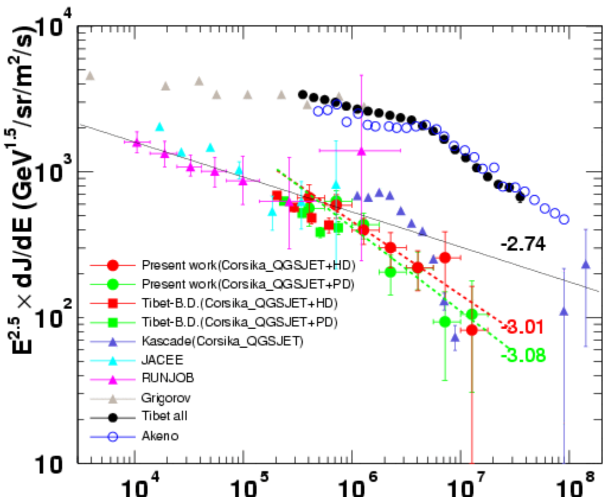

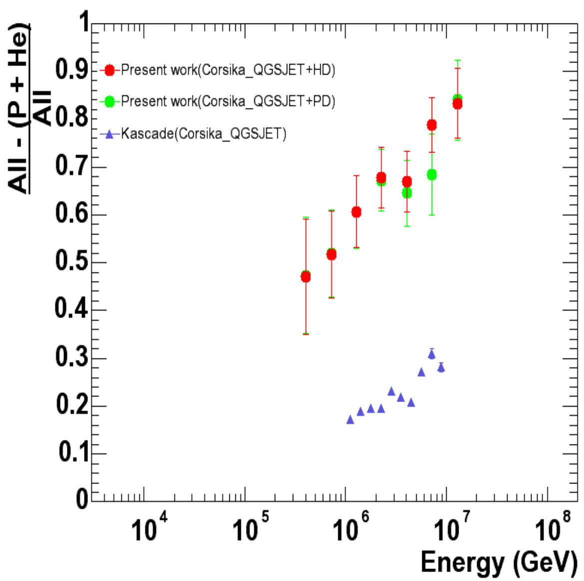

CORSIKA_SIBYLL

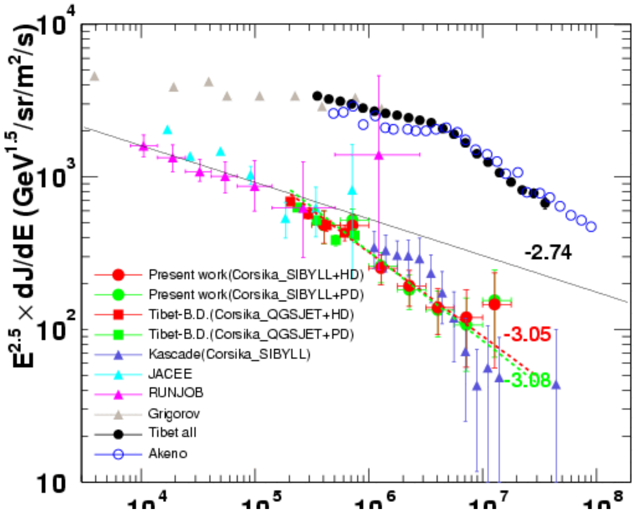

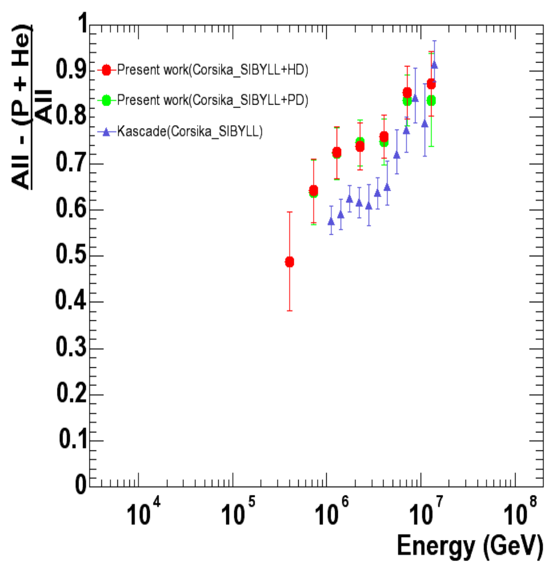

Proton

Small model dependence

(30 %)

$$\frac{\text{All} - (\text{p+He})}{\text{All}}$$

PL B632 (2006) 58-64

All Particle Energy Spectrum in the Knee region

10^{14}eV ～ 10^{17}eV (3 orders)

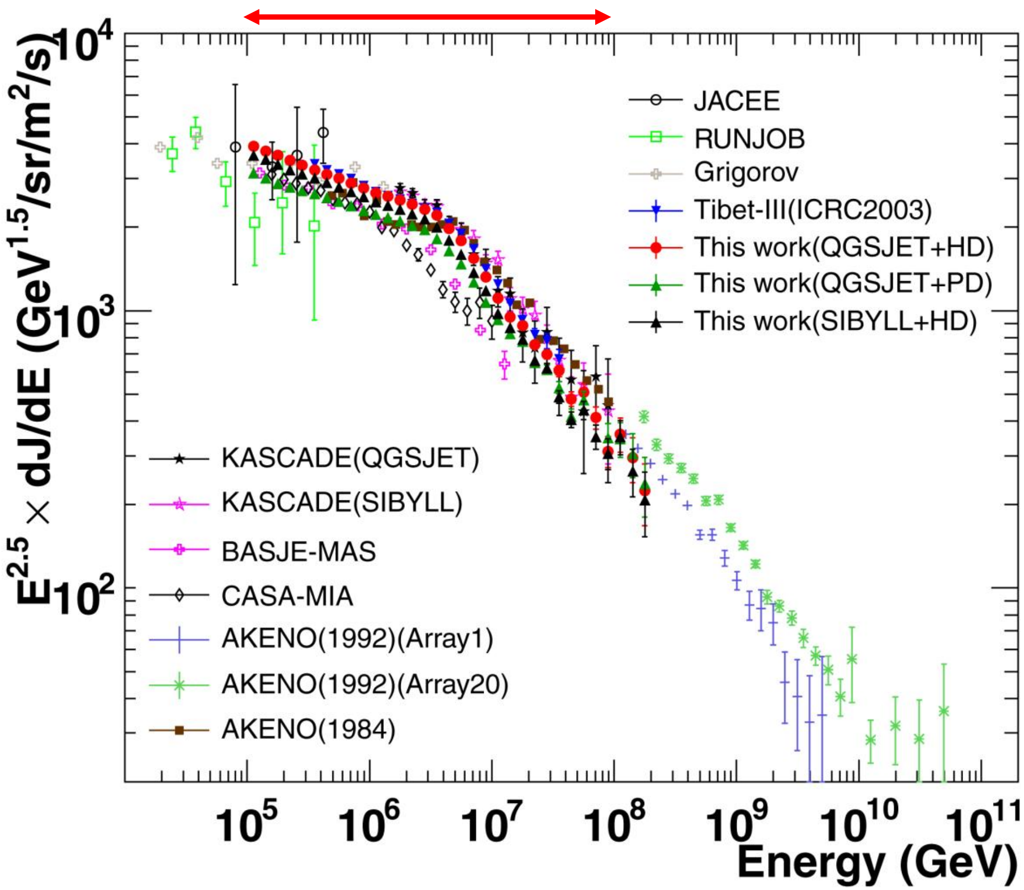

Amenomori *et al.*,
ApJ, **678**, 1165 (2008)

Model	Index of spectrum	Energy range (eV)
QGSJET +HD	−2.67±0.01	< 10^{15} eV
	−3.10±0.01	> 4×10^{15} eV
QGSJET +PD	−2.65±0.01	< 10^{15} eV
	−3.08±0.01	> 4×10^{15} eV
SIBYLL +HD	−2.67±0.01	< 10^{15} eV
	−3.12±0.01	> 4×10^{15} eV

Multiple source model

(Slide from M.Shibata,Y.N.U.)

Cutoff spectrum is written as

$$\frac{dj(E,\varepsilon)}{dE} = j_0 E^{-\gamma} \exp(-\frac{E}{\varepsilon}).$$

Distribution of sources with acceleration limit ε is assumed as,

$$S(x) = \frac{1}{\Gamma(\Delta\gamma)} \frac{1}{x^{1+\Delta\gamma}} \exp(-\frac{1}{x})$$

where $x = \varepsilon/\varepsilon_m$, ε_m is the minimum value of the acceleration limit. $S(x)$ is normalized as

$$\int_0^\infty S(x)dx = 1.$$

Then, superposition of the multiple sources gives following formula for cosmic-ray energy spectrum.

$$\frac{dJ}{dE} = \int_0^\infty \frac{dj(E,\varepsilon)}{dE} S(\frac{\varepsilon}{\varepsilon_m}) \frac{d\varepsilon}{\varepsilon_m} = \frac{j_0 E^{-\gamma}}{(1+E/\varepsilon_m)^{\Delta\gamma}}$$

$$\boldsymbol{\varepsilon_m \equiv \varepsilon_b}$$

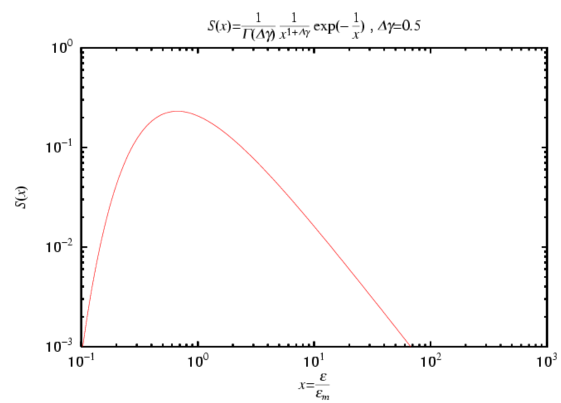

Distribution of acceleration power of cosmic rays

Proton Spectrum

Direct measurement and Tibet combined

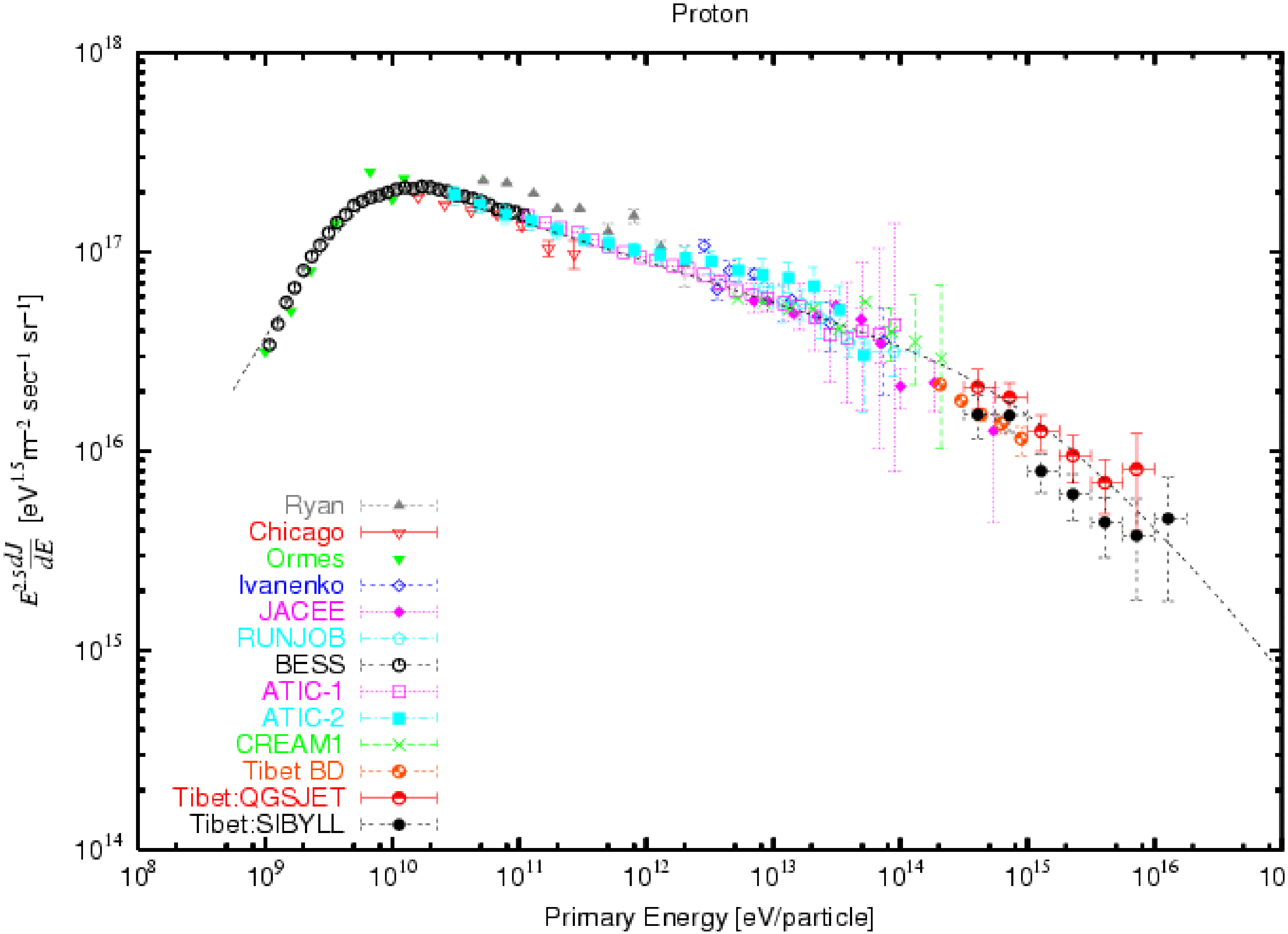

(Slide from M.Shibata,Y.N.U.)

Broken power law formula to describe proton spectrum

$$\frac{dj}{dE} = j_0 E^{-\gamma}[1+\frac{E}{\varepsilon_b}]^{-\Delta\gamma}$$

ε_b : break point (7×10^{14} eV for proton)
$\Delta\gamma$: difference of power index before and after the break point
（$\Delta\gamma$ ＝0.4）

(Slide from M.Shibata, Y.N.U.)

All particle spectrum around the knee

(Slide from M.Shibata, Y.N.U.)

CASA/MIA HEGRA KASCADE

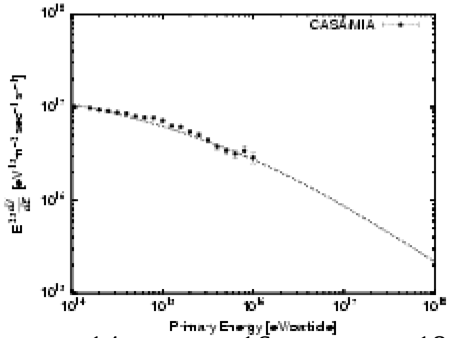

10^{14} 10^{16} 10^{18}

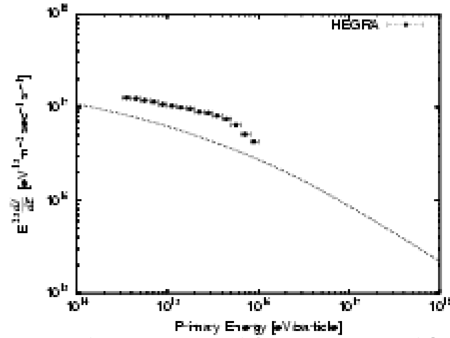

10^{14} 10^{16} 10^{18}

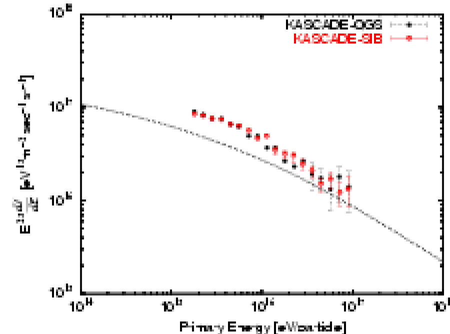

10^{14} 10^{16} 10^{18}

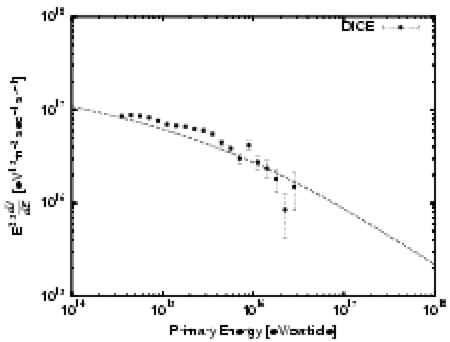

10^{14} 10^{16} 10^{18}

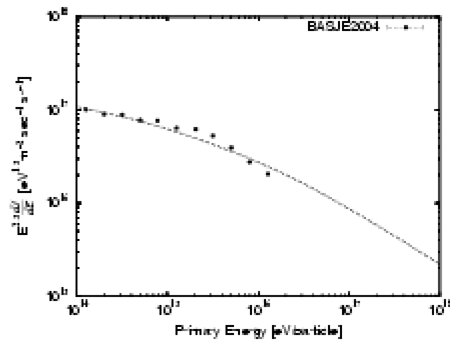

10^{14} 10^{16} 10^{18}

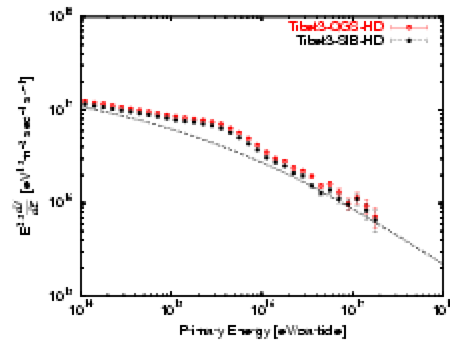

10^{14} 10^{16} 10^{18}

DICE BASJE TIBET

Extra component

All data agree if we apply energy scale correction within 20% by normalizing to direct observations.

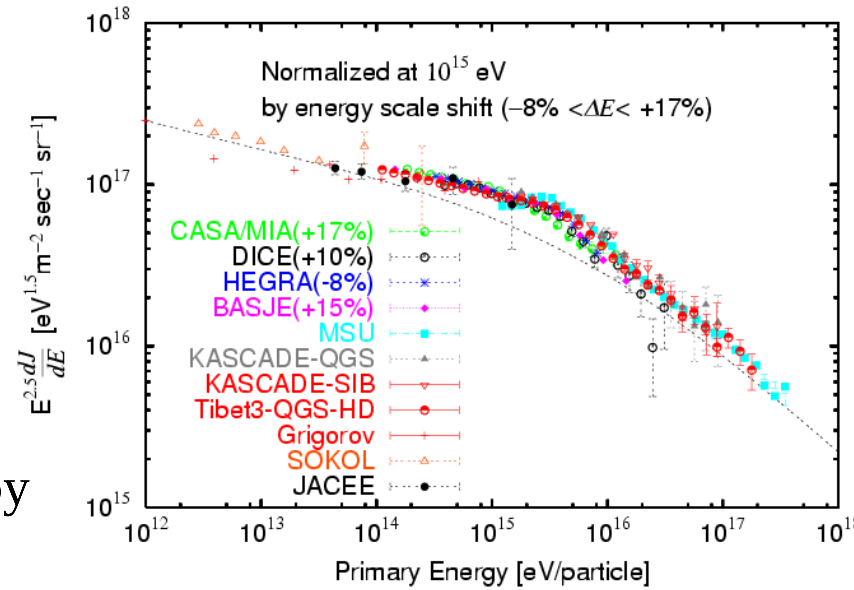

Extra component can be approximated by

$$E^{-2}\exp[-\frac{E}{4\mathrm{PeV}}],$$

suggesting **nearby source(s).**

Since P and He component do not show the excess at the knee, the extra component should be attributed to heavy element such as Fe.

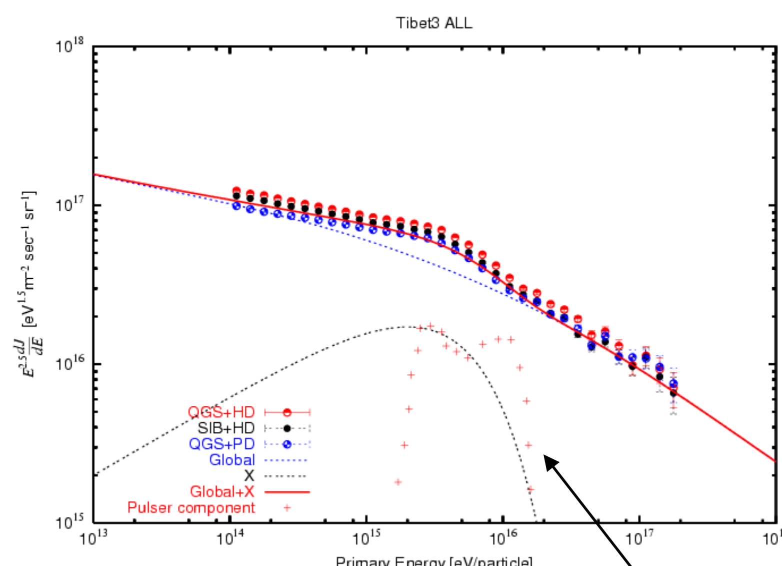

(W.Bednarek and R.J.Protheroe ,2002,APh)

(Slide from M.Shibata, Y.N.U.)

Tibet P +He spectrum does not show excess at the knee

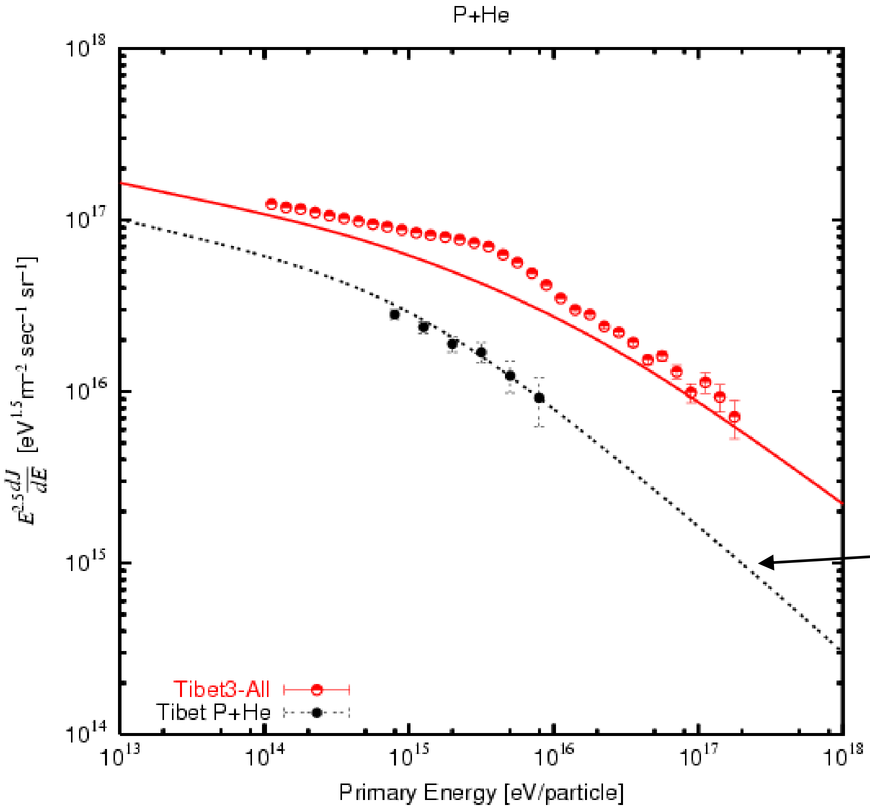

Tibet All particle
Data vs. Expected by multiple source model

P+He
Data vs. Expected by multiple source model

(Slide from M.Shibata, Y.N.U.)

(Slide from M.Shibata Y.N.U.)

Chemical composition of SN ejecta

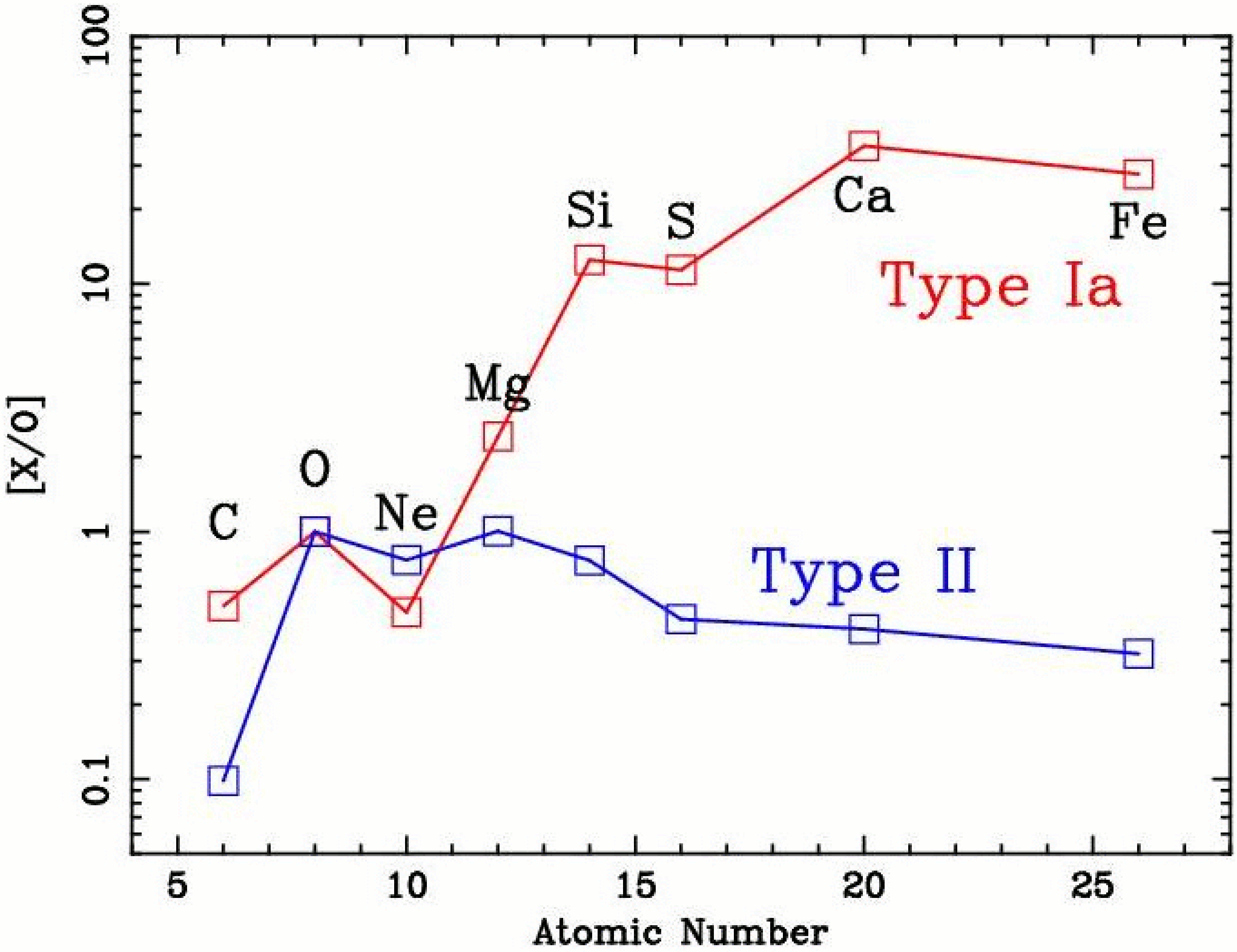

(Nomoto,K et al. Nucl. Phys. A, 621, 467, 1997)

4. Anisotropy

Compton-Getting Anisotropy at Solar Time Frame

Amenomori et al., ApJL, 672 (2008) L53

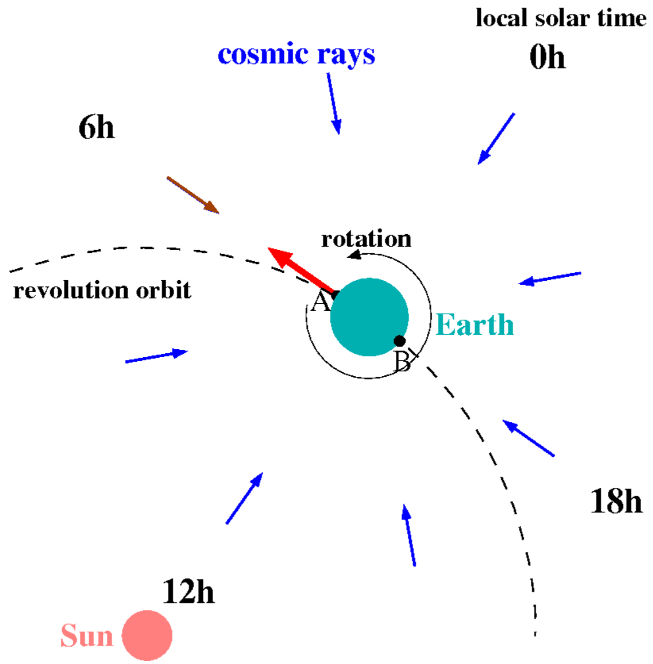

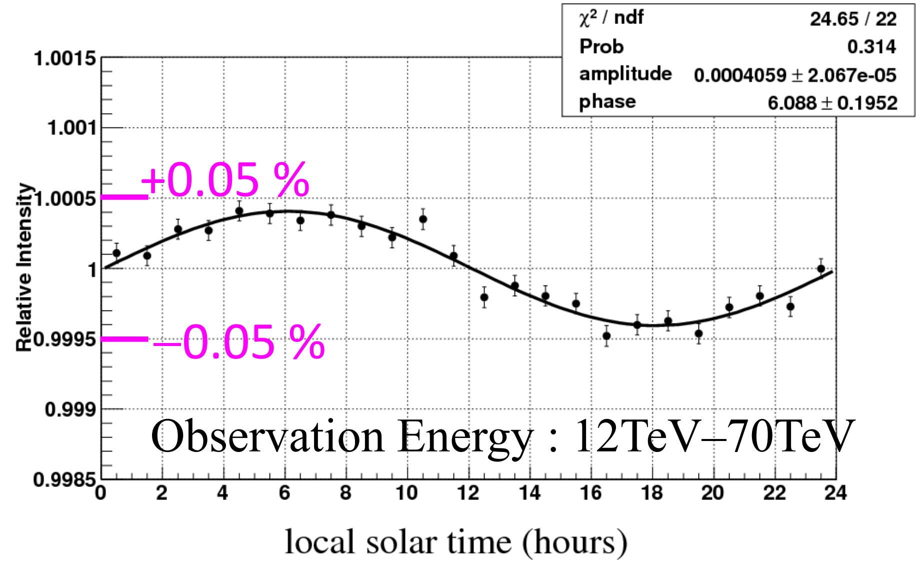

Expected	Amplitude 3.86×10^{-2} %	Phase 6 [hr]
Data	Amplitude $(4.06 \pm 0.21) \times 10^{-2}$ %	Phase 6.1 ± 0.2 [hr]

➡ **CG detected at 19.6σ consistent with expected**

- Reliability and calibration for sidereal anisotropy (~ 0.01%)
- Only Tibet ASγ experiment showing a clear sinusoidal curve

Modeling Sidereal Anisotropy : Origin of anisotropy

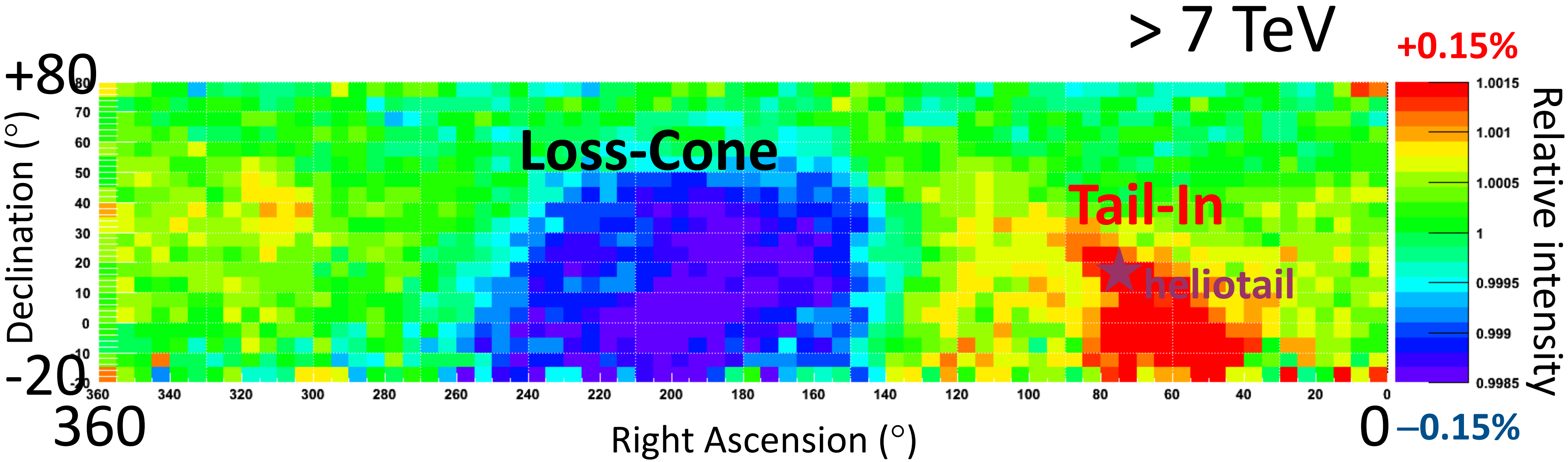

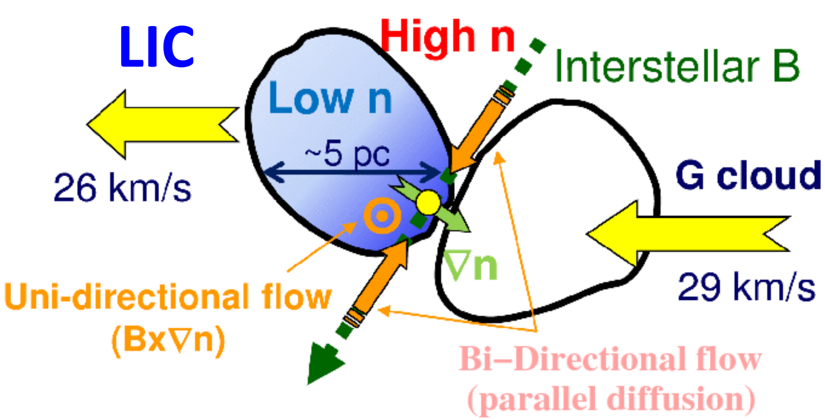

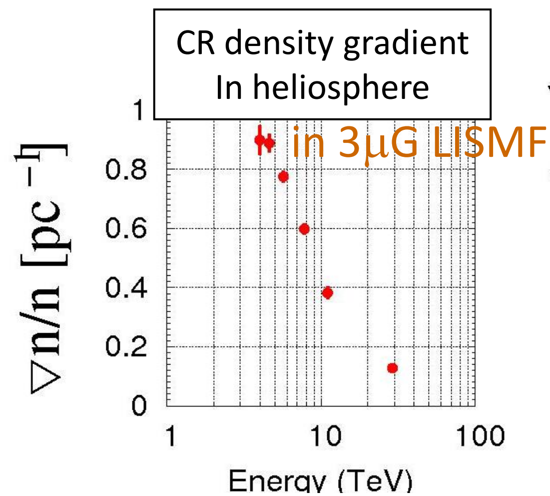

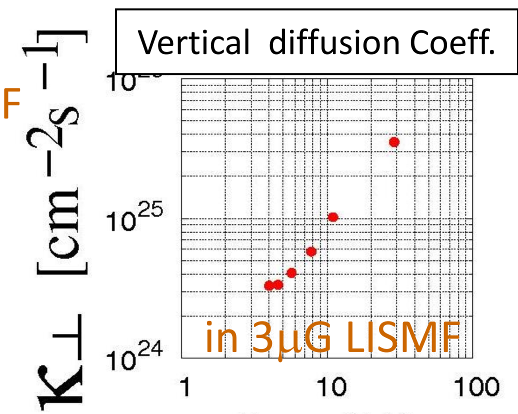

➡ Stimulus to CR transport theory and future space-ship experiment like Voyagers

Sidereal Anisotropy : Yearly Variation of Loss-Cone Amplitude?

Amenomori et al., App, 36 (2012) 237

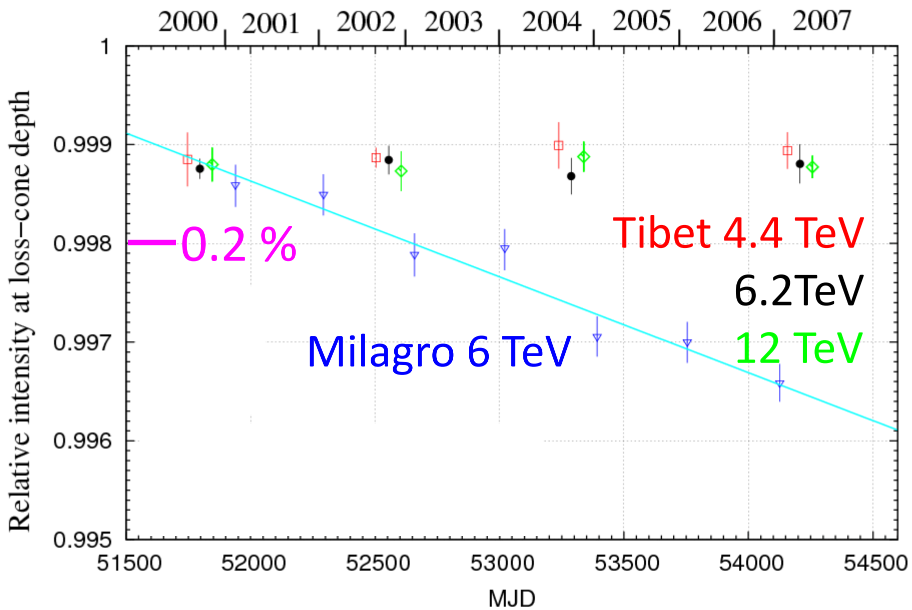

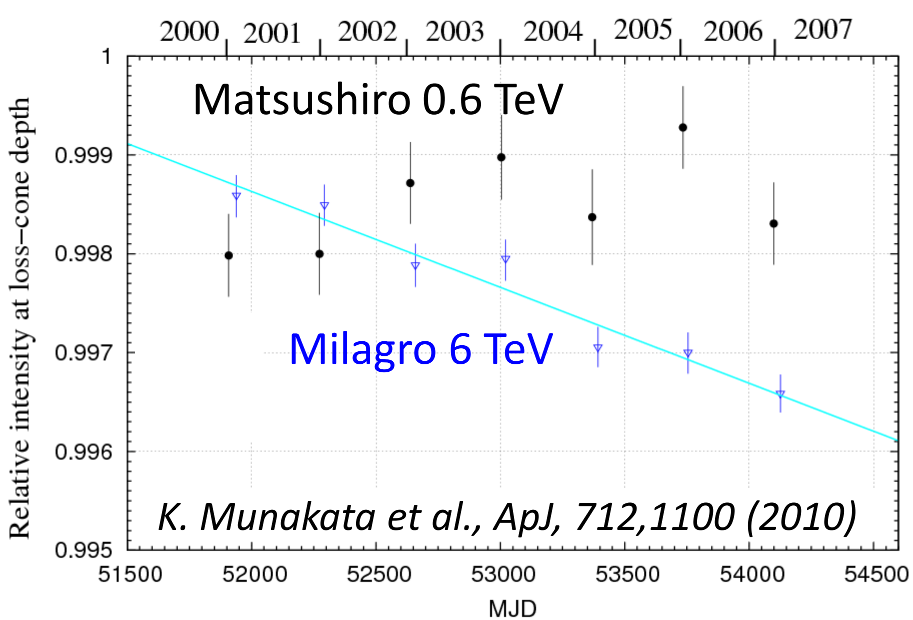

Fitting by α (MJD–53000) + β

Milagro 6 TeV

α = (0.97 ± 0.11) x 10^{-4} % [/day]

Tibet 4.4 TeV

α = (0.05 ± 0.13) x 10^{-4} % [/day]

inconsistent with Milagro (6.1σ)

6.2 TeV

α = (0.004 ± 0.099) x 10^{-4} % [/day]

inconsistent with Milagro (6.6σ)

11 TeV

α = (–0.002 ± 0.095) x 10^{-4} % [/day]

inconsistent with Milagro (6.7σ)

Matsushiro 0.6 TeV

p0 = (0.32 ± 0.22) x 10^{-4} % [/day]

inconsistent with Milagro (5.3σ)

Milagro's yearly variation of Loss-Cone amplitude ruled out at multi-TeV & sub-TeV

5. The Sun’s Shadow

The Sun's Shadow

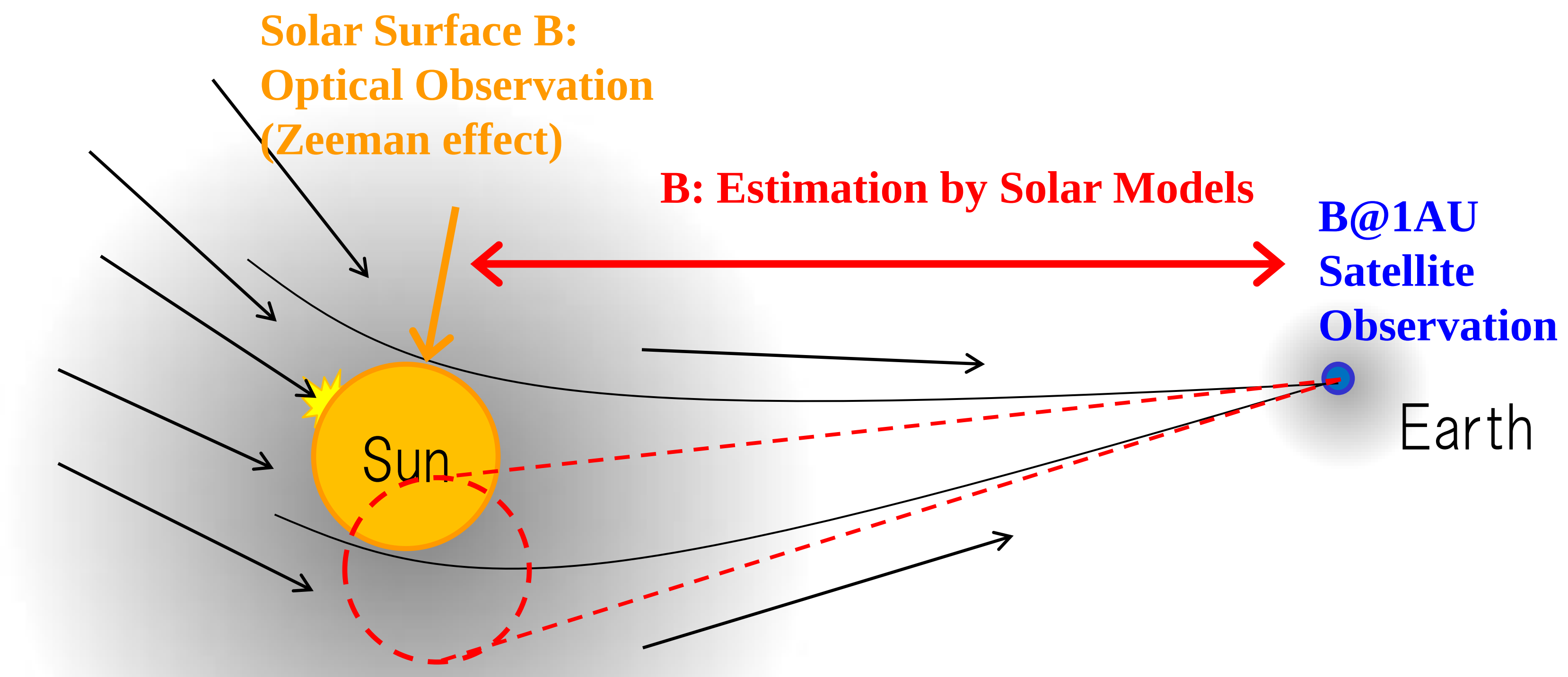

Shielding of CR
by the Sun

TeV CR (Protons)→Charged
Larmor Radius
～7.4AU (B=30μG around Earth)
～$0.16R_{\odot}$(B=300mG around Sun)
Probing magnetic structure in heliosphere

Observation of Sun's Shadow in Ecliptic Coordinates at 10TeV

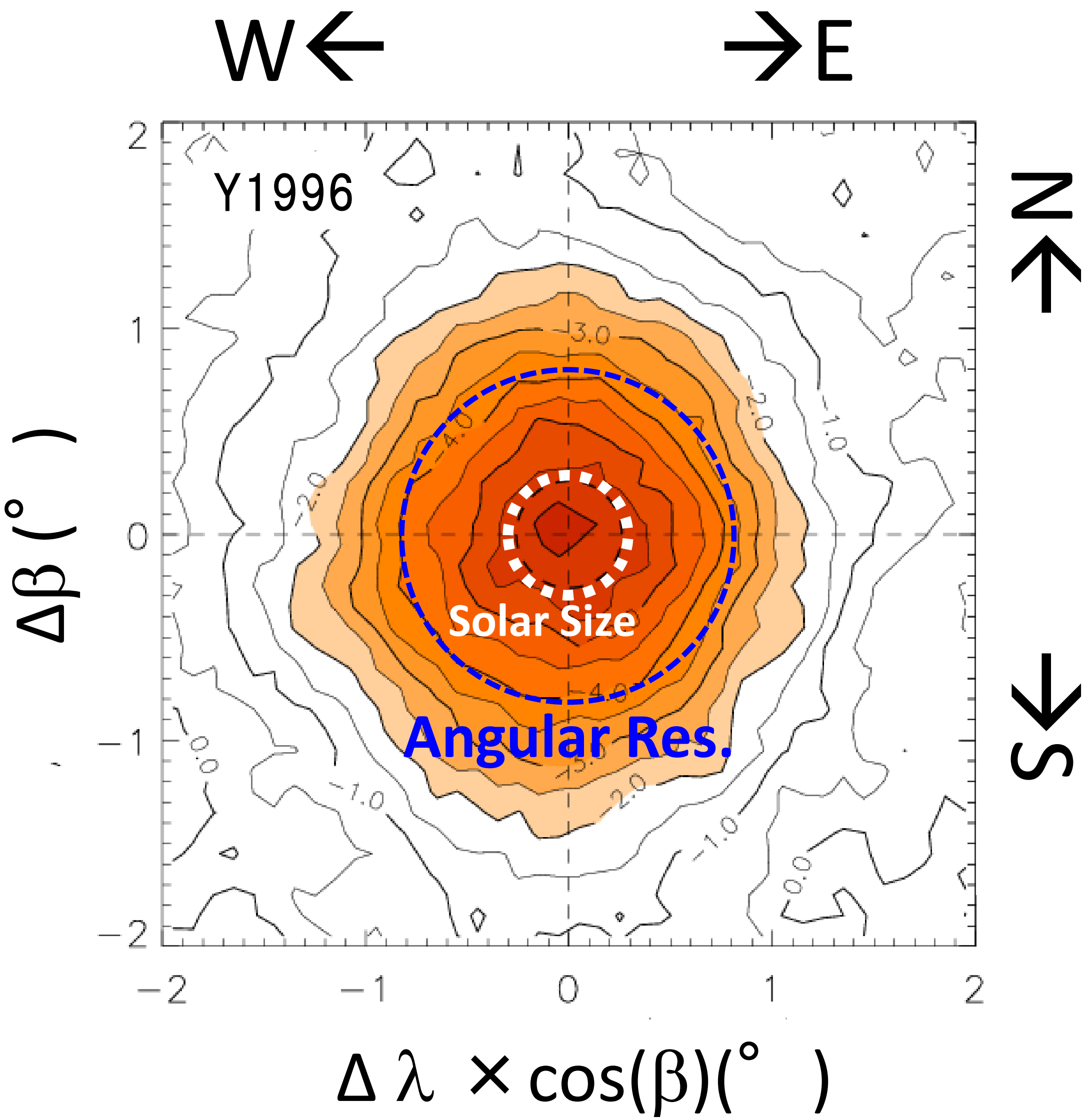

CR intensity map
In the 4° × 4° window
centered at Sun

Shadow smeared by σ_θ ∼0.9° apparent $R_\odot$ (∼ 0.26°)

6 % shielding effect expected in average CR flux

Shadow position and depth sensitive to B in heliosphere

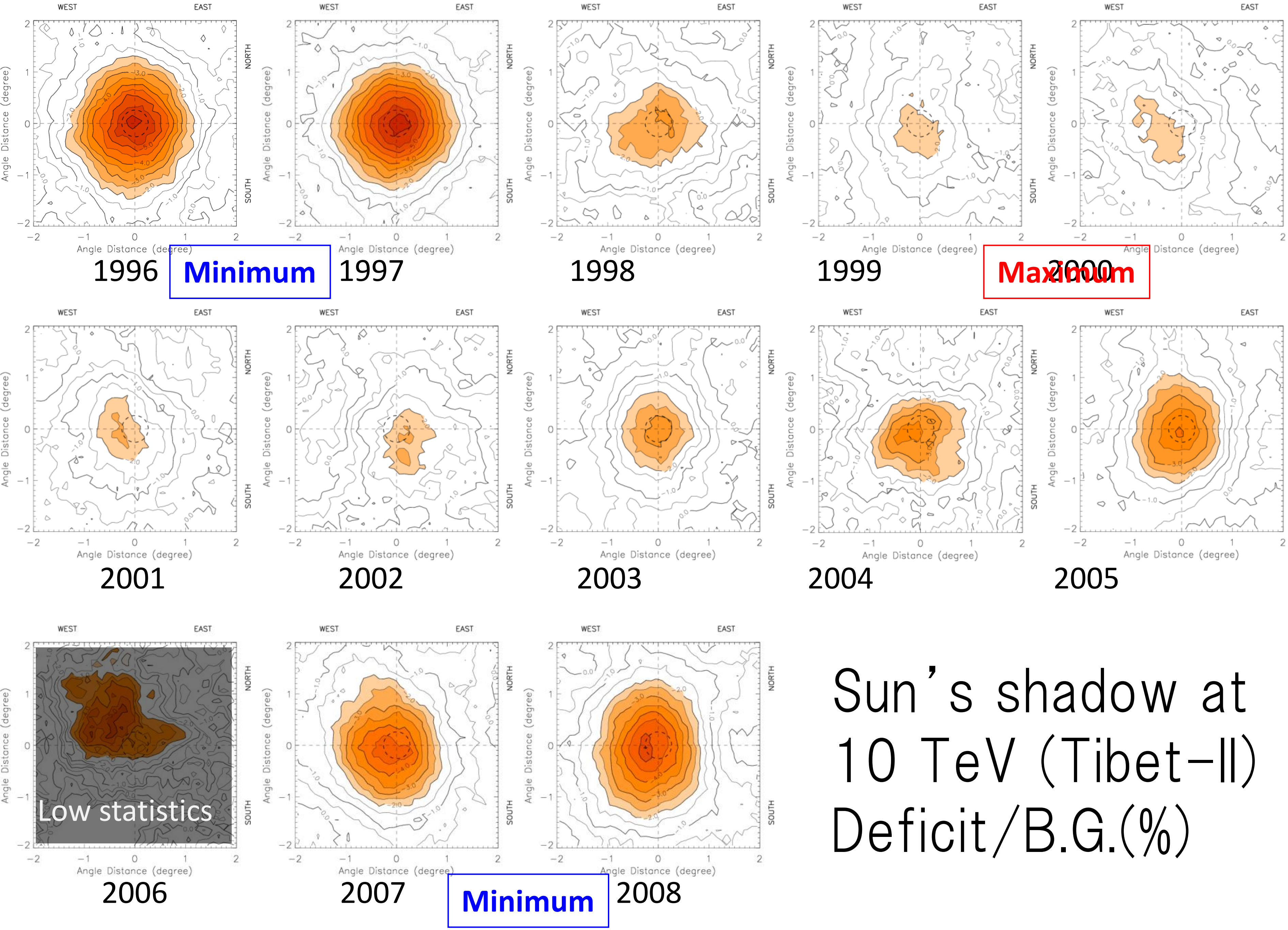

Sun's shadow at
10 TeV (Tibet-II)
Deficit/B.G.(%)

MC simulation of Sun's Shadow

Magnetic Field models in the heliosphere assumed,
Calculation of anti-CR trajectory from Earth to Sun
→ Anti-CR hitting Sun = Sun's shadow

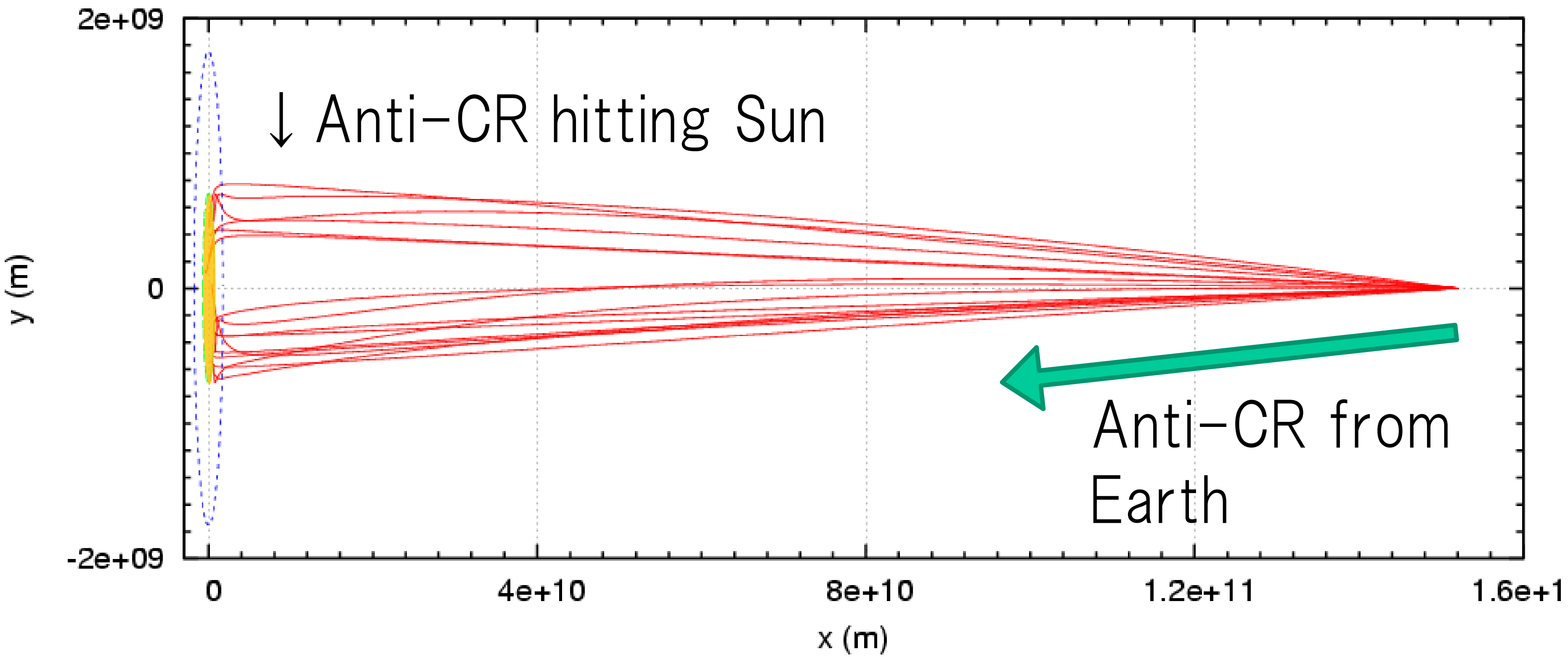

Magnetic Field Models assumed

Coronal Magnetic Field($<2.5R_{\odot}$)

→ PFSS model or CSSS model
Based on surface magnetic field observed by Kitt Peak averaged over 1 rotation period (~27 days)

Interplanetary Magnetic Field ($>2.5R_{\odot}$)

→ Parker's spiral model

Geomagnetic Field

→ Dipole Magnetic Field

Mininum(1996)
qA>0(+Positive)

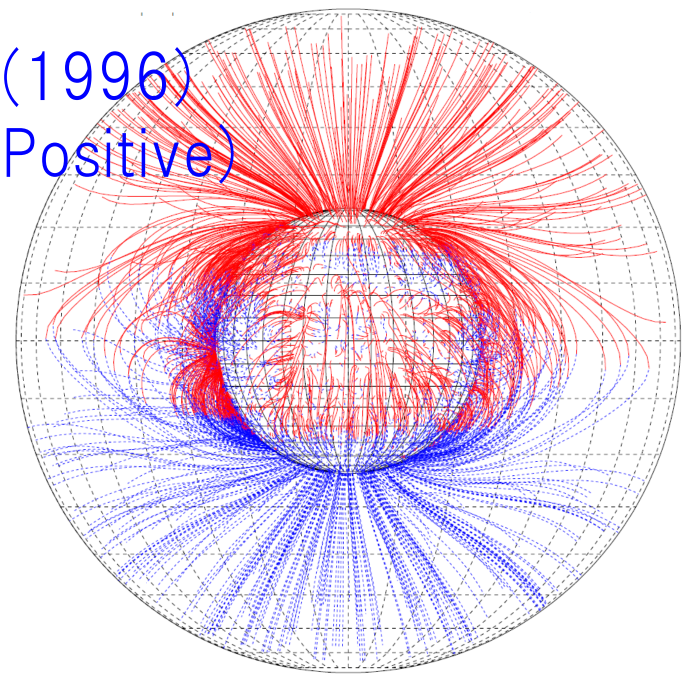

Maximum(2000)

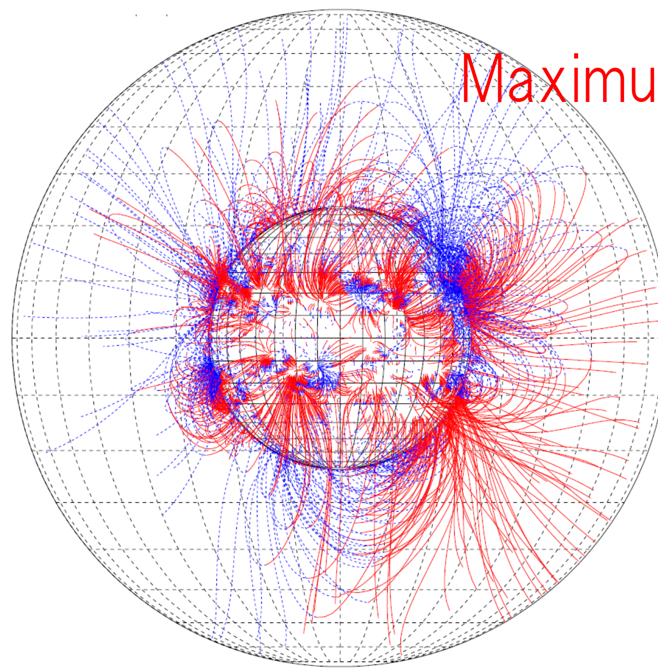

Example of MC simulation

CR chemical composition, energy spectra, experimental Condition(detector response, data analysis..) included

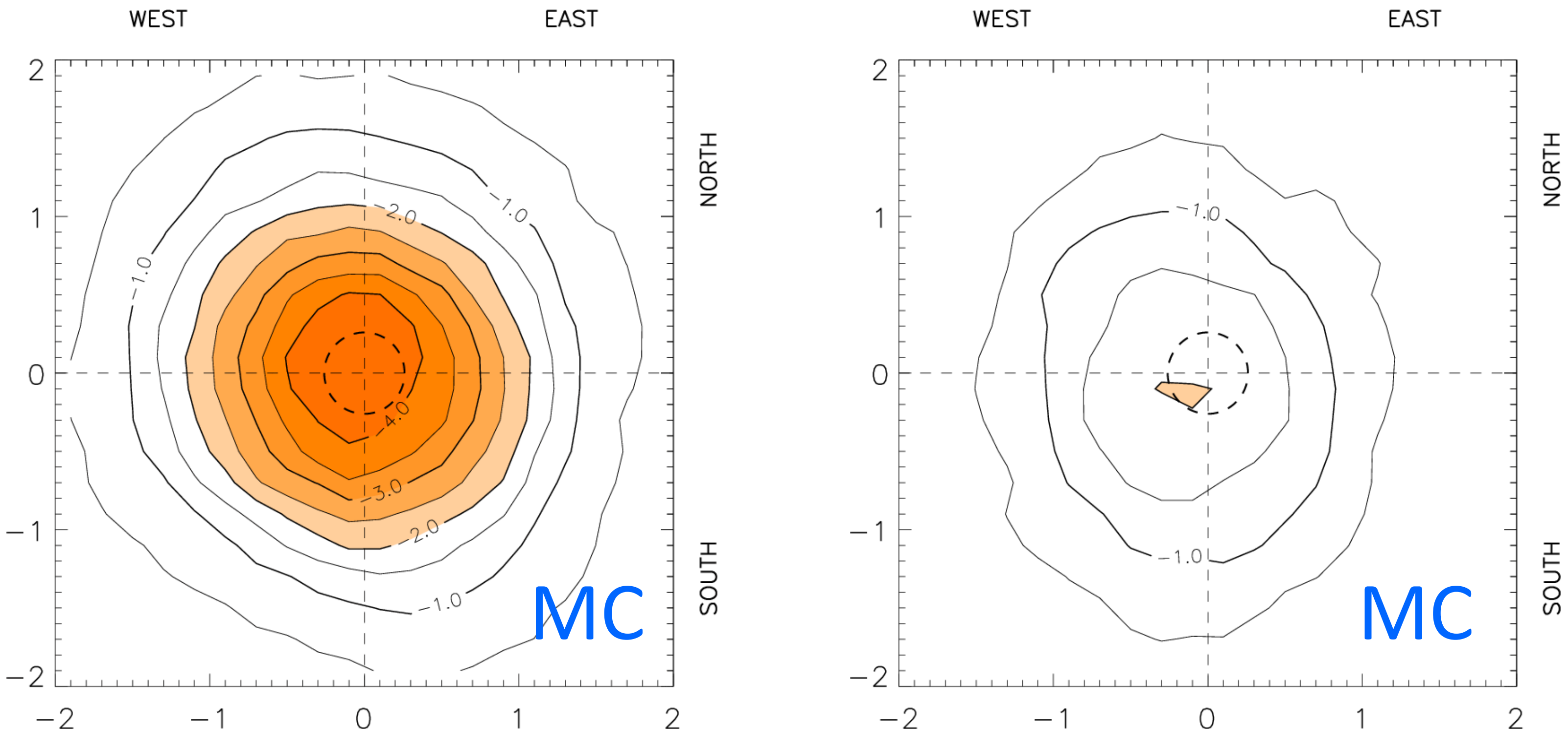

Minimum Y1996(CR1910)

Maximum Y2001(CR1978)

Potential Field Source Surface (PFSS) Model

Altschuler and Newkirk, Solar Physics, 9, 131 (1969)
Hakamada, Solar Physics, 159, 89 (1995)

Plasma velocity is small (β/c << 1) → $\frac{\partial E}{\partial t} << j$

Local and short-lived electric currents are ignored → $j = 0$

Current-free

Maxwell equations

$$\nabla \times \mathbf{B} = 0 \quad \rightarrow \quad \mathbf{B} = -\nabla \Psi$$

$$\nabla \cdot \mathbf{B} = 0$$

Scalar potential Ψ has to satisfy the Laplace equation

$$\nabla^2 \Psi = 0$$

Scalar potential Ψ can be expanded to spherical harmonic series

Spherical Harmonic Series

$$\Psi(r,\,\theta,\,\phi) = r_\odot \sum_{n=0}^{\infty} \sum_{m=0}^{n} P_n^m(\theta) \times$$

$$\times \left[\left\{ c_n^m \left(\frac{r}{r_\odot}\right)^n + (1 - c_n^m) \left(\frac{r_\odot}{r}\right)^{n+1} \right\} g_n^m \cos m\phi + \right.$$

$$\left. + \left\{ d_n^m \left(\frac{r}{r_\odot}\right)^n + (1 - d_n^m) \left(\frac{r_\odot}{r}\right)^{n+1} \right\} h_n^m \sin m\phi \right] ,$$

Boundary condition at Rss

$$\Psi(R_{ss},\theta,\phi) = 0$$

$$\rightarrow B_r \neq 0, B_\theta = 0, B_\phi = 0$$

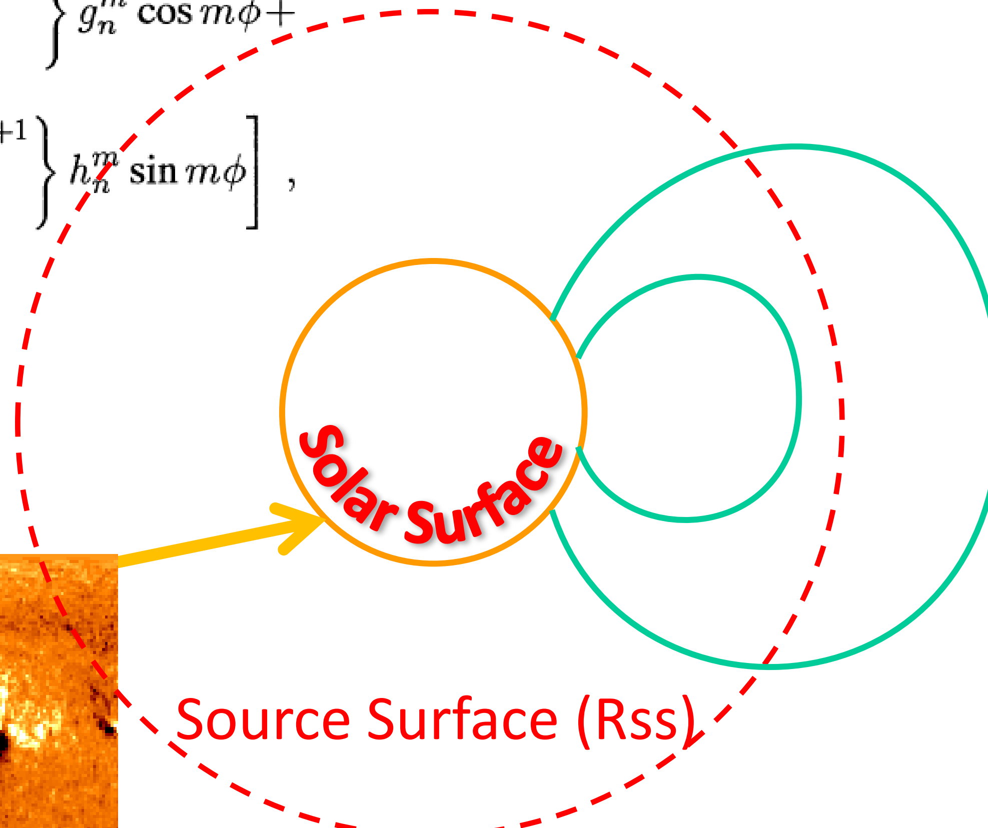

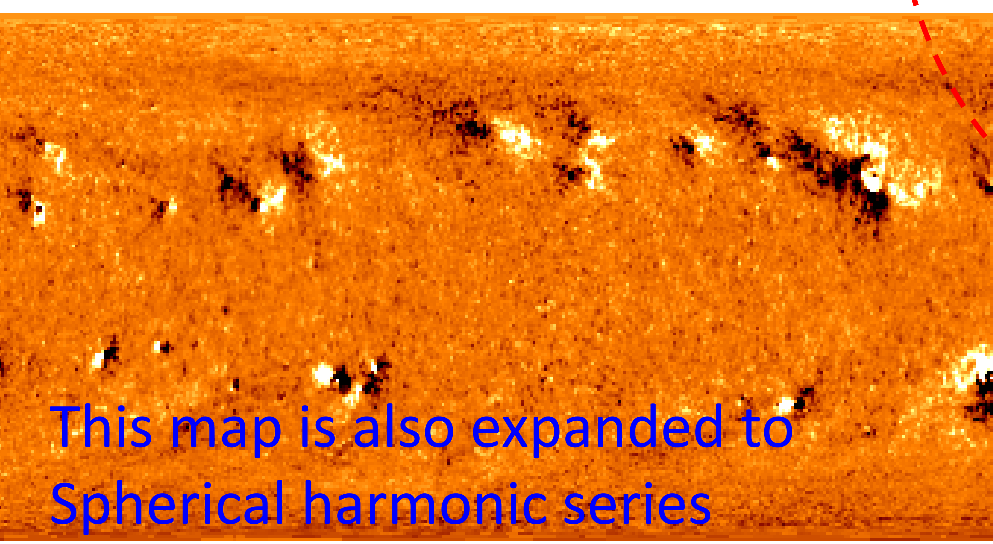

Solar surface magnetograph
with the Kitt Peak Vacuum Telescope
utilizing the Zeeman effect
(FeI 868.8, 630.1 and 630.2nm)

Spherical Harmonic Series

$$\Psi(r,\,\theta,\,\phi) = r_\odot \sum_{n=0}^{\infty} \sum_{m=0}^{n} P_n^m(\theta) \times$$

$$\times \left[\left\{ c_n^m \left(\frac{r}{r_\odot} \right)^n + (1 - c_n^m) \left(\frac{r_\odot}{r} \right)^{n+1} \right\} g_n^m \cos m\phi + \right.$$

$$\left. + \left\{ d_n^m \left(\frac{r}{r_\odot} \right)^n + (1 - d_n^m) \left(\frac{r_\odot}{r} \right)^{n+1} \right\} h_n^m \sin m\phi \right] \;,$$

Boundary condition at Rss

$$\Psi(R_{ss}, \theta, \phi) = 0$$

$$\rightarrow B_r \neq 0, B_\theta = 0, B_\phi = 0$$

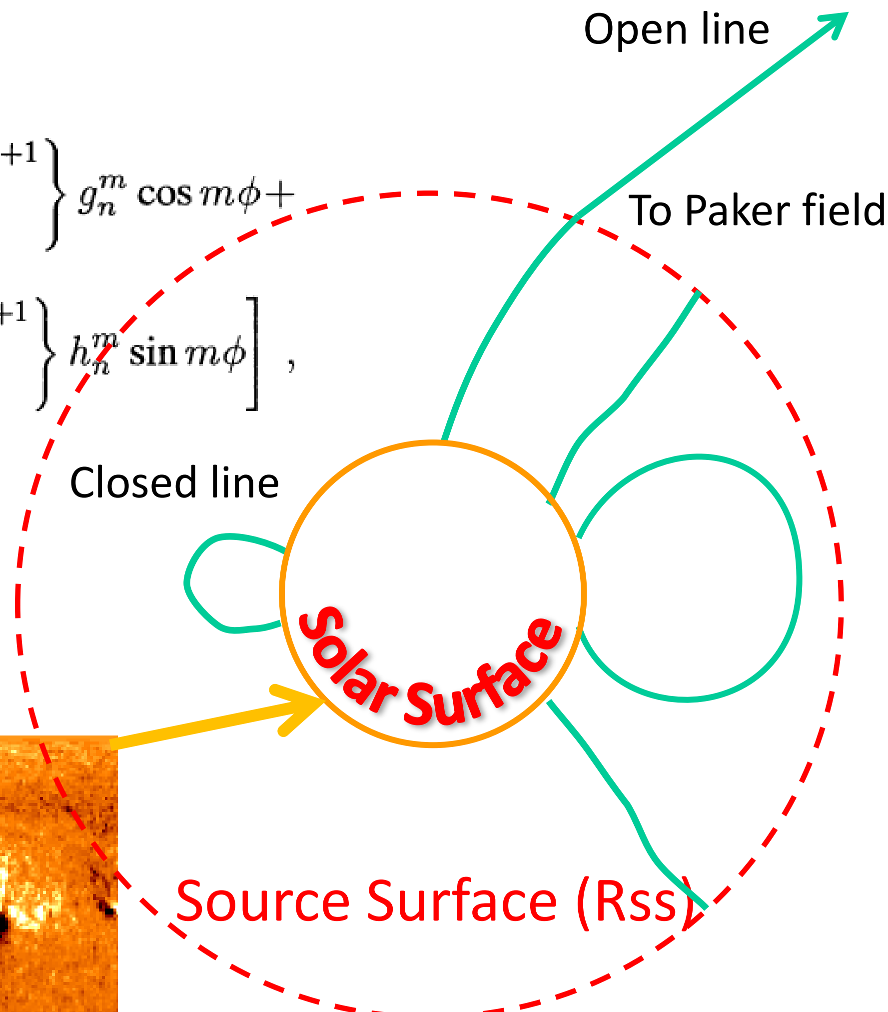

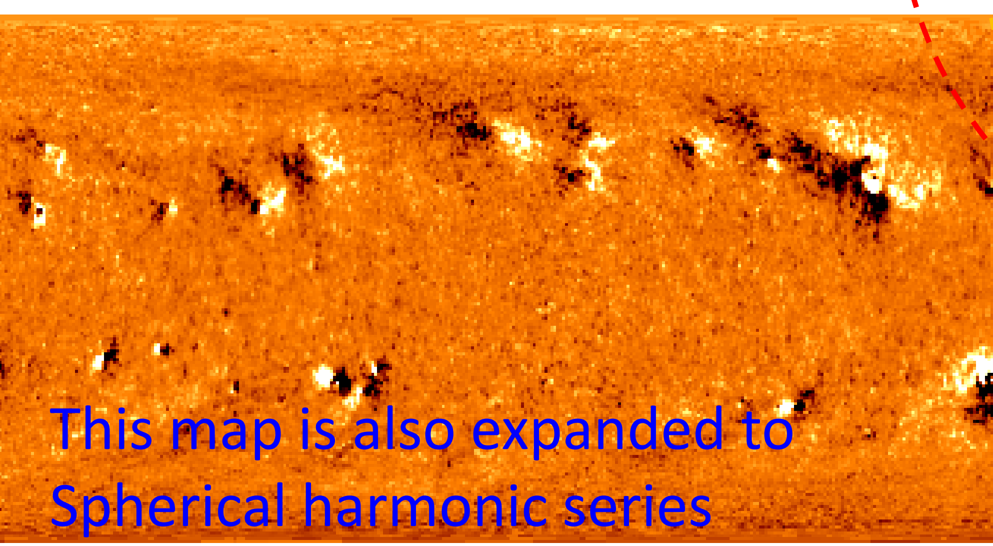

Solar surface magnetograph
with the Kitt Peak Vacuum Telescope
utilizing the Zeeman effect
(FeI 868.8, 630.1 and 630.2nm)

Magnetic Field Lines by PFSS Model

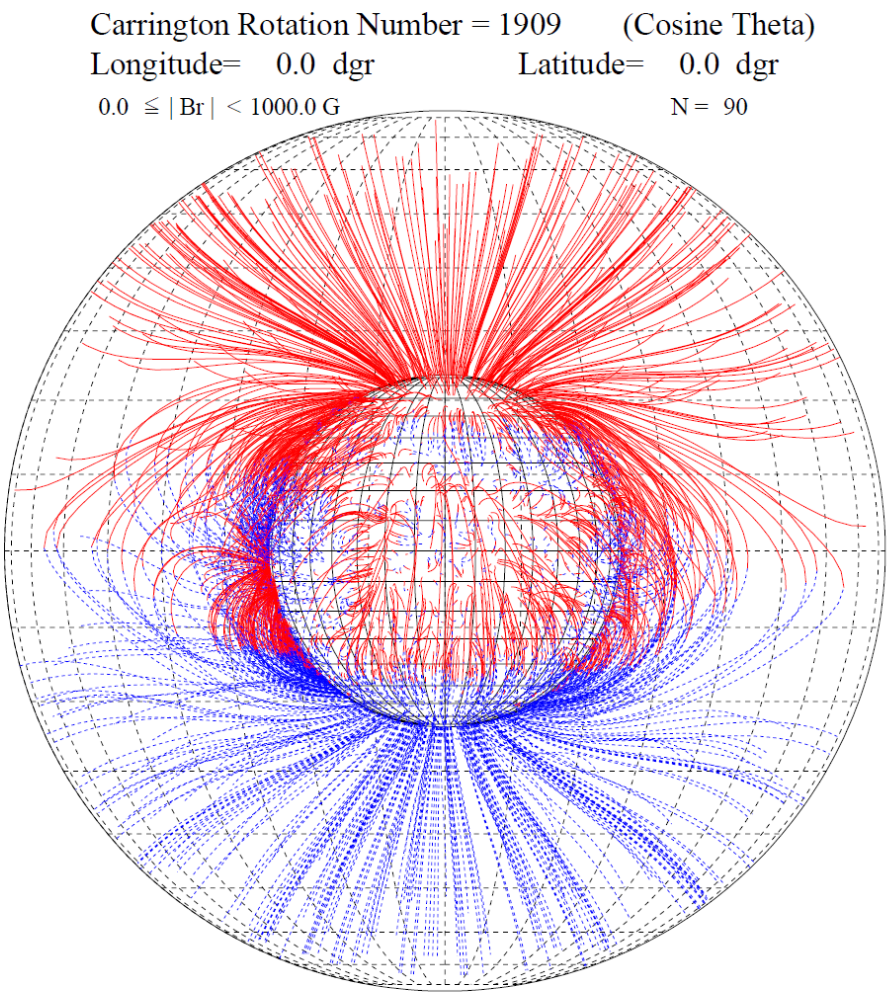

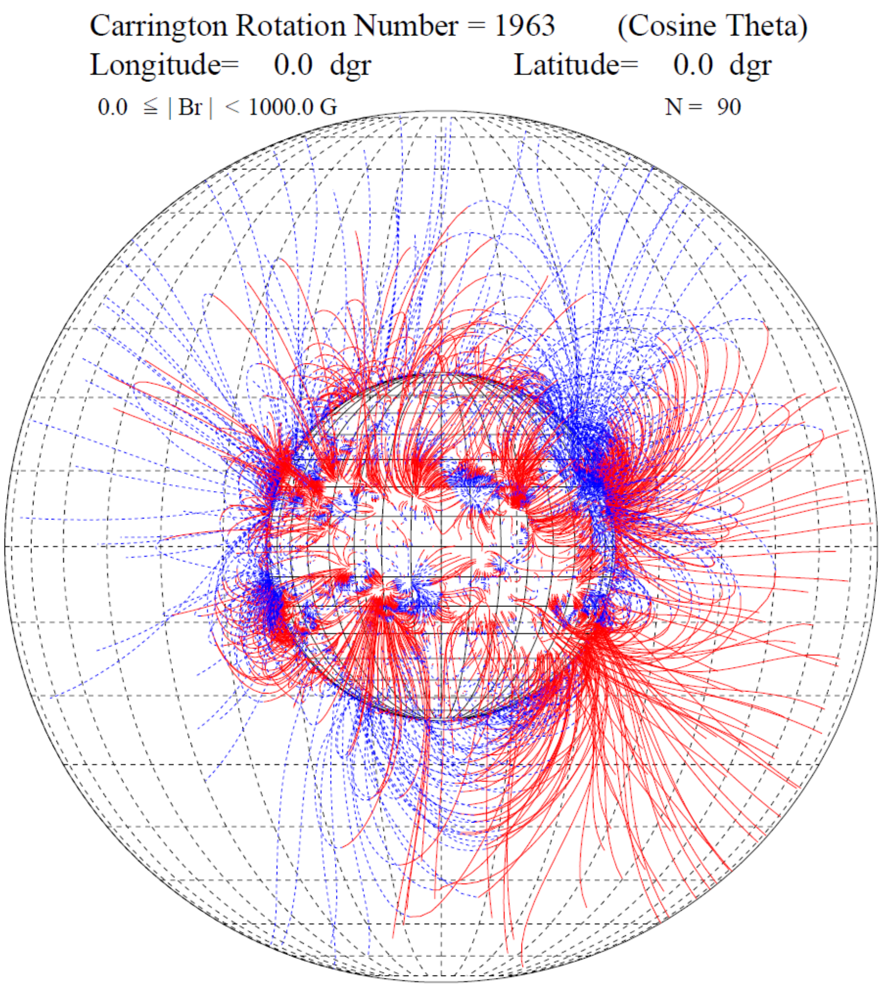

Courtesy: K. Hakamada

White light image

This photograph of a total solar eclipse was taken by Miloslav Druckmüller and colleagues from Brno University of Technology, Czech Republic, during an eclipse on July 22, 2009.

Current Sheet Source Surface (CSSS) Model

Xuepu Zhao & Todd Hoeksema, JGR, 100, 19 (1995)

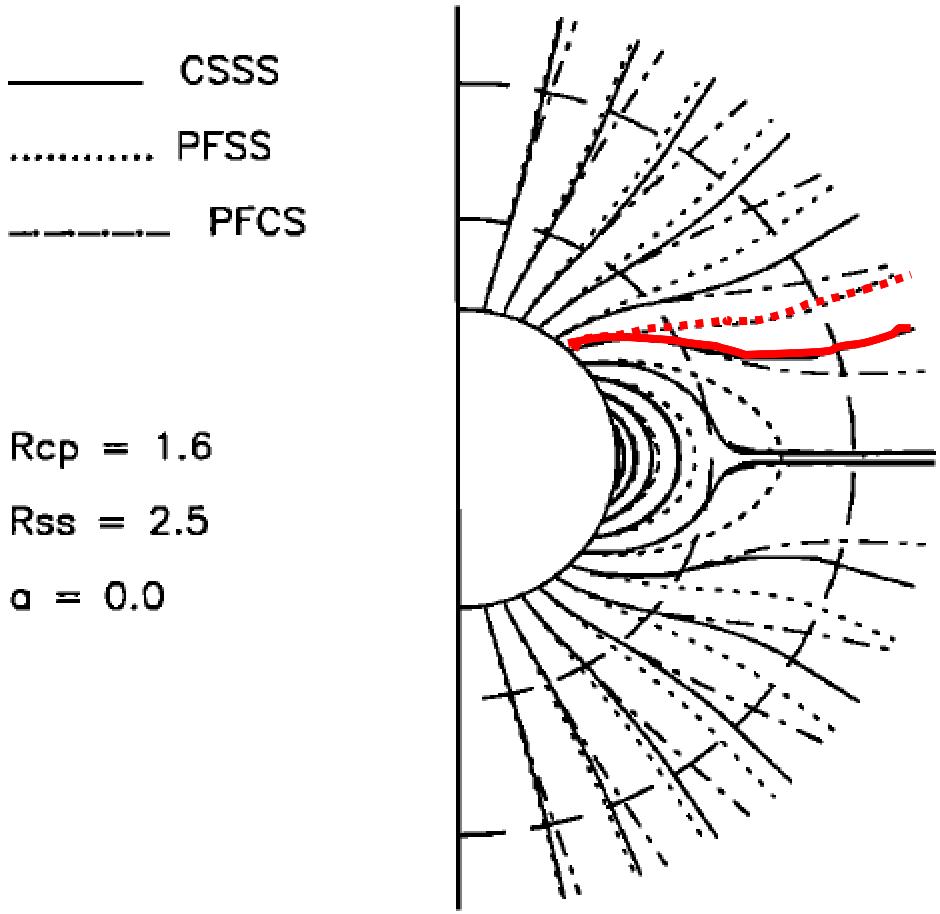

Abstract:

The model **includes the effects of the large-scale horizontal electric currents flowing in the inner corona** of the warped heliospheric current sheet in the upper corona, and of volume currents flowing in the region where the solar wind plasma totally controls the magnetic field. **The model matches the MHD solution** for a simple dipole test case better than earlier source surface and current sheet models

磁気静水圧平衡

Bogdan & Low, ApJ, 306, 271 (1986)

Low, ApJ, 293, 31 (1985)

Magnetostatic force balance

current (J)

$$\frac{1}{4\pi}(\nabla\times\mathbf{B})\times\mathbf{B}-\nabla\mathbf{p}-\rho\frac{GM}{r^2}\hat{\mathbf{r}}=0$$

Magnetic force, gas pressure and gravity

Analytical solutions

$$\mathbf{J}=\frac{1}{\mu_0 r}[1-\eta(r)]\left[\frac{1}{\sin\theta}\frac{\partial^2\Psi}{\partial\phi\partial r}\hat{\theta}-\frac{\partial^2\Psi}{\partial\phi\partial r}\hat{\phi}\right]$$

$$\mathbf{B}=-\eta(r)\frac{\partial\Psi}{\partial r}\hat{r}-\frac{1}{r}\frac{\partial\Psi}{\partial\theta}\hat{\theta}-\frac{1}{r\sin\theta}\frac{\partial\Psi}{\partial\phi}\hat{\phi}$$

$$\eta(r)=\left(1+\frac{a}{r}\right)^2$$

a : length scale of horizontal electric currents in the corona

Xuepu Zhao & Todd Hoeksema, JGR, 100, 19 (1995)

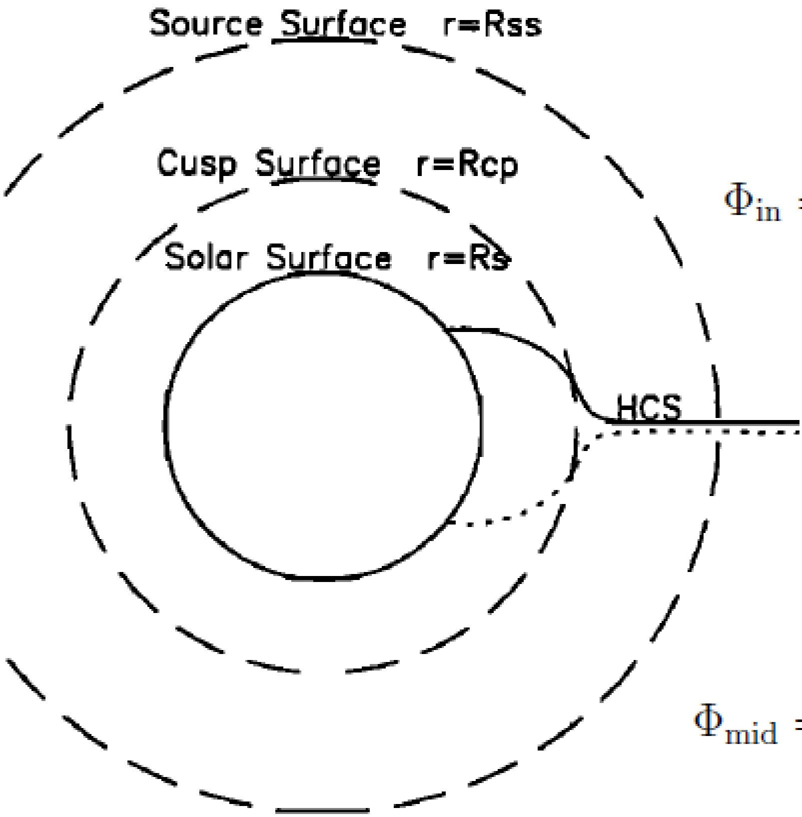

Inner region (Rs < r < Rcp)

$$\Phi_{\rm in} = \sum_{l=1}^{N_\odot} \sum_{m=0}^{l} R_l^\odot(r)\ P_l^m(\cos\theta)\ (g_{lm}^\odot\ \cos m\phi + h_{lm}^\odot\ \sin m\phi)\,,$$

$$R_l^\odot(r) = \frac{R_\odot(1+a)^l}{(l+1)(r+a)^{l+1}}$$

Middle region (Rcp < r < Rss)

$$\Phi_{\rm mid} = \sum_{l=0}^{N_\odot} \sum_{m=0}^{l} R_l^c(r)\ P_l^m(\cos\theta)\ (g_{lm}^c\ \cos m\phi + h_{lm}^c\ \sin m\phi)\,,$$

$$R_l^c(r) \;=\; R_\odot \left[\frac{l+1}{R_{\rm cusp}^2(R_{\rm cusp}+a)^l} + \frac{l(R_{\rm cusp}+a)^{l+1}}{R_{\rm cusp}^2(R_{\rm ss}+a)^{2l+1}}\right]^{-1} \times \left[\frac{1}{(r+a)^{l+1}} - \frac{(r+a)^l}{(R_{\rm ss}+a)^{2l+1}}\right]$$

Free parameters

- a : length scale
- Rcp : cusp surface
- Rss : source surface
- N : Maximum principal index

Coronal Magnetic Field at the Solar Minimum

CSSS

CR1910
(Year1996)

PFSS

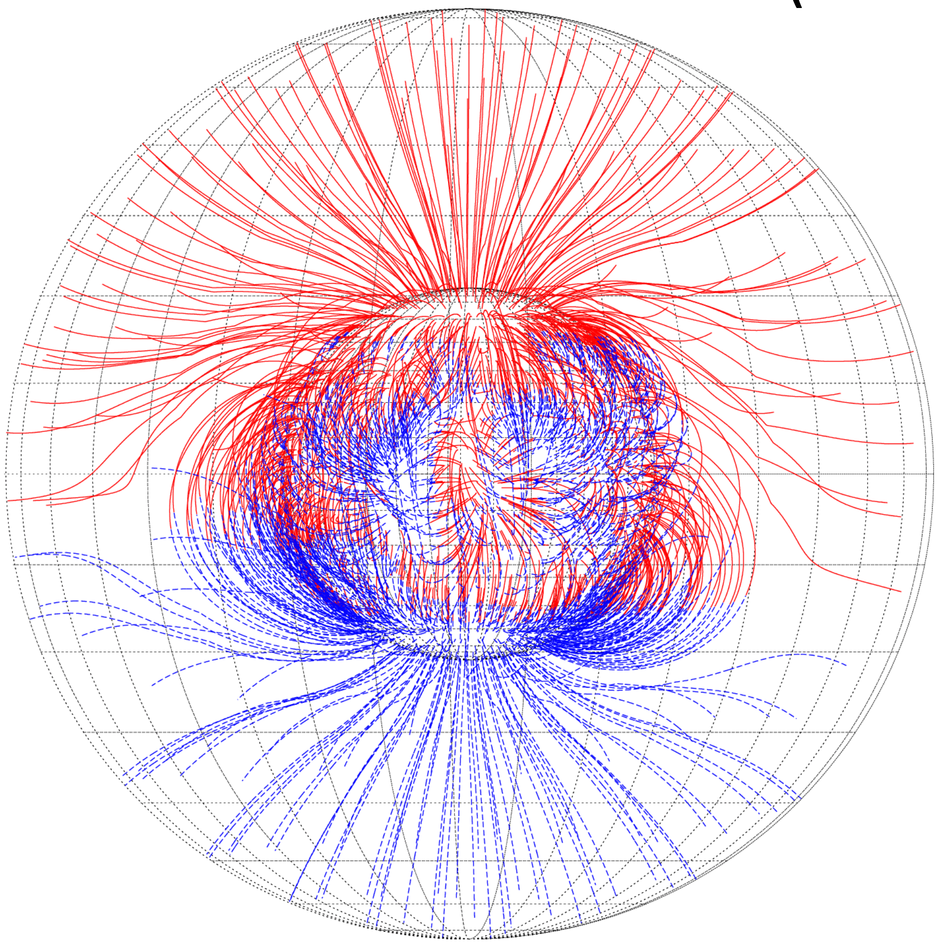

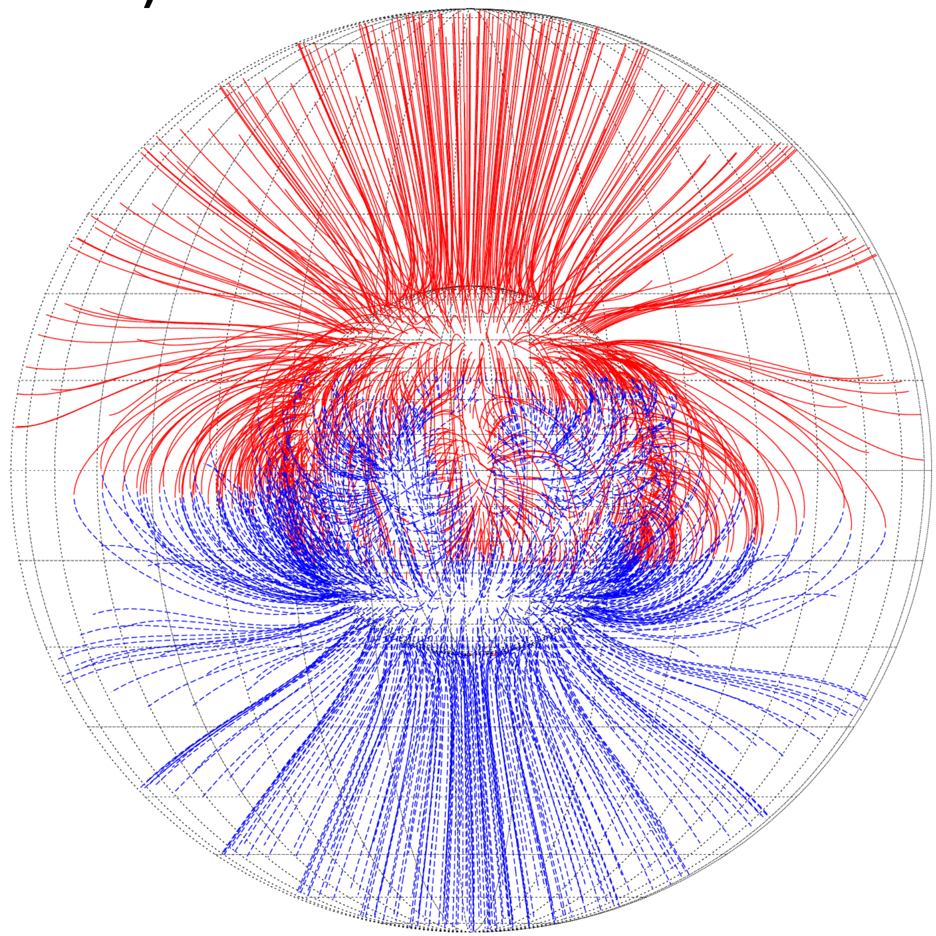

Comparison between CSSS and PFSS

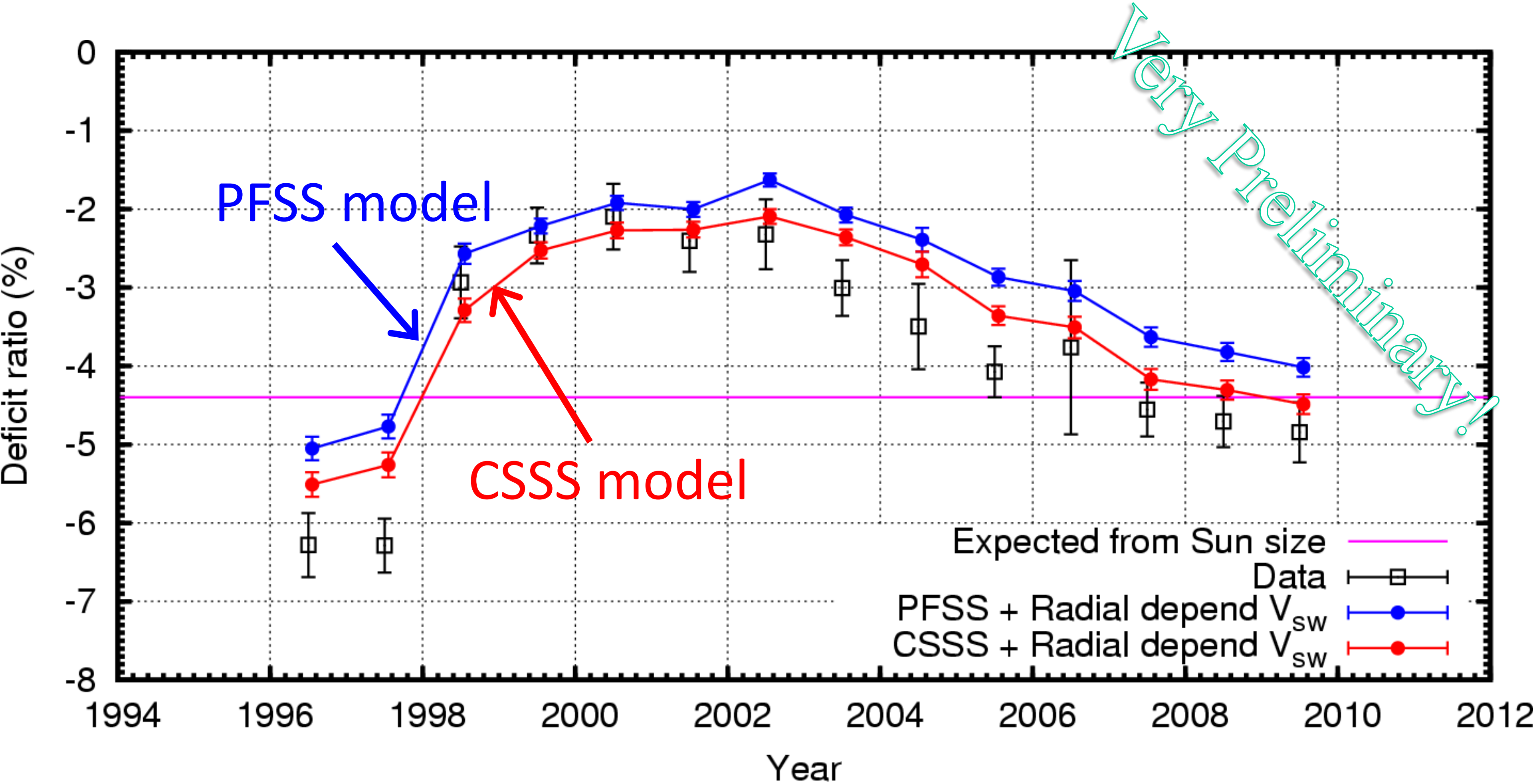

Data – MC(PFSS) χ^2/dof = 68.7/14 (5.7σ)

Data – MC(CSSS) χ^2/dof = 24.3/14 (1.7σ)

Sun’s shadow summary

- Observation of the Sun’s shadow (1996～2009) covering Solar Cycle 23

  → anti-correlation to 11-yr period solar activities

- Sensitivity to Sun-Earth magnetic field

  → Sun’s shadow sensitive to coronal magnetic field
  → CSSS magnetic field model adopting currents in the coronal atmosphere reproducing DATA better than PFSS model

6. Future Prospects

What we have found out:

Crab, Mrk501 , Mrk421, Fermi-source Correlation observed,

Possible diffuse γ-ray signal from Cygnus region?

P, He, all-particle E-spectrum (Galactic cosmic rays accelerated to the knee region ~10^{15} eV)

Sharp Knee!?

What we should do next:

1. 100 TeV (10 – 1000 TeV) region γ-ray astronomy

   Where do galactic cosmic rays under knee come from?

2. E-spectrum of heavy component around ‘ knee’

   All-particle knee = CNO? Fe knee?

□ Next Plans

Gamma ray: Tibet Muon Detector (MD) Project

&

Cosmic Rays: Tibet Yangbajing Airshower Core (YAC) Detector Project

Tibet Muon Detector (MD) Project

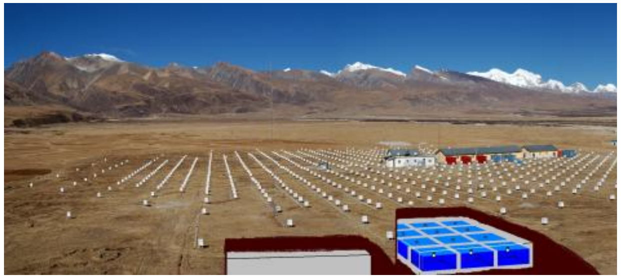

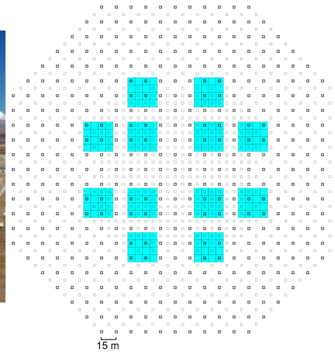

10-1000TeV Gamma

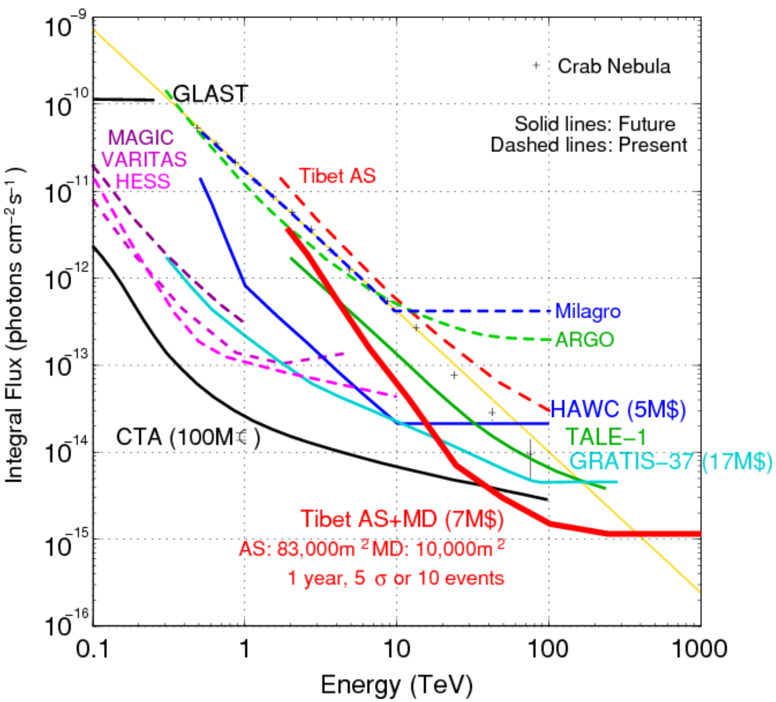

Tibet Air Shower Core Detector (YAC) Project

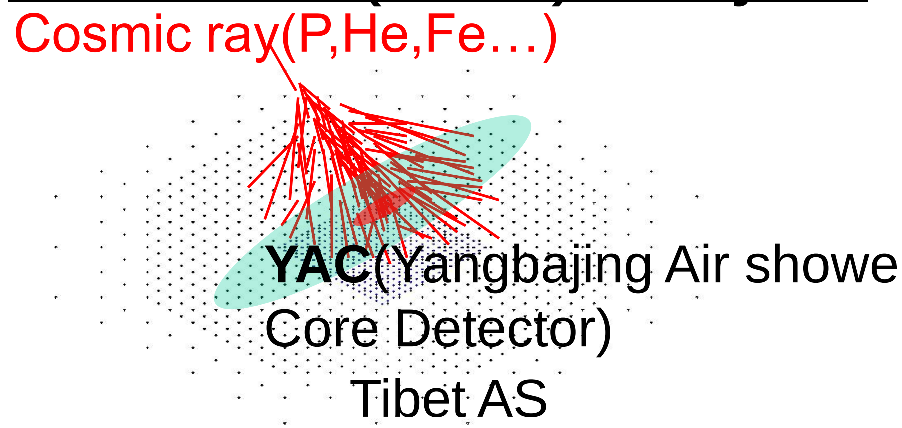

Chemical Compsition In the Knee

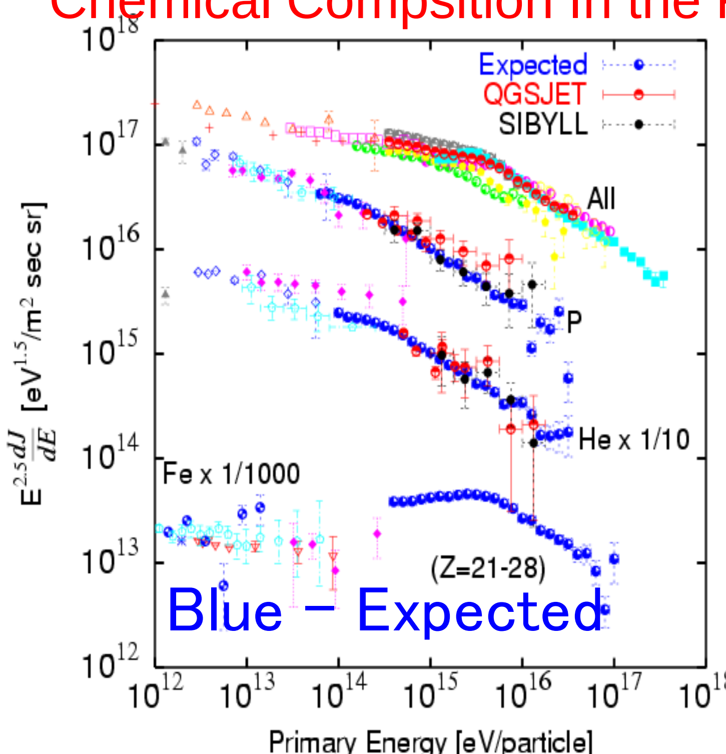

1. 100 TeV γ-ray astronomy

Let's see 100 TeV-region (10-1000TeV) gamma rays by

Tibet-III (AS) + a large underground

muon detector array (MD)

(~10000m^2 in total)!

>Origin of cosmic rays and acceleration mechanism and limit at SNRs.

>Diffuse gamma rays

p/γ discrimination by muons

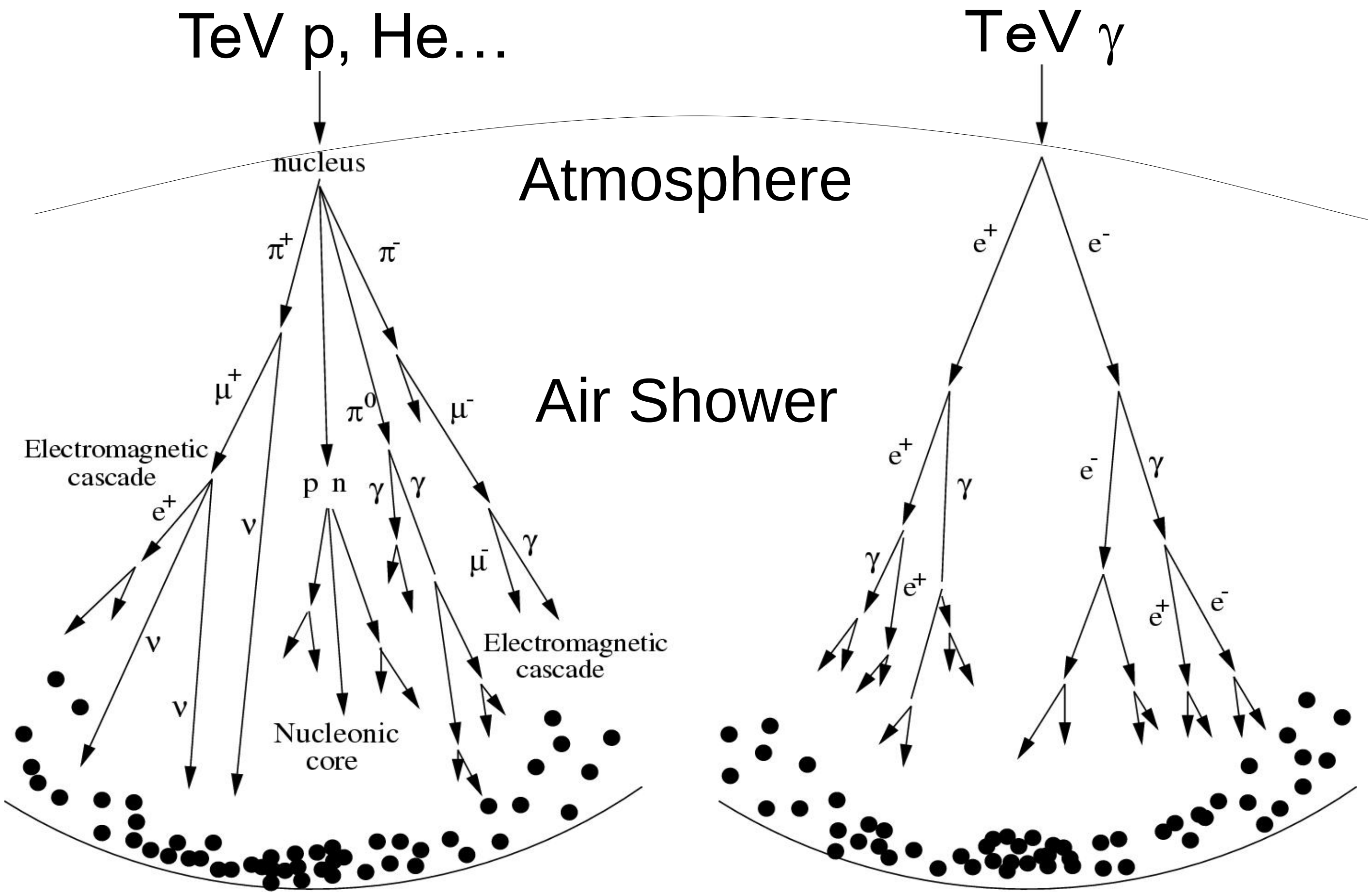

Number of muons（<100 m from core, 4300m a.s.l.）

100TeV Proton ~50

100TeV Gamma ~1

Tibet Muon Detector (MD) Array

7.2m x 7.2m x 1.5m depth Water pool

20"ΦPMT x 2 (HAMAMATSU R3600)

Underground 2.5m (~515g/cm^2~19X_0)

Material:

- Concrete pool
- White paint

192 detctors

Total ~10,000 m^2

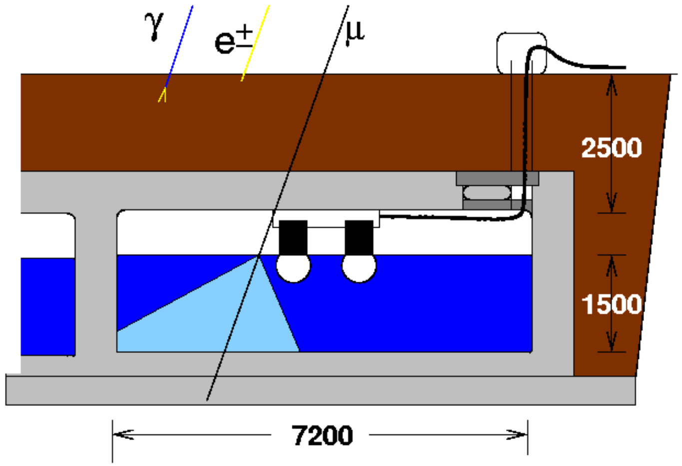

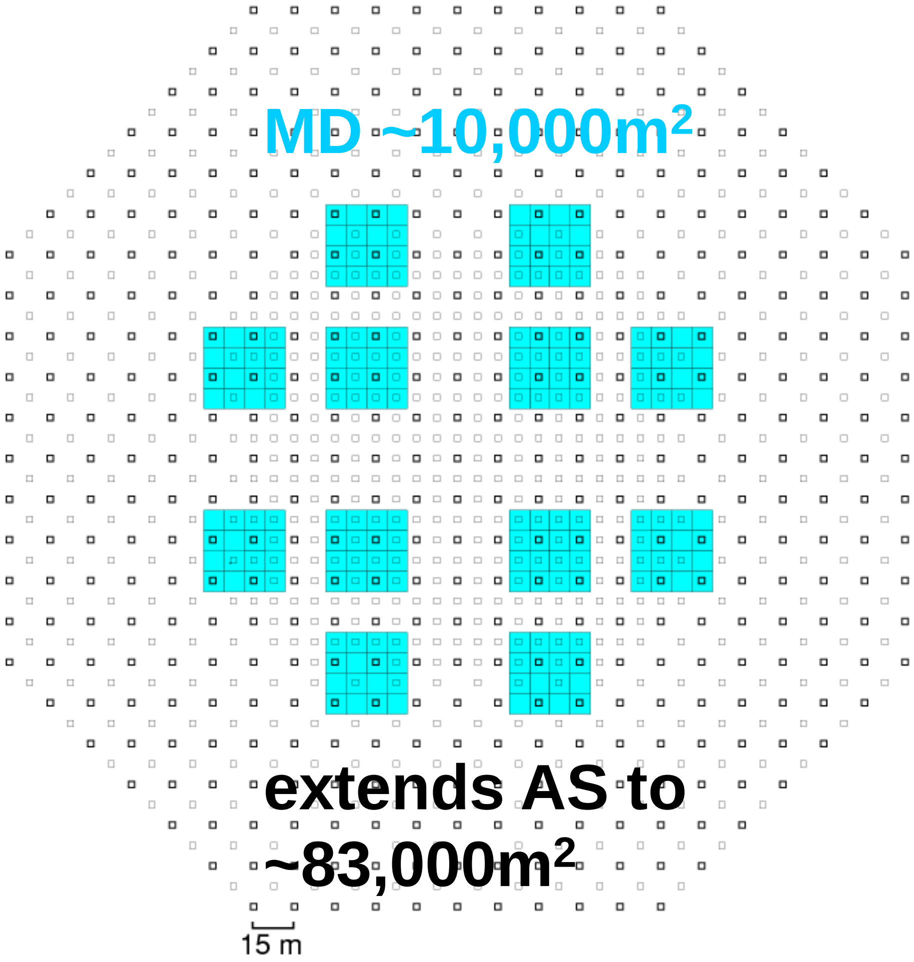

Counting the number of muons accompanying an air shower

➡ p/γ discrimination

Muon Number vs. Shower Size (Simulation)

$\Sigma\rho$: Sum of particle density by all scintillation det.
>> Shower Size

ΣN_{PE}: Sum of photoelectrons by all muon det.
>> Muon number
(Threshold of MD N_{PE} >10 p.e.)

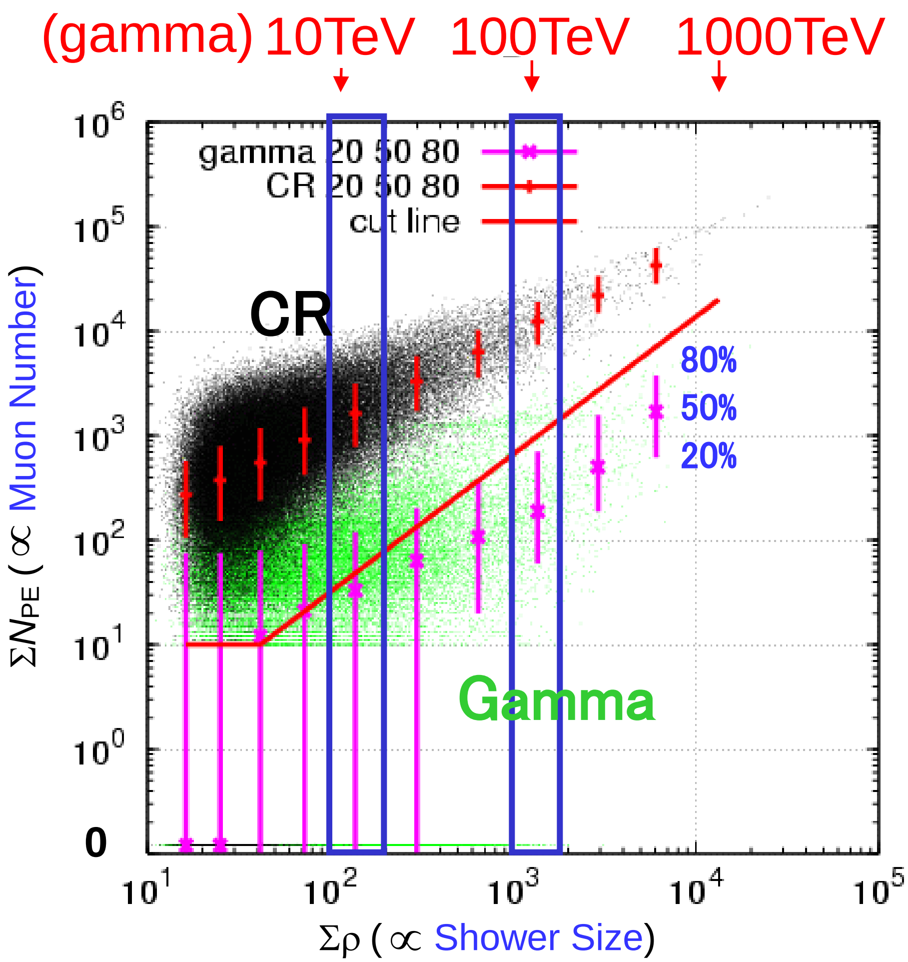

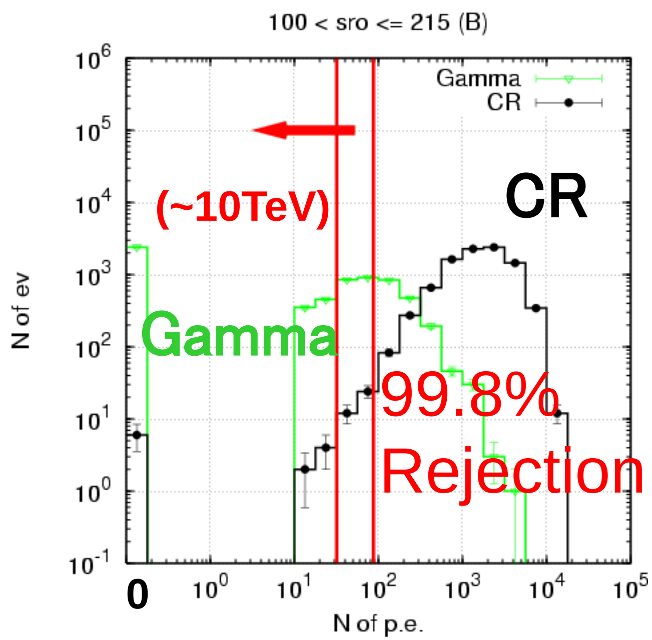

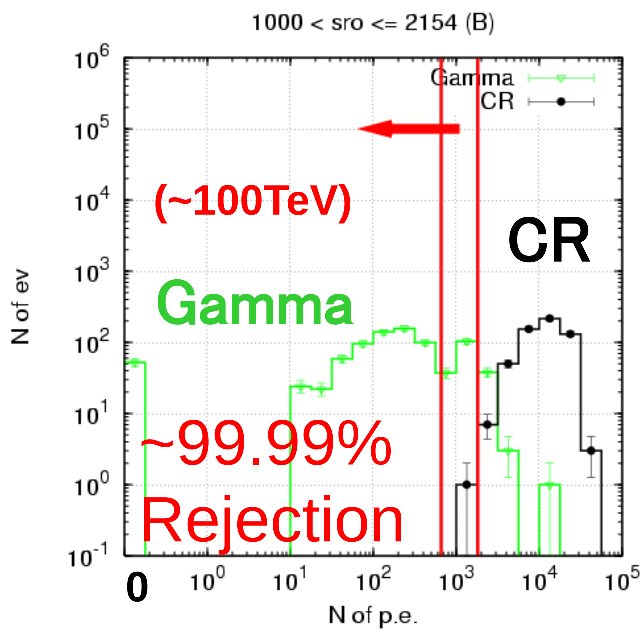

Other Future Plans（5σ or 10 events）

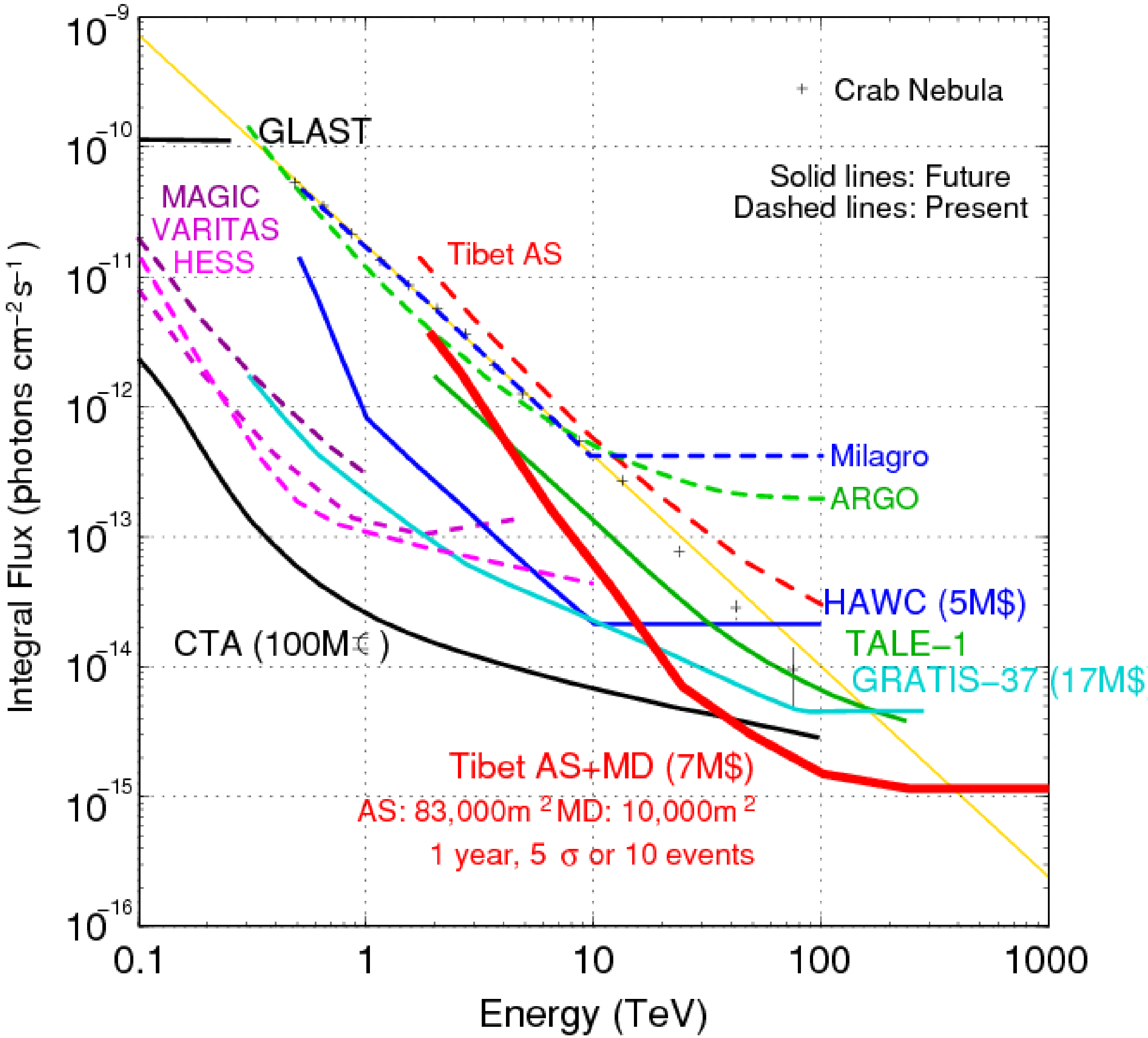

Gamma Ray Observation in the 100 TeV region

TeV J2032+4130 (~5% Crab)

1. Hard spectral index at TeV energies
2. Faint in other wavelengths

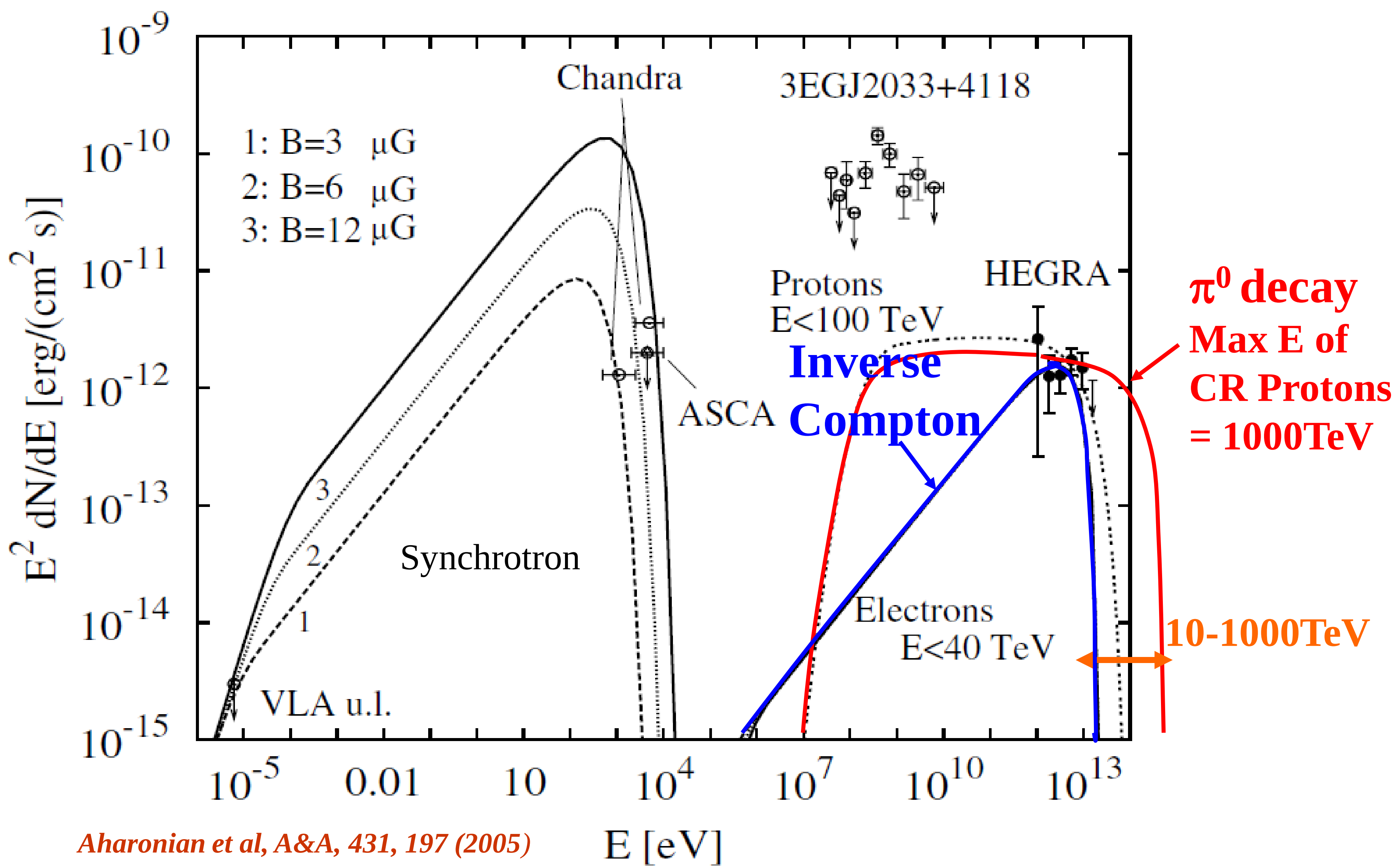

Aharonian et al, A&A, 431, 197 (2005)

TeV J2032+4130 and π^0 decay model

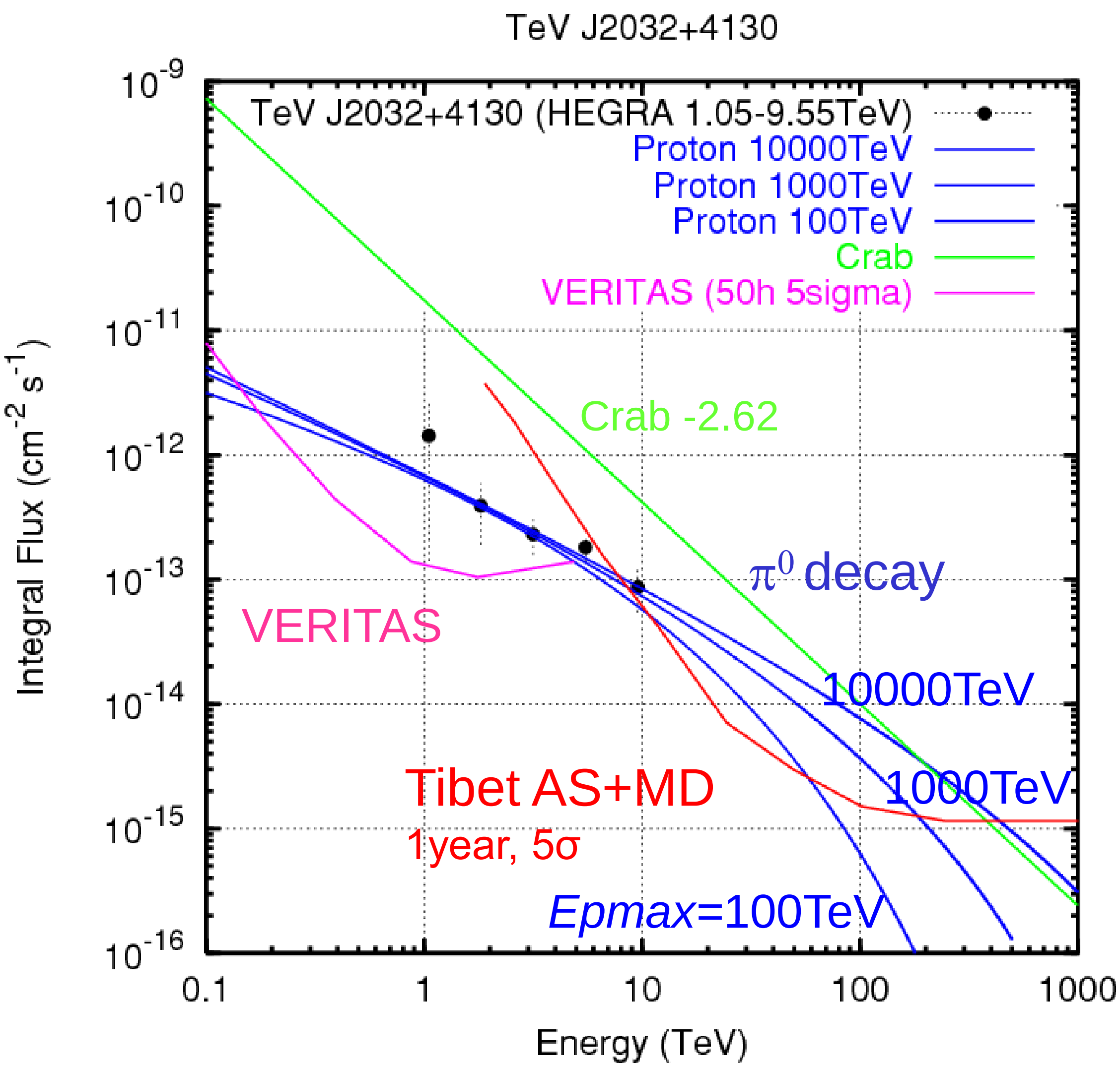

TeV J2032+4130
Unidentified source
Cyg X-3 in Cyg OB2
HEGRA obs.~158 hours
Extended ~6.2′

π^0 decay model
Aharonian et al. A&A, 464, 235(2007)
Kelner et al., PRD 74, 034018 (2006)

Aharonian et al, A&A, 431, 197 (2005)

Diffuse gamma rays from Galactic Plane

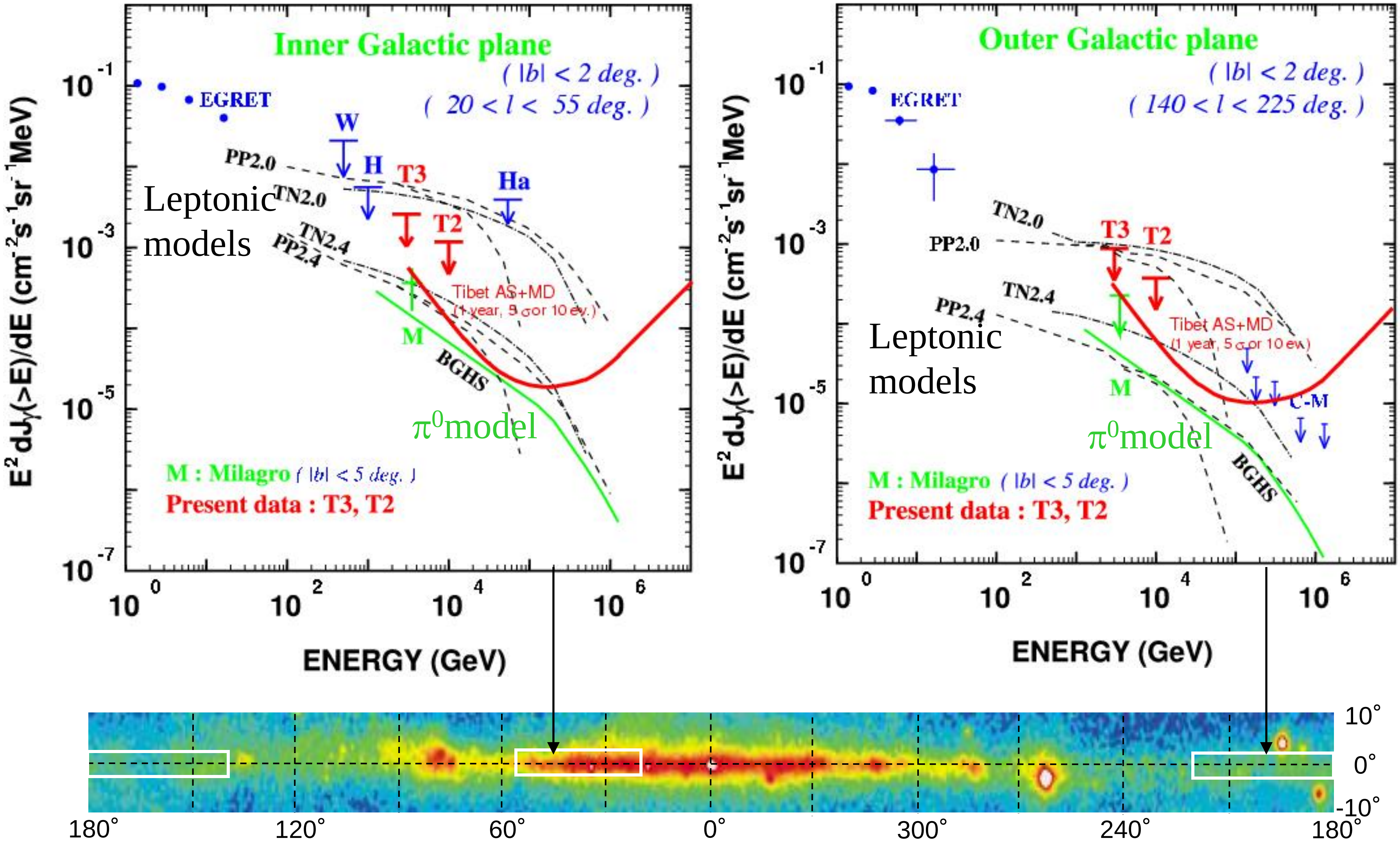

EGRET data

MD summary

Tibet MD

～83000 m^2 Airshower Array (AS) ＋

～10000 m^2 Water Cherenkov Muon Detectors (MD)

→100 TeV(10–1000TeV) γ–ray observation（CR acceleration limit & Diffuse γ)

Expected Sensitivity

F(>100(20)TeV) ～10^{-15} cm^{-2} s^{-1} ～10 (5) % Crabs

→More than 10 times better sensitivity

>HESS (>10–20TeV), >CTA (>30–40TeV)

Source Candidates for 100 TeV g–ray emission in our field of view.:

Possible (1 year) : Diffuse γ from Milky way,
Crab, TeV J2032+4130,
MGRO J2019+37, MGRO J1908+06, MGRO J2031+41
HESS J1837–069, Mrk 421

Interesting (Several years) : Cas A, M87, HESS J1834–089, HESS J0632+058
Mrk 501, LS I +61 303, IC443, Extragalactic Diffuse γ???

Unknown : several –10 !?

Prototype Muon Detector in Tibet

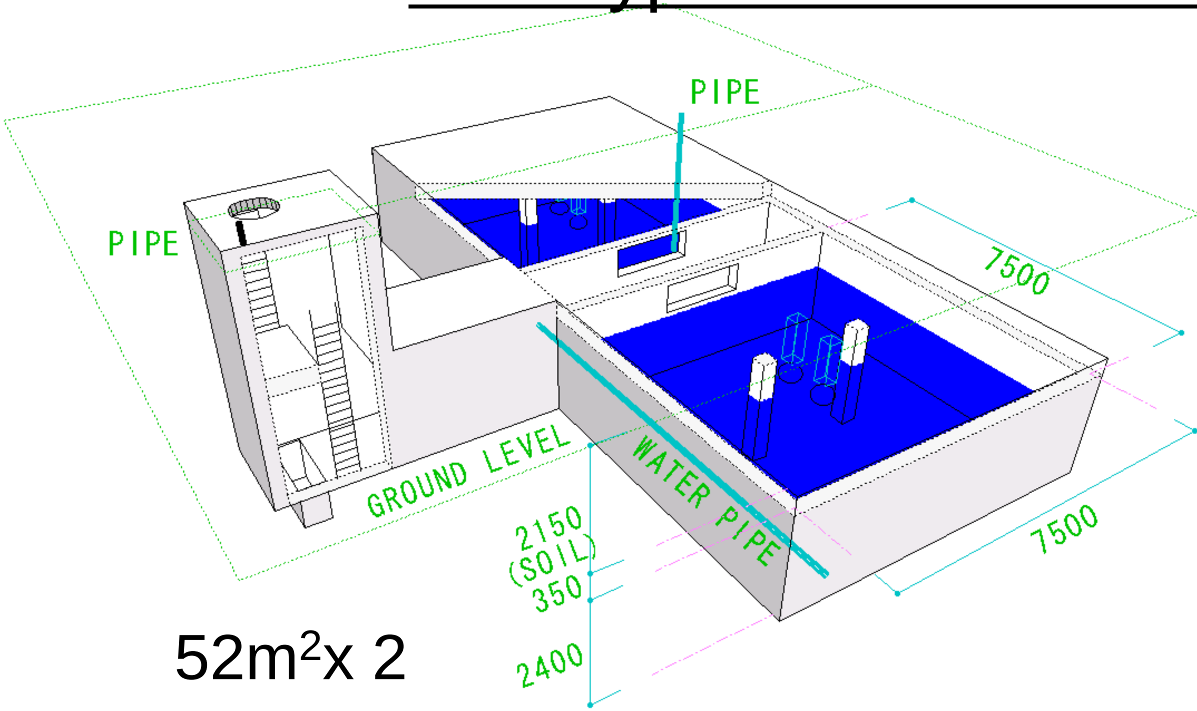

52m^{2}x 2

Construction from
Sep. 2007
Data taking from
Dec. 2007

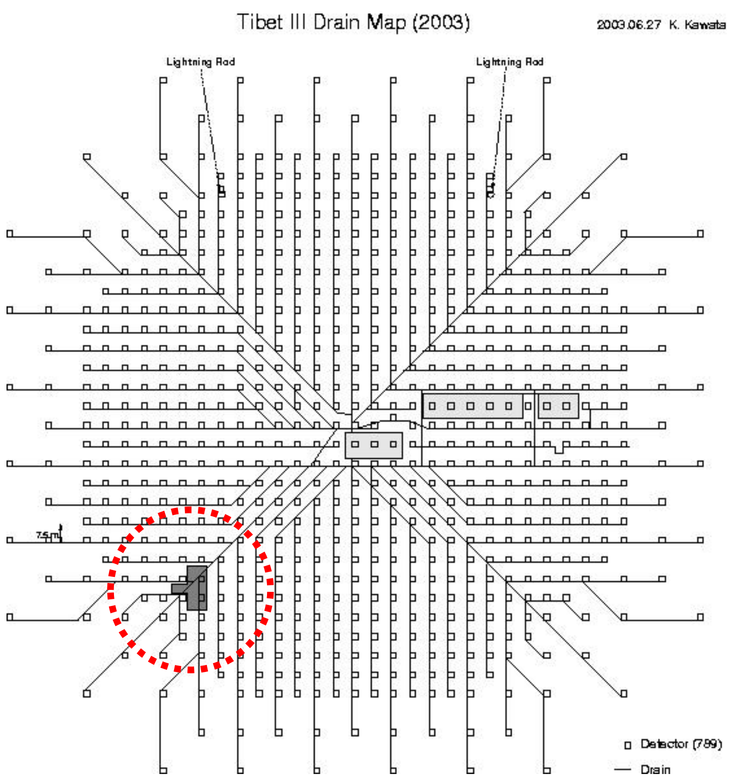

- Construction feasibility in Tibet ?
- MC simulation OK?
- γ observation above multi 100 TeV

16 November, 2007 Prototype Muon Detector

Prototype Muon Detector after backfilling

Inside of the Prototype MD

Clear underground water
from a nearby well

20”ϕ PMT x 3:
(Normal gain x 2, 1/100 gain x 1 for test)

Water depth : 1.5 m

White paint

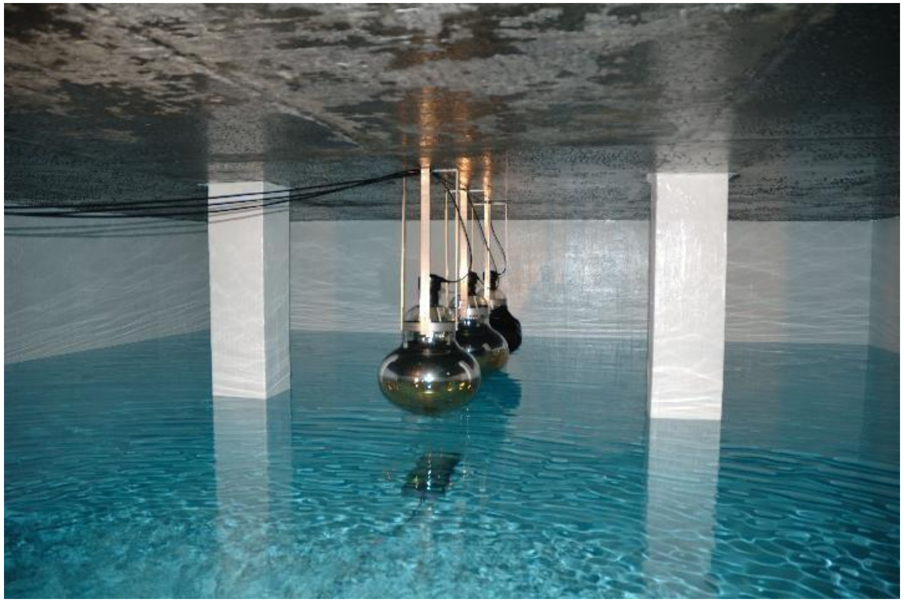

Pouring very clear well-water

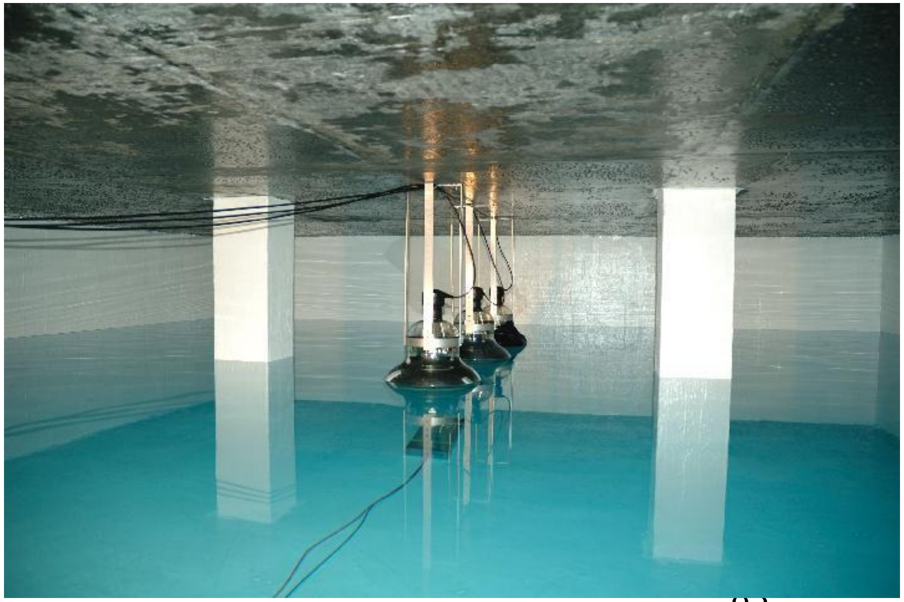

Filled up water 1.5 m in depth

Number of muons

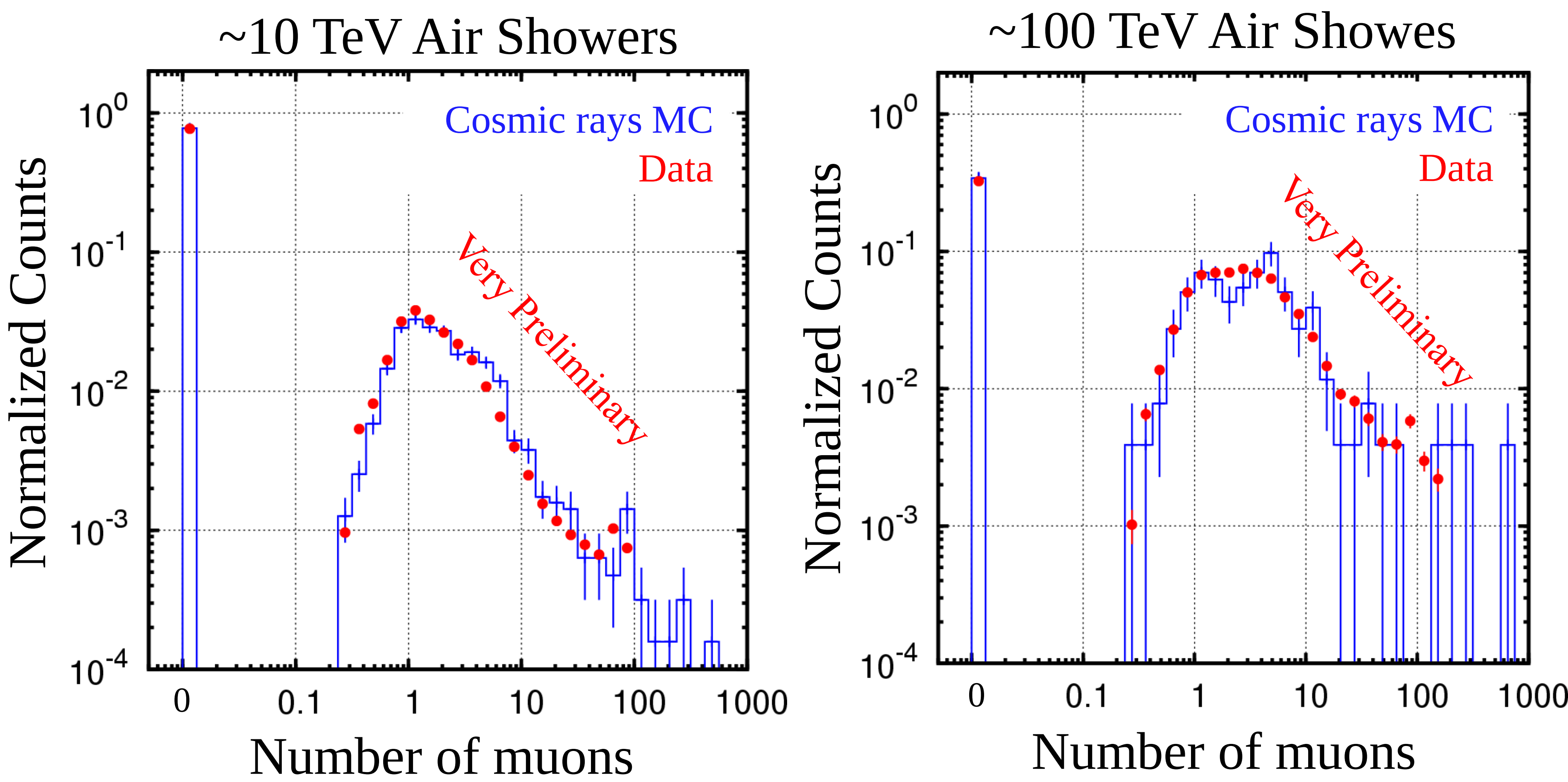

Cosmic Ray (Nucleus) Survival Ratio

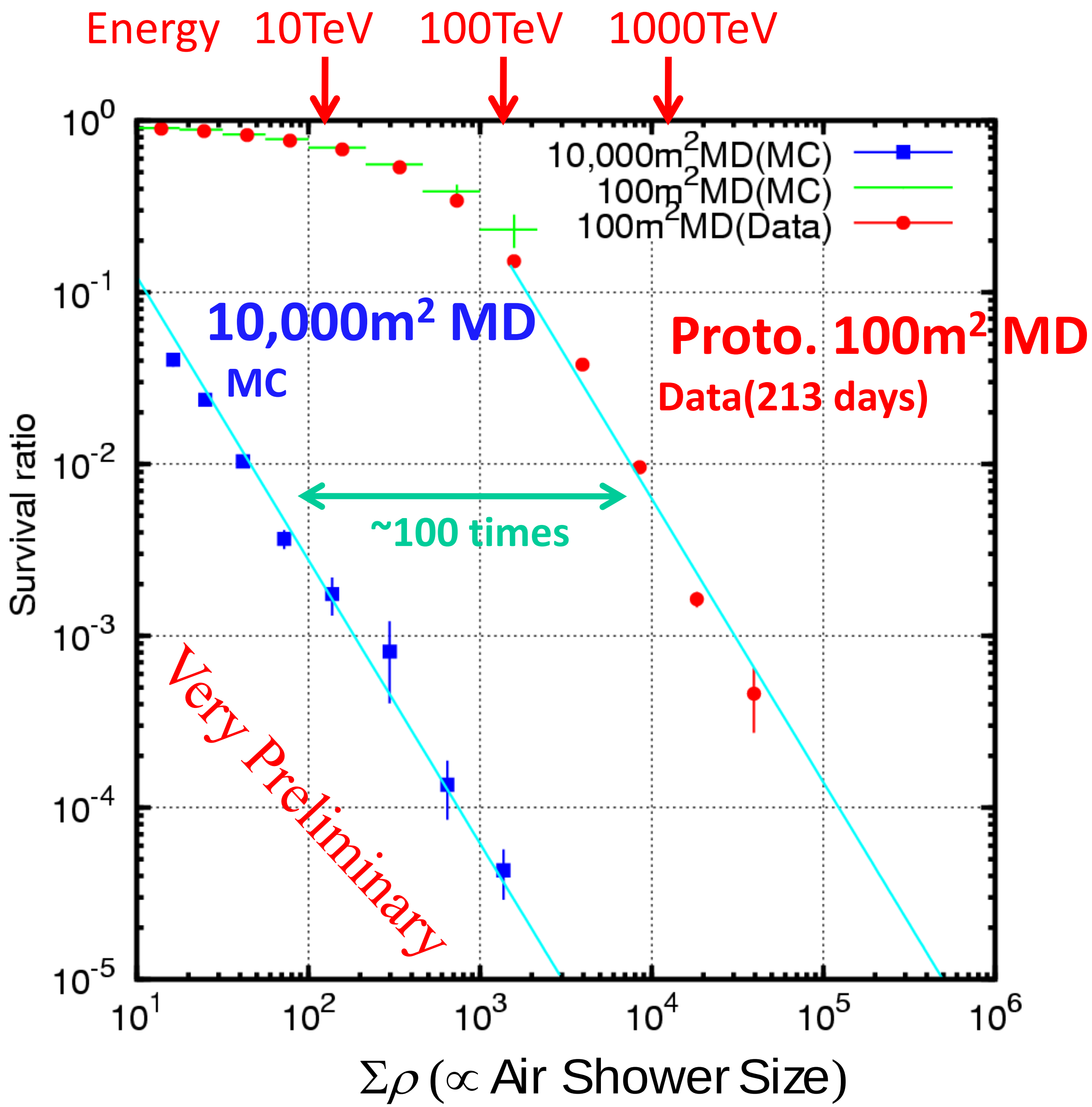

Status of MD Construction

5/12 Full MD under construction

Data-taking In 2013

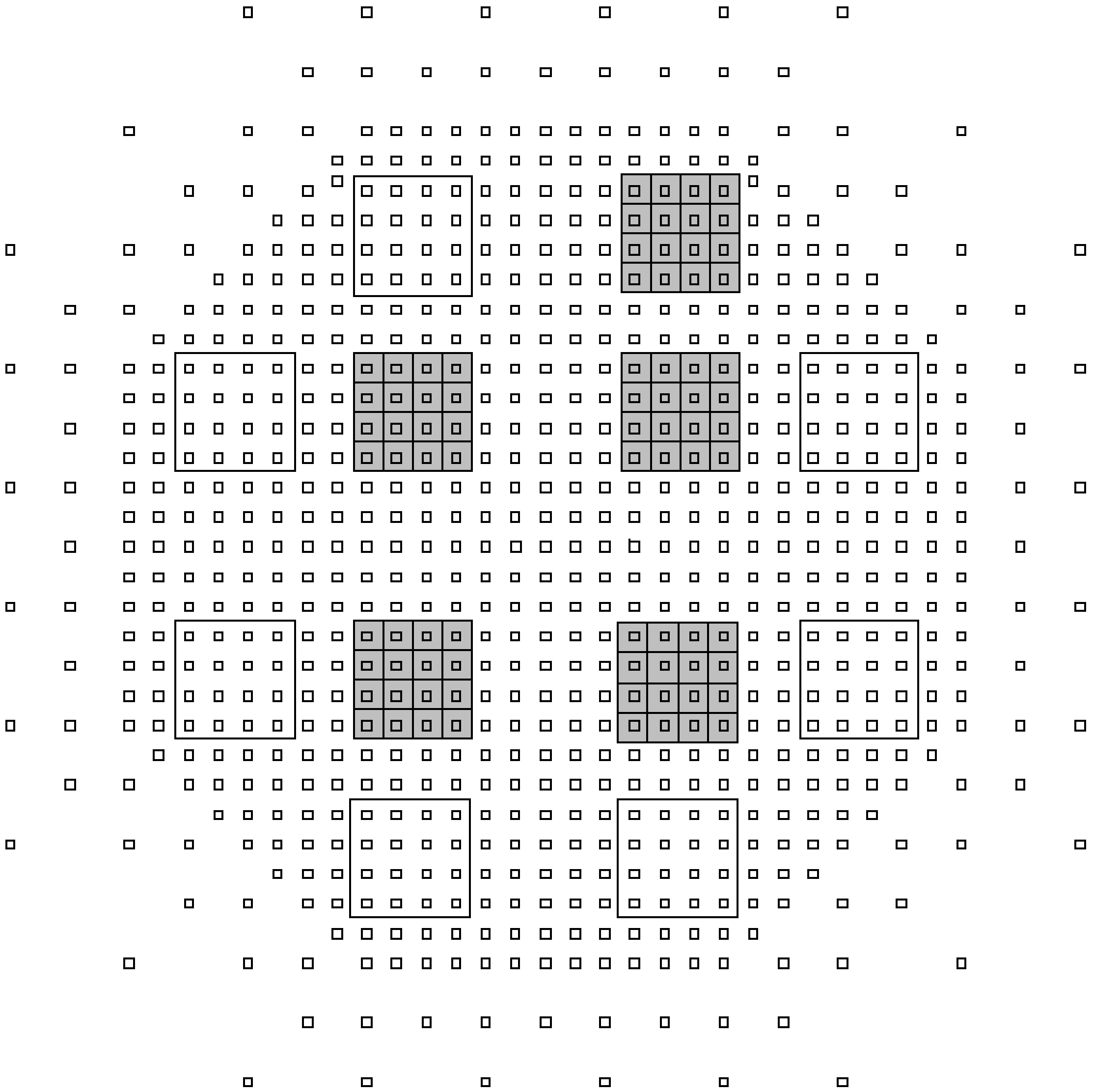

MD construction scene

Installing a 20 inch PMT in a MD cell.

Tyvek sheet walls and two 20 inch PMTs

MD Summary

Prototype MD (52 m^2 x 2 cells)

– **Successfully completed** (2007)

Data vs MC in reasonable agreement

CR survival ratio: ~0.2 %@~1 PeV

-> Full (10^{4}m^2) MD @~10 TeV

-> Full (10^{4}m^2) MD MC: OK up to ~10TeV

~1/3 Full MD under construction

Data-taking will start in 2013

YAC II

(Dense version)

（under construction）

YAC II detector consists of 100 burst detectors with 1.5m spacing between detectors.

Total area of the array is 160 m^2 located near the center of Tibet III AS array.

It is designed to measure proton and helium spectra in the knee region. **Expected number of protons (>100TeV) and helium (>200TeV) using HD model are 2300 and 800 per one year, respectively.**

Design of YAC-II

40cm x 50cm, 100 channels S=160m^2

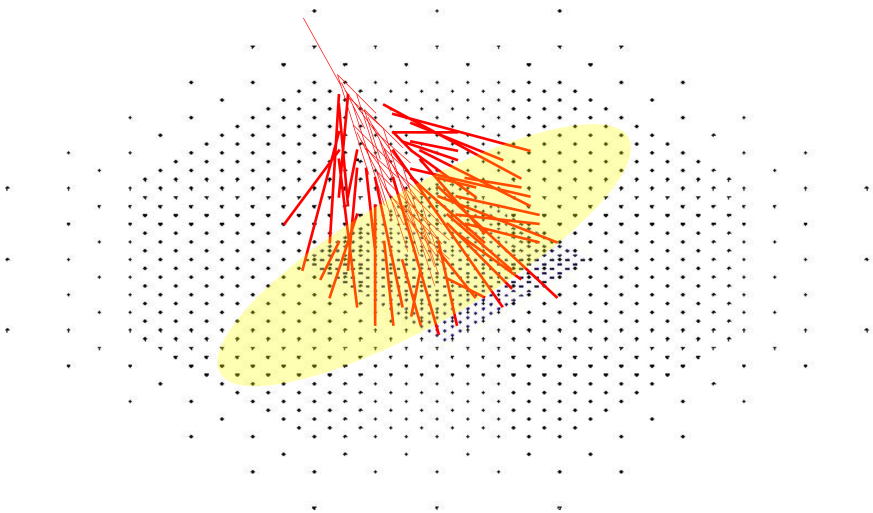

1.5m spacing 100ch
N_b>100electrons,
any 1 (>30GeV)

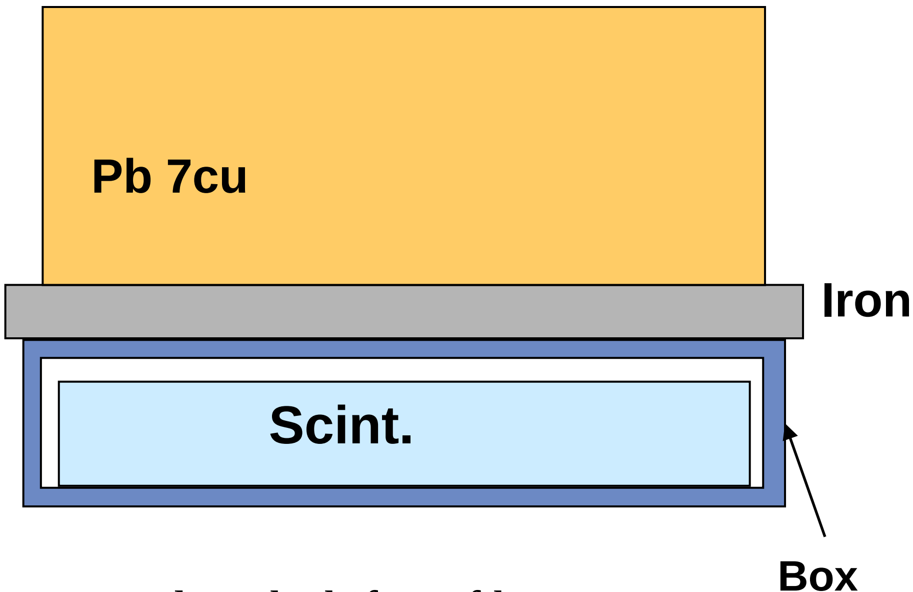

Wave length shifting fiber
+ 2 PMTs
(Low gain & High gain)
$10^2<N_b<10^6$

Tibet All, P, He spectrum

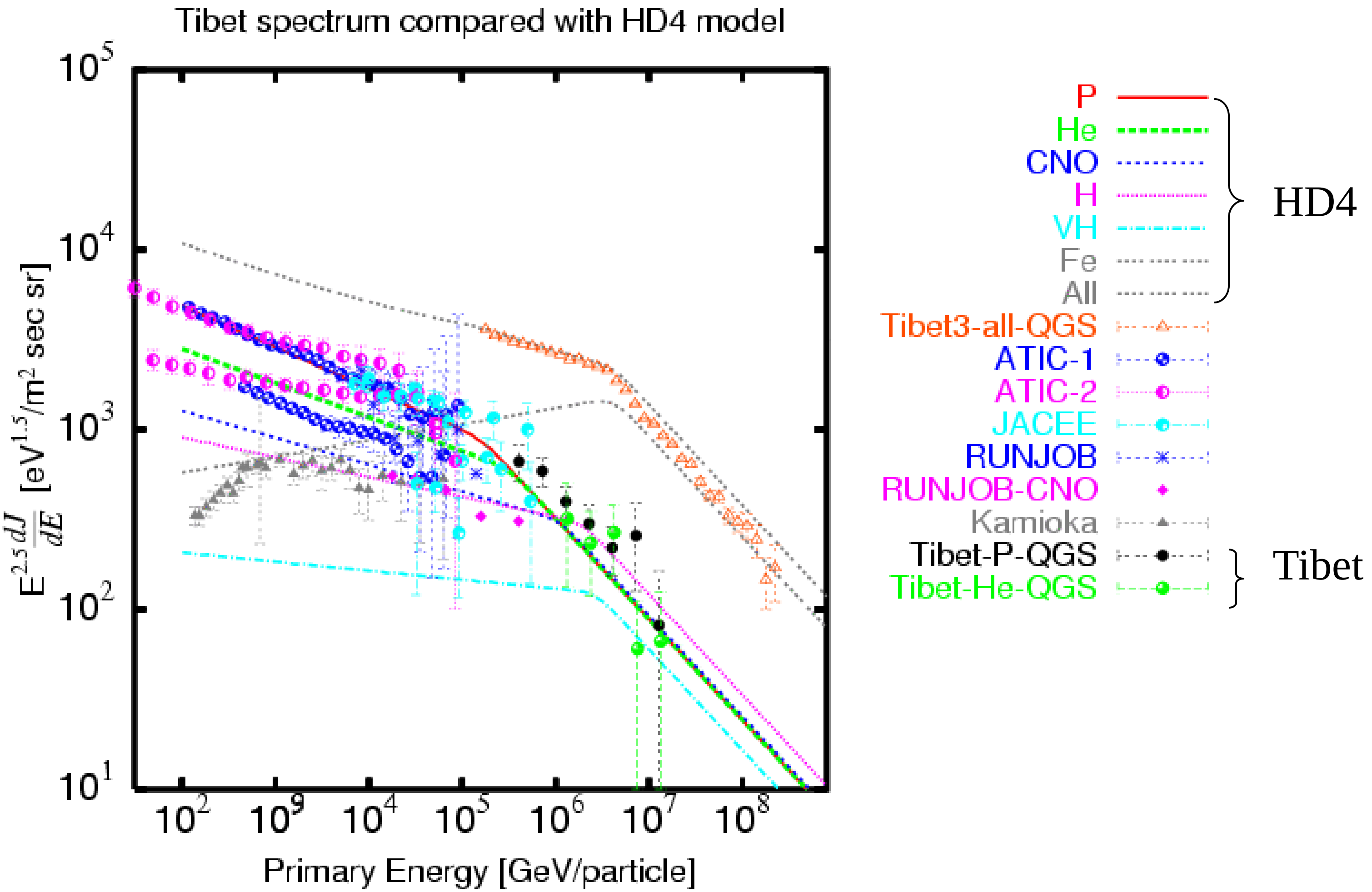

Features of YAC-II observables

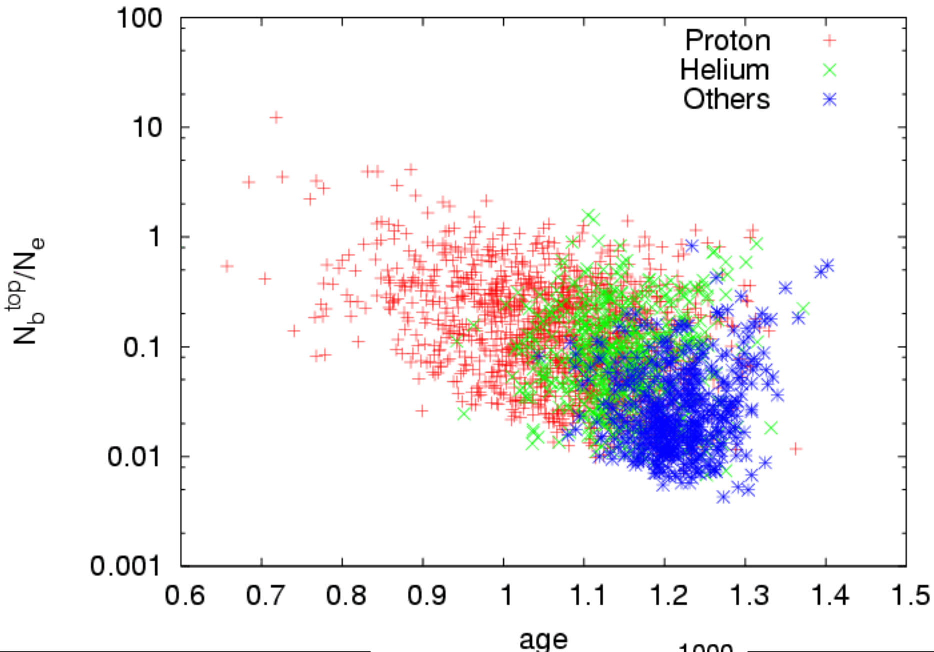

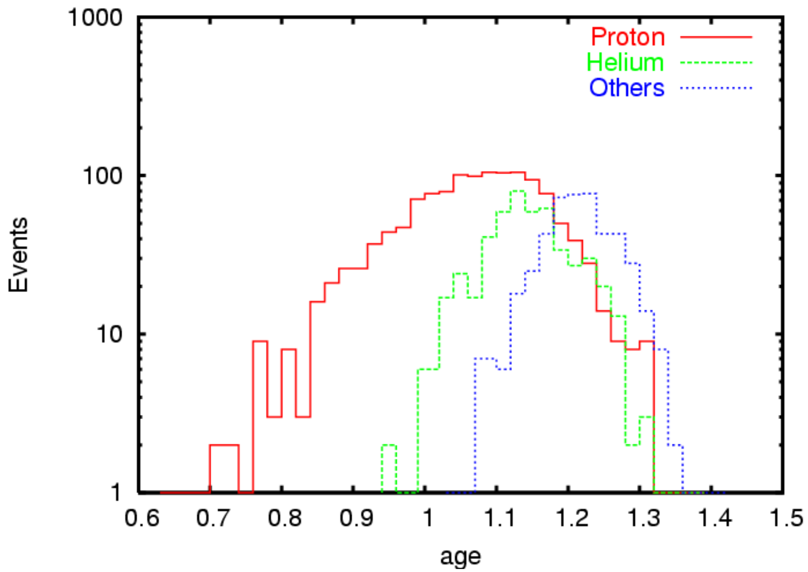

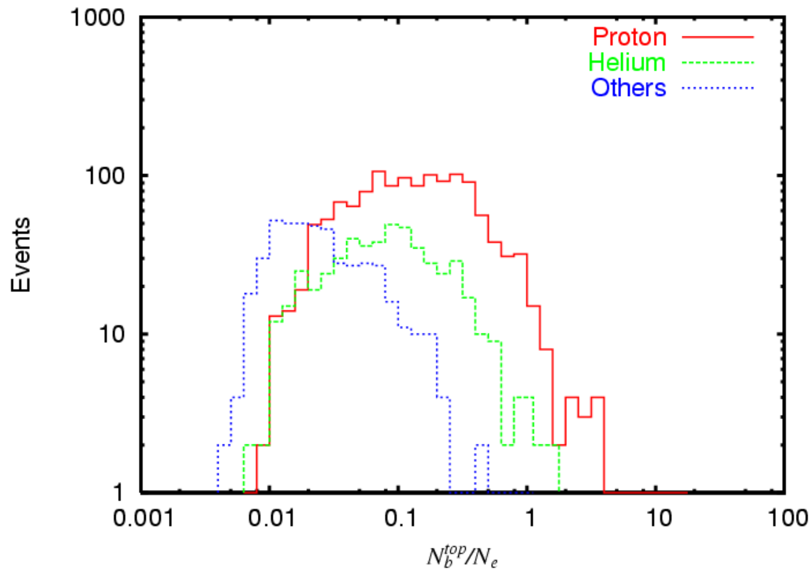

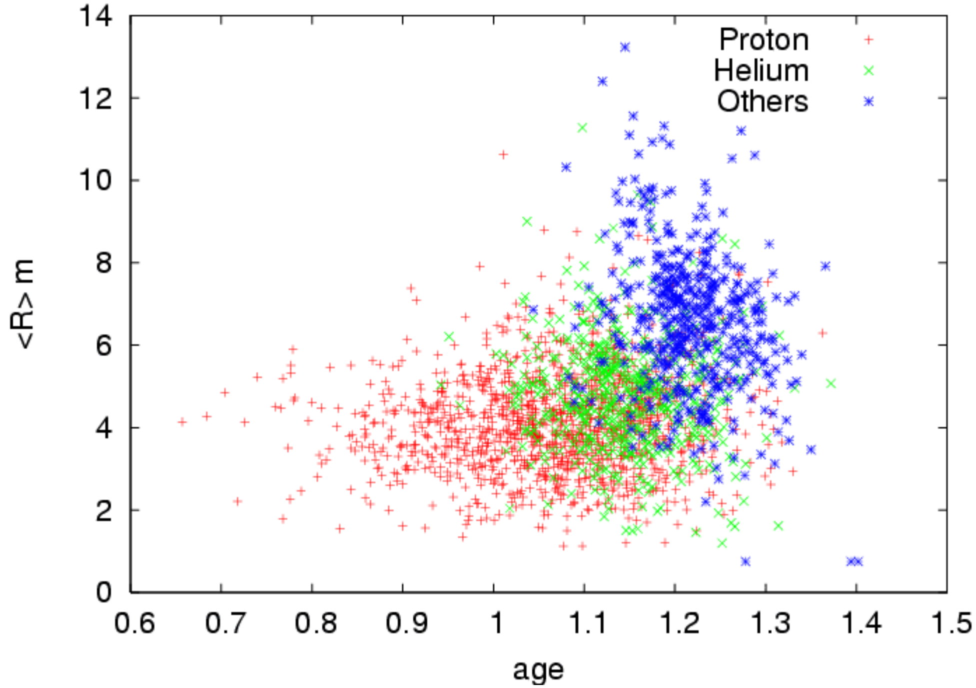

Proton
Helium
Others
<R> m
age

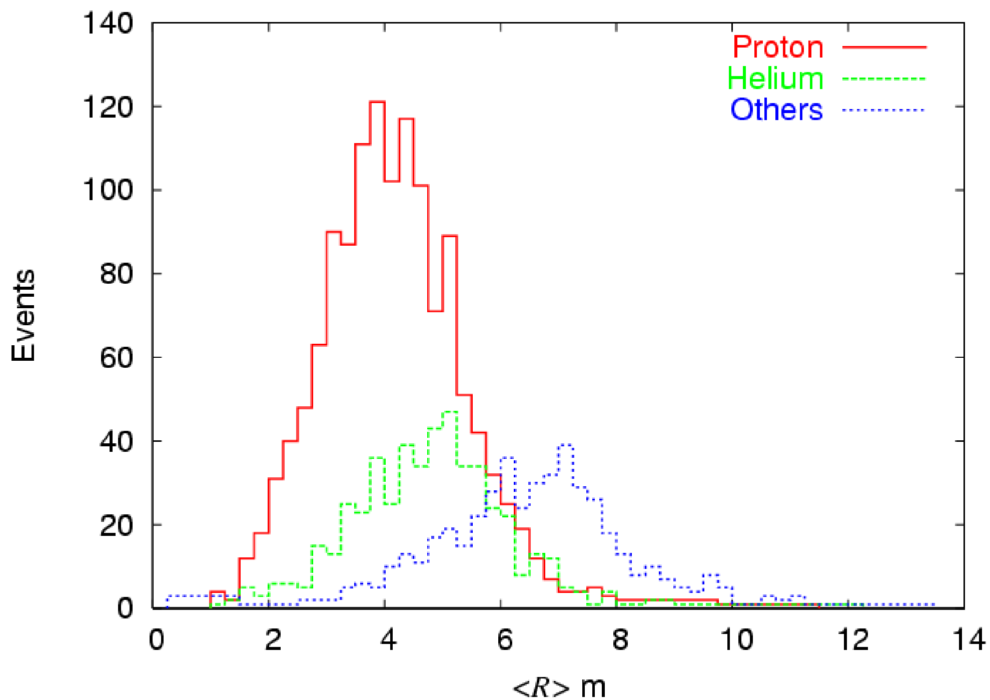

Proton
Helium
Others
Events
<R> m

ANN output

Proton separation

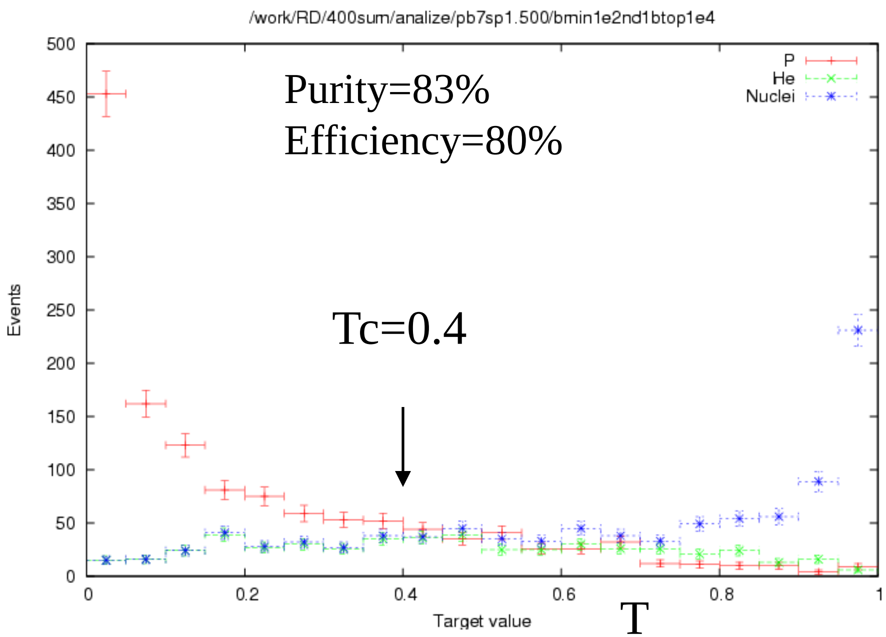

P+He separation

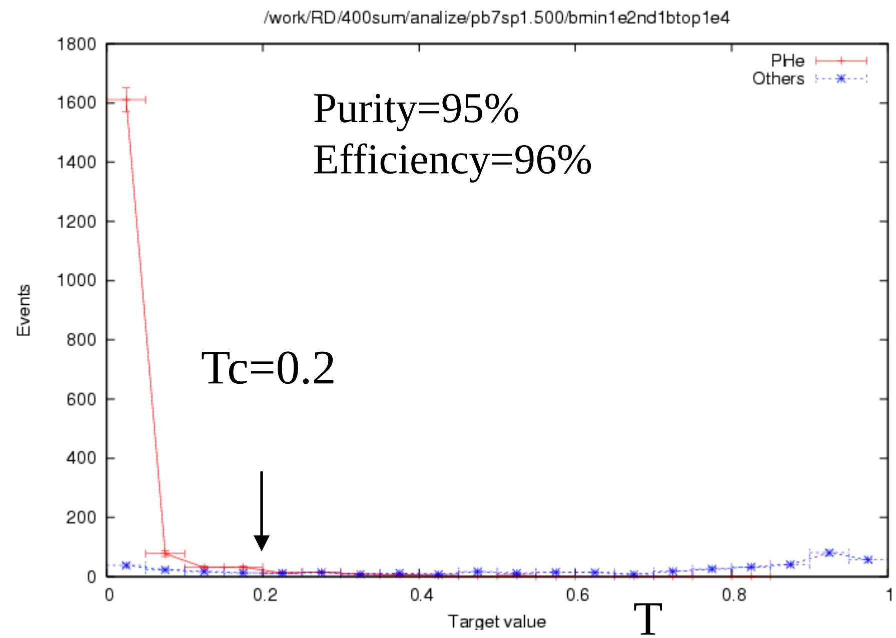

Contamination is exclusively by helium nuclei.
The fraction of helium events missidentified as protons is about 40% of helium events by Tc=0.4.

20% of heavier nuclei than helium contaminates to P+He region.

Expected proton spectrum (YAC-II)

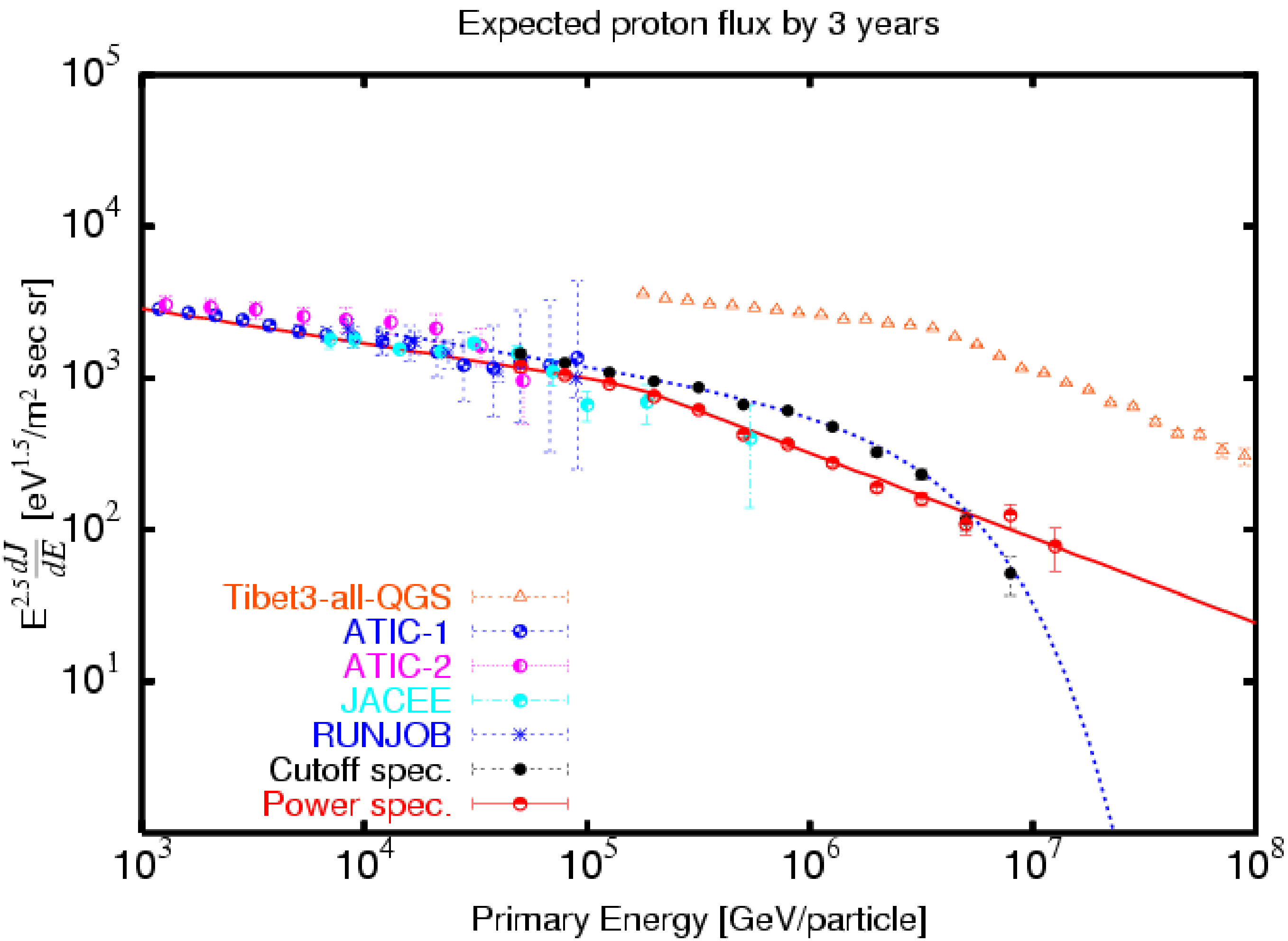

Expected He Spectrum (YAC-II)

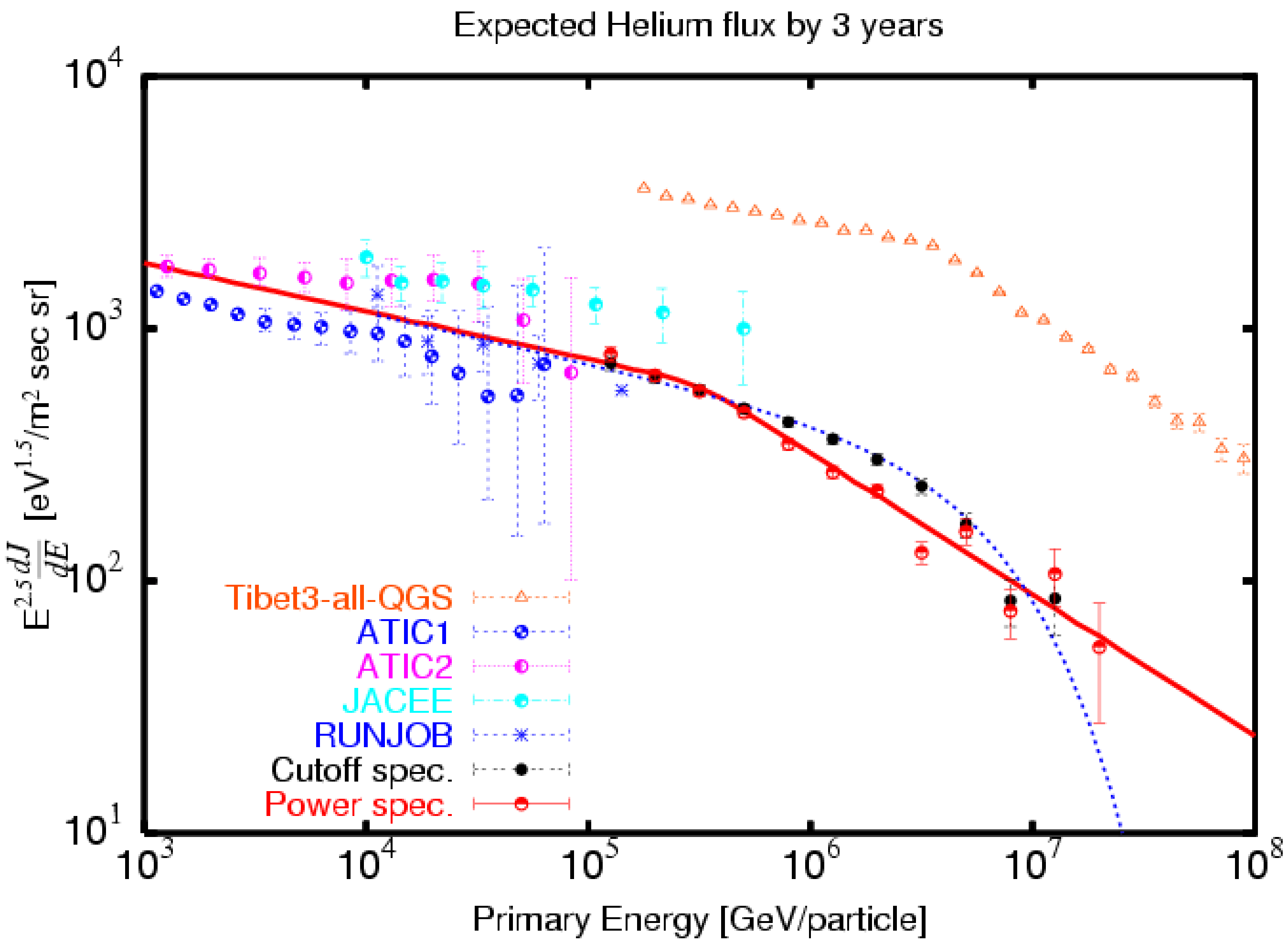

YAC III
(Wide version)   2.5 M USD

YAC III detector consists of 400 burst detectors with 3.75m spacing between detectors.

Total area of the array is 5000 m^2 located near the center of Tibet III AS array.

It is designed to measure iron group spectra in the knee region. <u>**Expected number of irons (>1000TeV) using HD model is 4400 per one year.**</u>

Design of YAC-III

40cm x 50cm, 20x20 channels
$S=5000m^2$

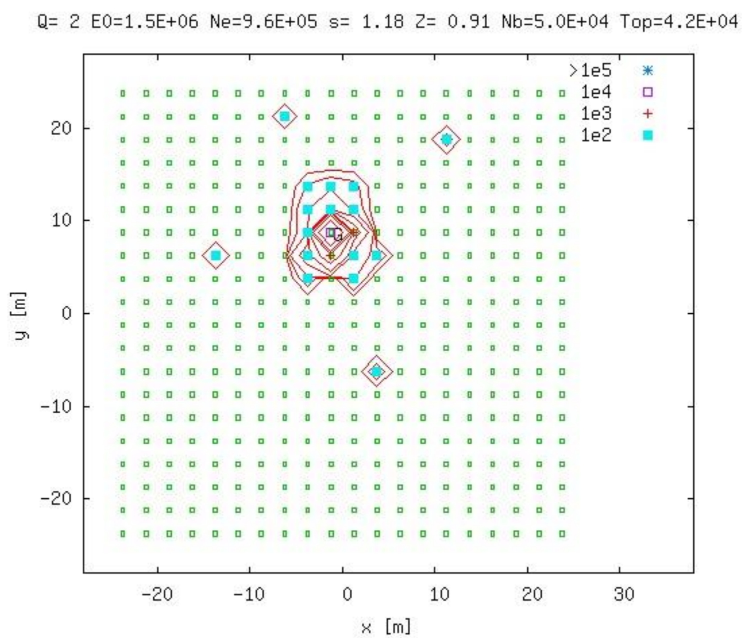

3.75m spacing 400ch
N_b>100, any 5
(>30GeV)

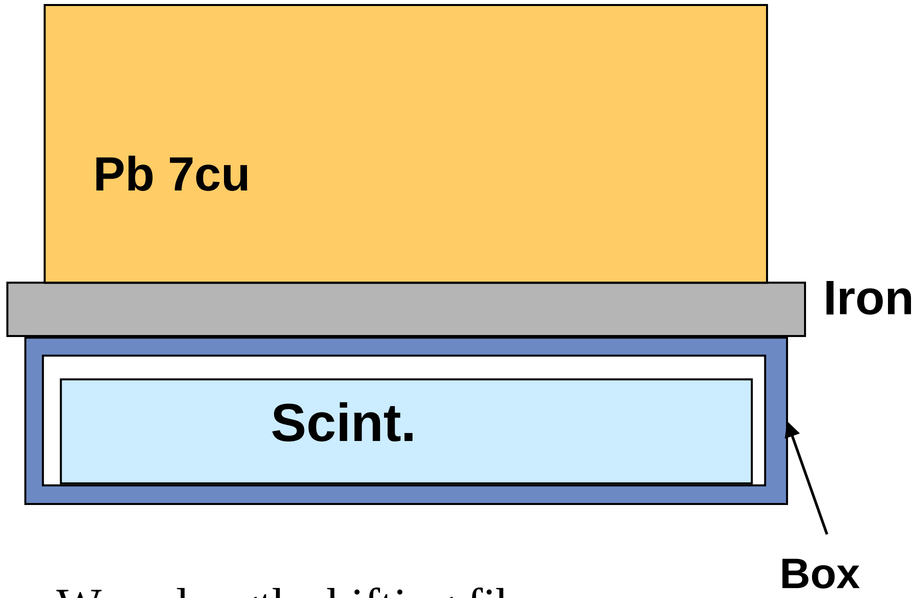

Wave length shifting fiber
+ 2 PMTs
(Low gain & High gain)
$10^2 < N_b < 10^6$

Separation of Fe by YAC III

$N_{hit} \geqq 21$

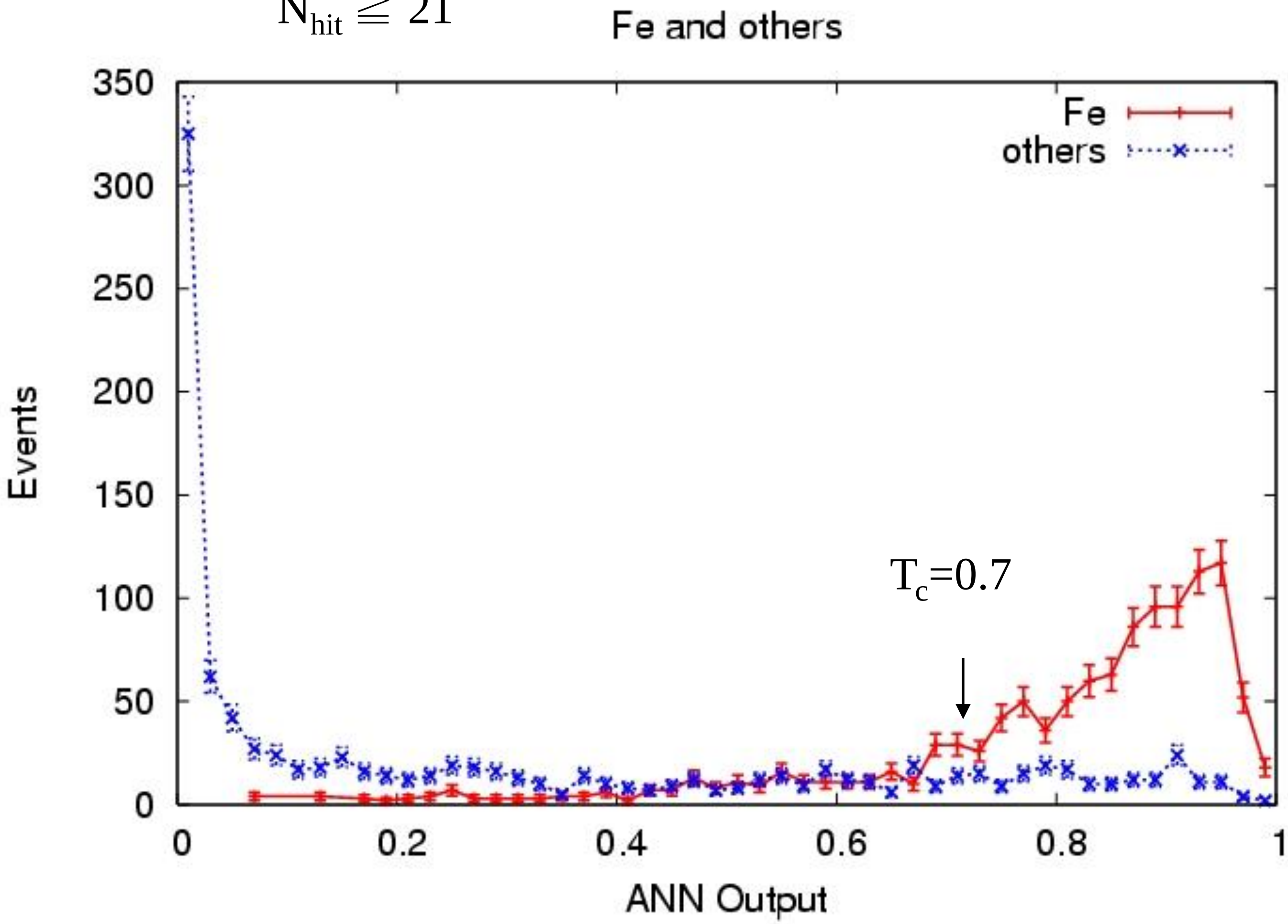

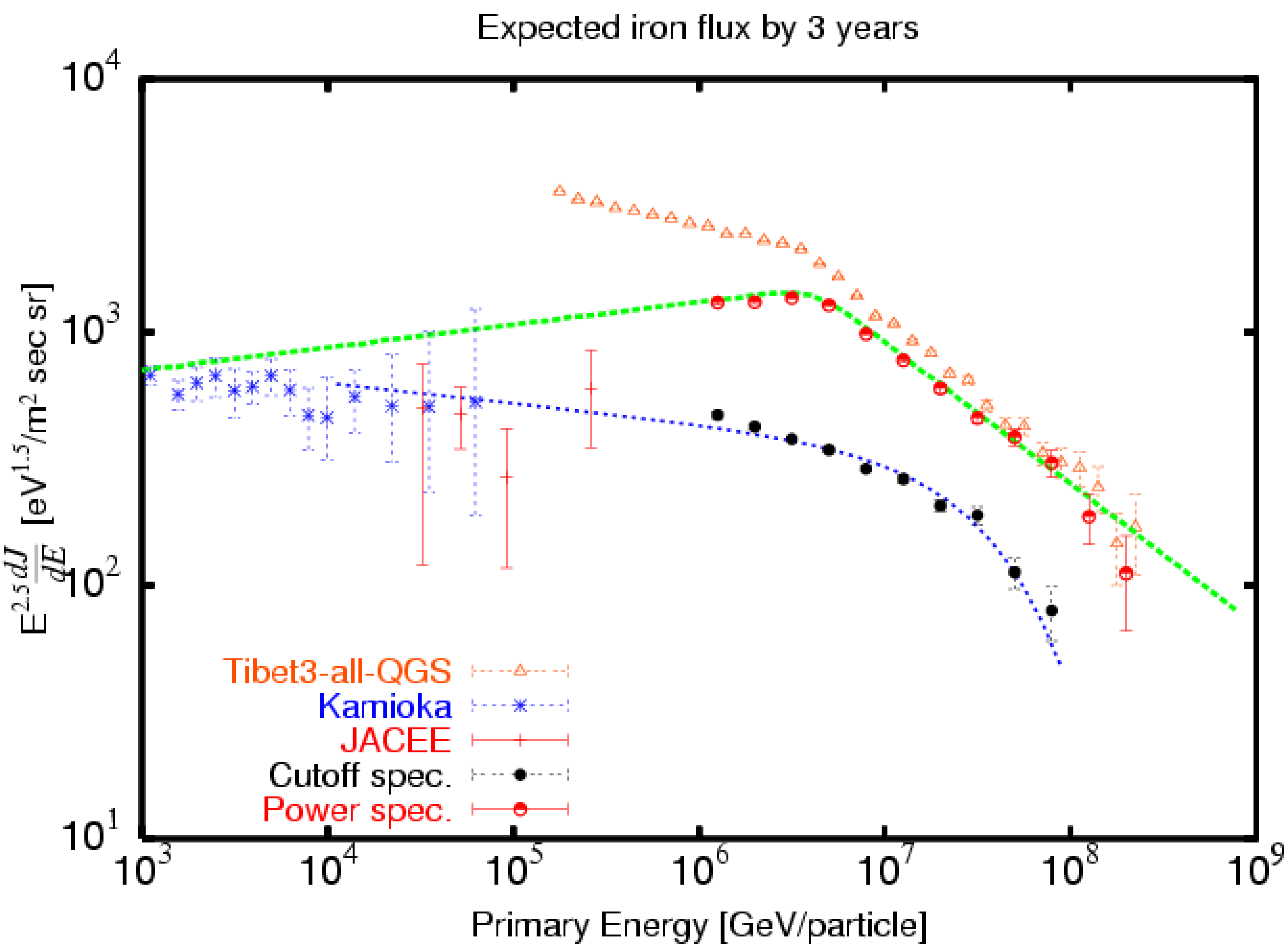
Expected iron flux by 3 years
$E^{2.5}\frac{dJ}{dE}$ [eV$^{1.5}$/m^2 sec sr]
Primary Energy [GeV/particle]
Tibet3-all-QGS
Kamioka
JACEE
Cutoff spec.
Power spec.

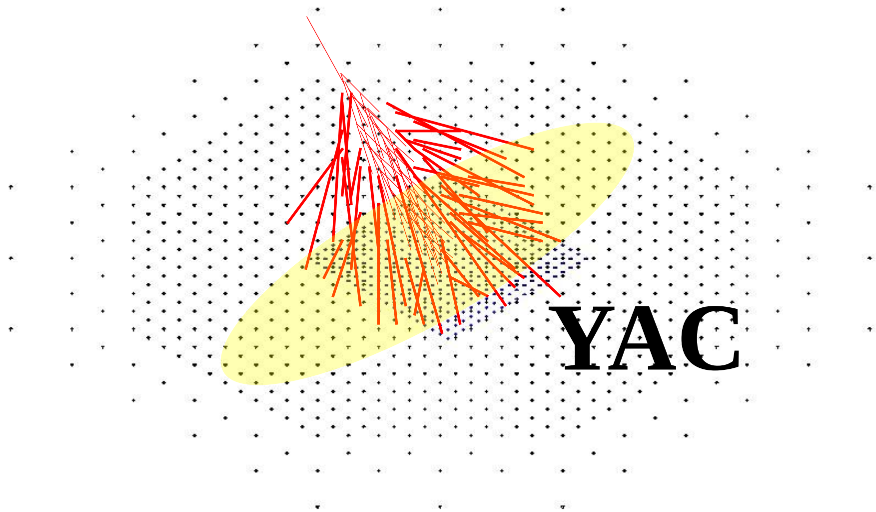

Proto-type YAC Detector

Prototype of YAC
(Yangbajing Air shower Core detector)

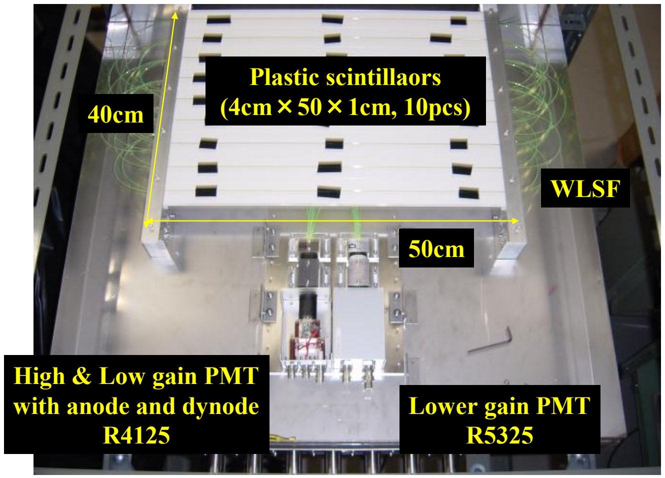

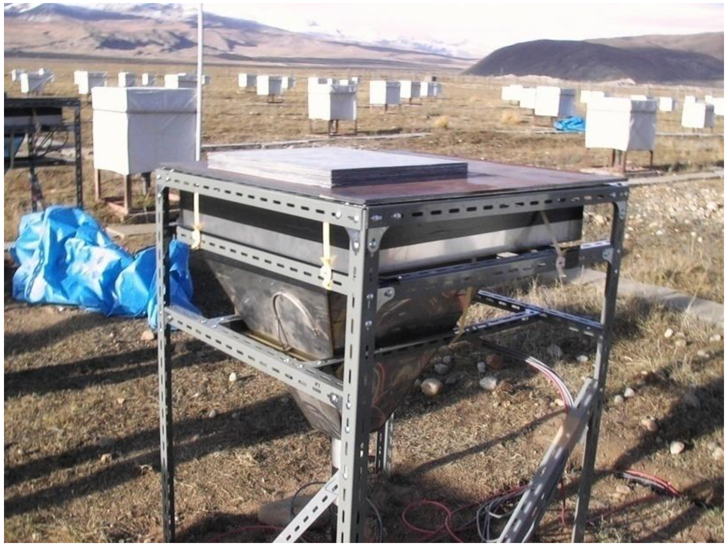

YAC-II under construction

Data-taking will start 2013

Sumary of MD & YAC status

- R&D DONE for MD&YAC
- 5/12 MD under construction

  YAC-II under construction

  Data-taking: in 2013
- Rest of the plan: if funded

End